LONG-TERM ANALYSIS OF AIR POLLUTANTS USING SATELLITE OBSERVATIONS, GROUND MEASUREMENTS, AND MODEL SIMULATIONS OVER ASIA

Pichnaree Lalitaporn

2014

Acknowledgement

First and foremost, I would like to express my deep gratitude to my supervisor, Prof. Yuzuru Matsuoka, for accepting me to be his student, and for his professional guidance and valuable support throughout the course of study. His willingness to give his time so generously has been very much appreciated. I also would like to express my very great appreciation to Assoc. Prof. Gakuji Kurata for his valuable and constructive comments and suggestions during the planning and development of this research work. Without his assistance and dedicated involvement in every step throughout the process, this research would have never been accomplished. I would like to thank you very much for his support and understanding over these past three years. Special thanks to Assist. Prof. Reina Kawase for her kind concern and support during my study. I would also like to extend my sincere gratitude to my committee member, Prof. Minoru Yoneda, for serving as my committee member, and for your brilliant comments and suggestions, thanks to you.

I would like to offer my special thanks to Dr. Narisara Thongboonchoo at King Mongkut's Institute of Technology Ladkrabang, Thailand and Dr. Vanisa Surapipith at Pollution Control Department, Thailand for their valuable support and collaboration during my internship in Thailand. My warm thanks to Dr. Prapat Pongkiatkul and Mr. Prawit Paravanich for providing very supportive advices on my research.

I owe my deepest gratitude to Ms. Emiko Hatanaka, the lab secretary for always helping my study run smoothly since I first came to Kyoto University, and for being a wonderful friend. Special thanks to Dr. Tran Thanh Tu for being my tutor and my good friend. Many thanks also to Kaku-san. I would not be able to adapt to my new life in Japan without you. To all lab members, I have been blessed with your friendships, thanks to you.

I have to thank Prof. Shigeo Fujii who directly interviewed me at Asian Institute of Technology (AIT), Thailand for the scholarship to pursue my PhD degree in Japan. Altogether, this research would have been impossible without the financial support from the Ministry of Education, Culture, Sports, Science and Technology (MEXT) of Japan for this three-year PhD course in Kyoto University.

Last but not least, I wish to thank my family for their support and encouragement throughout my study.

Abstract

The continuing rise of economic expansion and energy consumption are evidently seen as key drivers of the higher level of urban air pollution in Asian developing countries for the past decades. Monitoring air pollution is an essential component for air quality management to determine population exposure, health impact assessment, and compliance with national and international standards. Conventional ground-based monitoring of particulate matter and gaseous air pollutants is hampered by the limitation in spatial distribution. Satellite remote sensing recently gains increased attention due to its large spatial coverage which is particularly suitable for Asian developing countries with few ground-based monitors, high-level of pollutant emissions in industrial and populated areas, and high potential for long-range transport from biomass burning activities. The overall objectives of this study are to apply the use of satellite retrievals as a tool for long-term analysis of atmospheric pollutants, and to develop methodology to validate and improve emission inventories by using integrated satellite observations and model simulations.

Long-term analysis of tropospheric NO_2 columns retrieved from GOME, SCIAMACHY, OMI and GOME-2 satellites, CO columns from MOPITT satellite and AODs from MODIS satellite was performed for Southeast Asian countries and some parts of China and Japan over 17 years during 1996-2012. The results show that significant increasing levels of tropospheric NO_2 columns can be clearly observed during these years, especially above eastern part of China regions which are around 16 and 11 % per year for Shanghai and Beijing, respectively. For CO columns and AODs, the annual trends of these pollutants are relatively constant during the study period. The cities located in different latitude zones present the seasonal cycle of NO_2 columns, CO columns and AODs differently. For the cities located in mid-latitude zone and upper part of low-latitude zone, the maximum levels of NO_2 and CO columns can be observed in the winter (November-March) and the minimum in the summer (June-September). On the contrary, the maximum levels for the cities near Equator zone are revealed in dry season (June-October). In case of AODs, the maximum peaks normally occur during biomass burning

season and Asian dust-storm period. Ground monitoring concentrations of NO_2, CO and PM_{10} were also comparably analyzed with satellite NO_2 columns, CO columns and AODs, respectively in order to validate satellite observations. The results reveal that satellite data are in agreement with ground-based monitoring in term of seasonal variability, especially for NO_2. However, there are still some discrepencies between AODs and surface PM_{10}, since AODs do not directly represent PM_{10} concentrations. More analysis focused on the improvement of relationship between AODs and surface PM_{10} concentrations over Thailand. The regression was performed without and with cloud screening procedure. The latter gave stronger correlations. The multiple linear regression models were then developed by using 5-year (2008-2012) data of AODs with the correction of surface meteorological parameters including surface relative humidity (RH), wind speed (WS), and temperature (T). Such models were applied to estimate surface PM_{10} mass concentrations and evaluated with those measured from ground monitoring for year 2007 and 2013. The estimated results are reasonably correlated with the actual ones in term of both quantitative levels and diurnal variations, particularly for the cities in North Thailand.

Emission inventories of anthropogenic and biomass burning emissions for NO_x and CO were derived to investigate the consistency with satellite retrievals. The results illustrate that satellite observations are able to capture high episodes and seasonal variability of the pollutant emissions in some cities. The discrepancies were found probably due to the effect of meteorological conditions or the underestimation of the emissions. Furthermore, the comparisons between satellite retrievals and model simulations were conducted to validate emission inventories used in the models. Generally, simulated model results agree well with those retrieved from satellite measurements for spatial distribution and seasonal pattern. However, the modeled results underestimate satellite data by the factor around 2-5 which are possibly due to the inaccuracy in emission inventories, the inaccuracy of spatial and temporal allocations, and the uncertainties in the satellite retrievals.

The overall results highlight that incorporating satellite retrievals with ground measurements and air quality models can provide useful information for long-term air quality study and can be used as a tool to assess the accuracy of the emission inventories, especially in the limited in situ availability.

Table of Contents

List of Figures

List of Tables

Abbreviations

ACE-FTS	Atmospheric Chemistry Experiment Fourier Transform Spectrometer
AERONET	Aerosol Robotic Network
AIRS	Atmospheric Infrared Sounder
AQM	Air Quality Management
AOD	Aerosol Optical Depth
CEC	Central East China
CF	Cloud Fraction
CH_4	Methane
CMAQ	The Community Multi-scale Air Quality
CO	Carbon Monoxide
CO_2	Carbon Dioxide
EANET	The Acid Deposition Monitoring Network in East Asia
GEOS–Chem	The Goddard Earth Observing System-Chemical Transport Model
GOME	Global Ozone Monitoring Experiment
HCHO	Formaldehyde
HNO_3	Nitric Acid
IASI	Infrared Atmospheric Sounding Interferometer
MACCity	Monitoring Atmospheric Composition & Climate and CityZen
MH	Mixing Height
MISR	Multi-angle Imaging SpectroRadiometer
MODIS	Moderate Resolution Imaging SpectroRadiometer
MOPITT	Measurements Of Pollution In The Troposphere
NAAQS	National Ambient Air Quality Standard (NAAQS)
N	Number of the data
NO_2	Nitrogen Dioxide
NO_x	Nitrogen Oxide
O_3	Ozone
OMI	Ozone Monitoring Instrument

PCD	Pollution Control Department, Thailand
Pb	Lead
PBL	Planetary Boundary Layer
PM	Particulate Matter
REAS	Regional Emission inventory in ASia
RH	Relative Humidity
RMSE	Root-Mean-Square Error
SCIAMACHY	SCanning Imaging Absorption spectroMeter for Atmospheric CartograpHY
SD	Standard Deviation
SEA	Southeast Asia
SO_2	Sulphur Dioxide
T	Temperature
TES	Tropospheric Emission Spectrometer
VOC	Volatile Organic Compound
WHO-AQG	World Health Organization-Air Quality Guidelines
WS	Wind Speed

Chapter 1 Introduction

1.1 Research background

1.1.1 Air pollution problem in Asia

Population growth and economic development are evidently seen as key drivers of environmental change for the past decades. In 2011, the human population reached 7 billion and is expected to reach 10 billion by 2100 with the largest population in the Asia and Oceania region (UNEP 2012). In Asian region, increased economic development with industrialization, motorization, and consequent changes in land use has led to rapid and unplanned urbanization with a large number of people being concentrated in urban areas. However, the air quality management capacity has not been developed at the same pace causing Asian megacities to face more serious air pollution problems than similar cities in developed countries (Kim Oanh 2012). Due to the continuing rise of economic expansion and energy consumption, the level of urban air pollution in Asian developing countries is projected to increase considerably for the next three decades (APMA 2002). In some countries, the use of low quality fuel and inefficient energy production devices in vehicles and industrial facilities, together with the lack of legal frameworks for enforcement are the main causes of releasing large quantities of air pollutants. As a result, air pollutant levels in many large cities of Asian countries have been reported to exceed the World Health Organization-Air Quality Guidelines (WHO-AQG) and the respective National Ambient Air Quality Standard (NAAQS). High anthropogenic emissions of air pollutants in several cities in China affect not only the local and regional but also global atmospheric environment which has aroused global concern (Xing et al. 2011). Nearly 45% of the 522 cities cannot meet the Class II NAAQS of China (Hao et al. 2007). For example, the annual average of $PM_{2.5}$ (particulate matter with the aerodynamic diameter, $d_a < 2.5$ μm) at some locations in Beijing was reported above 100 μg/m^3 which is well higher than the Class II NAAQS of China (35 μg/m^3) and the WHO-AQG (10 μg/m^3) (WHO 2006; Cao 2013; Matsui et al. 2009). For the other cities of developing Asia, the recorded data also show that the levels of PM_{10} (particulate matter with the aerodynamic diameter, $d_a < 10$

μm) normally exceeded the WHO-AQG by the factor of three or more. Figure 1.1 presents 5-year (2000–2004) averaged concentrations of PM_{10} and, also SO_2 and NO_2 in selected Asian cities (WHO-AQG: PM_{10} annual average 20 μg/m^3; SO_2 24-hr average 20 μg/m^3; NO_2 annual average 40 μg/m^3).

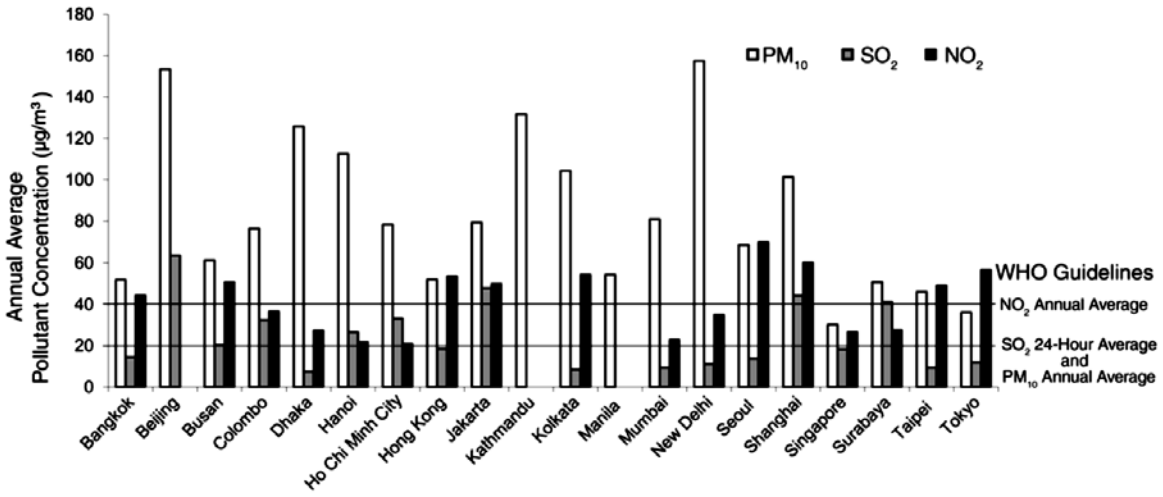

Figure 1.1 Five-year averaged concentrations of PM_{10}, SO_2, and NO_2

Data source: HEI (2010)

The most important air pollutants in Asian developing cities are particulate matter (PM) and ozone (O_3). Other commonly measured pollutants include sulphur dioxide (SO_2), volatile organic compounds (VOCs), lead (Pb), carbon monoxide (CO), carbon dioxide (CO_2) and nitrogen dioxide (NO_2), which vary significantly among cities (APMA 2002; Permadi and Kim Oanh 2008). On the regional scale, intensive emissions from large combustion sources (forest fires and coal/heavy oil-based facilities) with the support of strong convection during monsoons in Asia can introduce the long-range transboundary transport of pollutants, which subsequently lead to multiple effects on regional air temperature, precipitation, agriculture, air quality and human health (Kim Oanh 2012).

1.1.2 Satellite observations on air quality management

The goal of urban air quality management (AQM) is to control and reduce air pollution, and maintain acceptable air quality that avoids adverse effects to human health and welfare (APMA 2002). In order to achieve this air quality goal, it is necessary to develop appropriate air quality policies and strategies. Air quality monitoring, emission inventories, and air pollution modeling are parts of the key components of AQM. Monitoring air pollution is an essential component that provides inputs to AQM and determines population exposure, health impact assessment, and compliance with national and international standards. In general, traditional study of PM and gaseous air pollutants depends on spatial and temporal data series obtained from air quality ground monitoring networks. Such monitoring programs are limited in terms of spatial coverage. Ground-based monitoring stations are clustered in urban areas where there is highly localized population. While they are still scarce in many regions of the world, especially at remote sites where pollutant concentrations can be high due to biomass burning activities, natural emissions, and transport of pollutants from other sources. In this case, ground-based monitors do not provide sufficient tools for tracking and predicting the transport of atmospheric pollutants, whereas air quality is highly variable in space and time. Advancement in Earth observations made by satellite sensors has provided a new area of research for monitoring global air quality, and can be used to better assess the spatial structure of air pollution and interactions on global, regional, and local dispersion patterns when surface measurements are not available (Hadjimitsis 2009). Satellite-based data are provided in term of spatial averages which represent air quality information during satellite overpass time, but ground-based data represent information for a single location as time interval averages. With their own advantages and limitations, integration of these two based measurement complements each other and makes effective tools for AQM to set air quality policies, mitigation plans, and monitoring programs. Reliable emission inventory with adequate spatial and temporal distributions is also an essential component for prioritizing pollution control efforts and for preparing input datasets to air quality models. However, there are large uncertainties in traditional bottom-up emission inventories based on application of large amounts of statistical data (i.e. activity rates and emission factors), which are limited by the lack of continuity. Satellite observations can be

used to assess and improve the accuracy of emission inventories through a top-down approach based on inverse modeling. In term of air quality dispersion modeling, the lack of ground-based data makes it difficult to evaluate such models. For this reason, satellite-based data with global picture of pollutant distribution are necessary to evaluate and establish the model's credibility for future use (Kim Oanh 2012). Satellite remote sensing of trace gases and aerosols has been developed dramatically for air quality applications over an extended period of time. Currently, a global coverage for a wide range of species is retrievable by satellite observations including vertical columns of aerosols, O_3, NO_2, CO, formaldehyde (HCHO), and SO_2 (Martin 2008).

1.2 Research objectives

The overall goals of this study are to apply the use of satellite data as a tool for long-term analysis of atmospheric pollutants, and to develop methodology to validate and improve emission inventories by using integrated satellite observations and model simulations. In order to achieve the goals, two main objectives are set as follows:

1. To investigate the capability of the satellite instruments to observe spatial and temporal variability of atmospheric pollutants (NO_2, CO, and aerosols) over Asian region.
    - 1.1 To investigate the consistency between the satellite products.
    - 1.2 To study the characteristics of spatial distribution, long-term trend, and seasonal variability of atmospheric pollutants observed by satellites.
    - 1.3 To investigate the consistency between surface measurements and satellite observations.
    - 1.4 To improve the relationship between satellite AODs and surface PM concentrations by developing linear regression model with the inclusion of meteorological parameters.

2. To develop methodology using atmospheric pollution information retrieved from satellite observations and those simulated from models in order to validate emission inventories.

2.1 To investigate the consistency between source emissions and satellite observations.

2.2 To investigate the consistency between model outputs and satellite observations.

1.3 Research scope

1. Satellite products in this study focus on (1) NO_2 columns retrieved from GOME, SCIAMACHY, OMI and GOME-2, (2) CO columns retrieved from MOPITT and SCIAMACHY, and (3) AODs retrieved from MODIS-Terra and MODIS-Aqua.
2. The area of study is focused on Asian region, especially for the capital cities of the countries in Southeast Asia, China, and Japan.
3. The period of study is from 1996 to 2012.
4. The emissions inventories used in this study are REAS and MACCity.
5. The models used in this study are GEOS-Chem and CMAQ.

1.4 Research originality

Recent satellite remote sensing has tremendous potential for providing a global picture of air quality that complements ground-based monitoring networks. Although the satellite retrievals of air quality are promising, to date, most of the recent studies that apply satellite observed information for air quality study were conducted in United States, Europe, and some part in Asia such as India, China, Japan, and Korea. However, in order to understand the effects of PM and trace gases on the Earth's climate system and human health, it is necessary to routinely monitor these pollutants on a global basis. Therefore, further studies are needed in other part of the world. Satellite retrieved data are particularly suitable for Asian developing countries with few ground-based monitors, high-level of pollutant emissions in industrial and populated areas, and high potential for long-range transport from biomass burning activities. This study has set the study area in Asian regions by focusing on Southeast Asia (SEA) countries and some parts of China and Japan. Long-term datasets of satellite observations were retrieved for trace gases and aerosols for air quality study over 17 years from 1996 to 2012. Moreover, the analysis in

this study has categorized the study area into different latitude zones in order to investigate the correlation of the spatial and temporal distribution patterns of the pollutants in each latitude zone.

Since satellite measurements are combined with science-based algorithms for retrievals of pollutant concentrations, the accuracy of such algorithms is still less certain whether the models adequately characterize the pollutants in the atmosphere. Thus, it remains a challenge to validate satellite-based data with ground-based data. In this case, mass concentrations of NO_2, CO, and PM_{10} were derived from 15 ground monitoring stations over Thailand in order to correlate with satellite-based data of NO_2 columns (retrieved from GOME, SCIAMACHY, OMI and GOME-2), CO columns (retrieved from MOPITT) and AODs (retrieved from MODIS), respectively. Considering more than one pollutant also enable the determination of source apportionment of the considered pollutants.

Correlation studies with ground-based measurements have found that satellite retrieved AODs can be served as a proxy for PM. However, the relationship between PM and AODs varies by locations and seasons. There are many factors that can influence the correlations such as the uncertainties in satellite retrieved algorithms, meteorological conditions (relative humidity, cloud cover, wind speed, mixing height, etc.), and pollutant types (sulfate, nitrate, carbon, dust, etc.). Long-term data are needed to develop statistical relationships of AODs-PM. This study attempted to improve the relationship between satellite retrieved AODs and ground-level PM_{10} concentrations by developing multiple linear regression models over Thailand using 5-year (2008-2012) data of satellite AODs, cloud cover, relative humidity, wind speed, and temperature. The regression models were then tested to estimate ground-level PM_{10} mass concentrations for the pre and post years (2007, 2013), and finally evaluated with those collected from ground monitoring stations.

Emission inventories of air pollutants are recognized as one of the most important uncertainties in the models. Although several emission inventories have been developed for Asia, uncertainties in these emissions are still large, especially due to the lack of ground observations with sufficient spatial and temporal resolution (Shi et al. 2008). Some studies have investigated the influence of using different emission databases on the

comparison between satellite retrievals and the results from simulated models, however, it has not been well addressed. In this study, the comparisons of long-term derived satellite data along with surface emissions of NO_x and CO were conducted to assess the consistency between these parameters. Furthermore, satellite observed data were examined with the results from simulated models in order to validate the accuracy of input emission inventories.

1.5 Research framework and organization

In order to achieve the above mentioned objectives of this thesis, the research framework is structured in the following manner as shown in Figure 1.2 which includes 13 activities in 9 chapters. First activity is setting objectives and scope of this study providing in chapter 1. Activity 2 is literature review of related information about this study which is provided in chapter 2. Activity 3-9 are set to complete objective 1 of this study. Details of data collection processes and discussions on the results of these activities are provided in chapter 3-6. Activity 10-12 are set to complete objective 2. Discussions on the results are provided in chapter 7-8. The last activity is conclusions and recommendation providing in chapter 9.

Chapter 1 introduces the research background of this thesis about air pollution problem in Asian region and the advantage of satellite retrievals on AQM. Research objectives, scope, originality, and framework and organization are also provided in this chapter.

Chapter 2 concentrates on literature review in which this research stands on. The content includes the previous studies of the applications of satellite remote sensing on air quality study.

Chapter 3 provides the details of satellite data collection and extraction processes, and discusses the results of inter-comparisons between satellite products (1) NO_2 columns (SCIAMACHY vs. GOME/OMI/GOME-2, and OMI vs. GOME-2), (2) CO columns (SCIAMACHY vs. MOPITT), and (3) AODs (MODIS-Terra vs. MODIS-Aqua).

Chapter 4 discusses the results of long-term analysis of satellite observations (NO_2 columns, CO columns, and AODs) in term of spatial distribution, long-term trend, and seasonal variability at different latitude zones during the period of 1996-2012.

Chapter 5 provides the details of ground-level data collection processes, and discusses the results of comparably analysis between satellite-based (NO_2 columns, CO columns, and AODs) and ground-based (NO_2, CO, and PM concentrations) measurements.

Chapter 6 focuses on the processes of improvement the relationship between satellite retrieved AODs and ground-level PM mass concentrations by developing linear regression models with the correction of meteorological parameters. Finally, the regression models were used to estimate surface PM mass concentrations and then compared with those measured from ground monitoring stations.

Chapter 7 provides the details on emission inventories applied in this study, and discusses the results of comparably analysis between retrieved satellite data (NO_2 columns and CO columns) and emission data (NO_x and CO).

Chapter 8 provides the details on model simulations and input data description, and discusses the results of comparably analysis between retrieved satellite data and the output from GEOS-Chem and CMAQ simulations (NO_2 columns and CO columns) which has been performed in order to validate emission inventories.

Chapter 9 concludes the highlights of this research and provides recommendation for future direction.

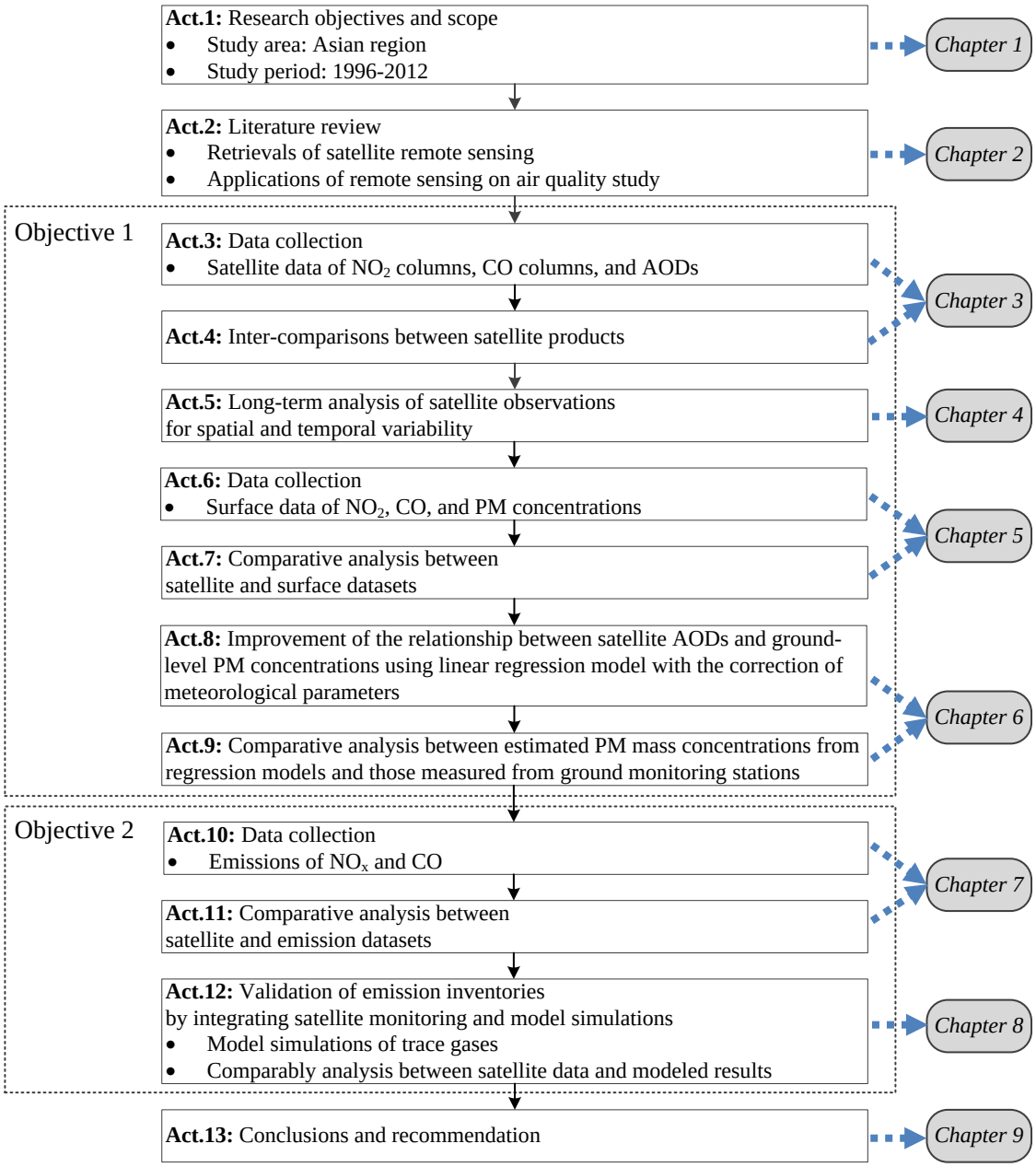

Figure 1.2 Research framework

Chapter 2 Literature Review: Satellite Observations on Air Quality Study

This research considered three atmospheric species retrieved from satellite remote sensing including NO_2, CO, and aerosol. Brief introduction to each species and previous studies are provided below. The basic information on the retrieval of satellite products is provided in Appendix A.

2.1 Nitrogen dioxide

Nitrogen oxide (NO_x=NO+NO_2) is one of the major air pollutants playing a key role in atmospheric chemistry. NO_x emissions have been built up at high concentration over Asia due to rapid economic growth during the past decade (Akimoto 2003; Ohara et al. 2007). The significant sources of NO_x can be distinguished into anthropogenic sources such as fossil fuel combustion and biomass burning, as well as natural sources such as soil emissions and lightning. NO_x can cause a wide variety of human health and environmental impacts due to its various compounds and derivatives in the family. The photolysis of nitrogen dioxide (NO_2) in the troposphere is the major source of O_3 production which is one of the hazardous components. In addition, during daytime NO_2 may react with OH and form nitric acid (HNO_3), the main component of acid precipitation, and also related particles. Nitrate particles and NO_2 can also block the transmission of light, reducing visibility in urban areas and on a regional scale. In term of greenhouse gas, NO_2 contributes significantly to the radiative forcing of climate over urban and industrial areas by perturbing methane (CH_4) and O_3 concentrations which are strong greenhouse gases (Solomon et al. 1999; Velders et al. 2001). Since, the lifetime of NO_2 in the troposphere is relatively short, varying from hours in the continental boundary layer to days in the upper troposphere and its sources and sinks are distributed heterogeneously, therefore, it is necessary to measure the concentration with a broad spectrum of spatial and temporal scales.

Over the past ten years, advances in satellite technology have allowed for observations of NO_2 vertical columns which provide a global picture and useful information for air quality study. Many researches have been studied on tropospheric NO_2 columns since the Global Ozone Monitoring Experiment (GOME) onboard ERS-2 was operated in 1995, followed by the SCanning Imaging Absorption spectroMeter for Atmospheric CartograpHY (SCIAMACHY) onboard ENVISAT in 2002, the Ozone Monitoring Instrument (OMI) onboard EOS-Aura in 2004, and GOME-2 onboard MetOp in 2006. Figure 2.1 shows the image of tropospheric NO_2 columns retrieved from OMI satellite during February 2014. Because of the short lifetime of NO_x in the troposphere, satellite observations of NO_2 are closely correlated to the surface emissions of NO_x (Itahashi et al. 2013). The comparisons between retrieved tropospheric NO_2 columns from satellite observations and in situ measurements have been conducted by many studies. The first validation of tropospheric NO_2 columns retrieved from GOME was performed using in situ NO_2 profiles derived from aircraft on a clear day over Austria (Heland et al. 2002). Martin et al. (2004) evaluated GOME measurements of tropospheric NO_2 columns by comparing with in situ data from aircraft campaigns over eastern Texas and the southeast United States. Blond et al. (2007) investigated the consistency of SCIAMACHY NO_2 observations, NO_2 surface measurements and air quality modeling results over Western Europe. The results of these studies reported reasonably well correlations between satellite and in situ measurements under certain conditions. Richter et al. (2005) reported that based on GOME observations, rapid increasing trend of tropospheric NO_2 columns was founded over Central East China (CEC) approximately 7% per year (1996 – 2002) due to an increase in industry and traffic. van der A et al. (2008) showed significant decreasing trends of NO_2 columns in Europe and parts of eastern United States (up to 7% per year), but a strong increasing trend in Asia, especially in China (up to 29% per year) for the period 1996 – 2006. Furthermore, recent studies have also used satellite products to validate air quality model and to assess the accuracy of the emission inventories. Ma et al. (2006) compared tropospheric NO_2 columns retrieved from GOME satellites with those from regional model simulations using different emission inventories over China. The simulated results show that with all the emission inventories, the model underestimates observed tropospheric NO_2 columns in all the regions in remote and rural areas of China. He et al. (2007) performed a numerical analysis of interannual and seasonal variability of tropospheric NO_2 columns based on a

combination of a regional chemical transport model and satellite observations of GOME and SCIAMCHY over East Asia during 1996 – 2005. Both modeling results and satellite observations reveal a sharp increase of NO_2 columns over CEC after the year 2000. However, the modeling results show that the emission inventories underestimate tropospheric NO_2 columns. The results in this analysis are consistent with other studies over the same region (Lin et al. 2010; Shi et al. 2008; Uno et al. 2007). Han et al. (2011) and Han et al. (2009) investigated NO_x emissions in East Asia by using model-predicted and satellite-derived NO_2 columns from GOME and OMI, respectively. The model-predicted NO_2 columns produce larger values by the factor around 1.46 compared to GOME retrievals and between 1.38-1.87 compared to OMI retrievals over South Korea, whereas the model-predicted results produce smaller values by the factor around 1.57 compared to GOME retrievals over North China. Itahashi et al. (2013) performed trend analysis over East Asia. They found rapid growth of tropospheric NO_2 columns above the CEC region which is beyond double between 2000 and 2010. In contrast, slightly decreasing trends were observed over Japan. Moreover, Irie et al. (2013) and Itahashi et al. (2013) also performed model simulations of NO_2 columns by using the updated REAS inventory version 2.1. The modeled NO_2 columns reasonably produced the annual trends and the absolute values observed by the satellites.

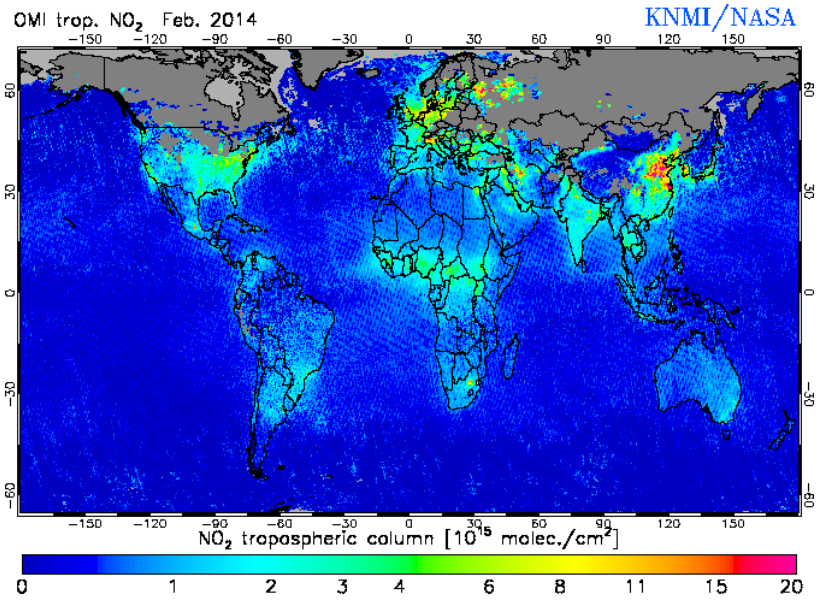

Figure 2.1 Image of tropospheric NO_2 columns retrieved from OMI satellite

Data source: TEMIS (http://www.temis.nl/airpollution/no2.html)

2.2 Carbon monoxide

Carbon monoxide (CO) is another important trace gas in tropospheric photochemical processes that can lead to the formation of tropospheric O_3 in the presence of NO_x and sunlight. It is also the major sink of OH radical which is the cleansing agent of the troposphere and thus controls the oxidative capacity of the atmosphere (Crutzen and Zimmermann 1991; de Laat et al. 2010a). Because it has a lifetime of several weeks to a few months, CO is a good tracer for long-range transport pollution (Shindell et al. 2006). The largest sources of atmospheric CO are incomplete combustion processes, mainly from seasonal biomass burning and fossil fuel combustion (Galanter et al. 2000; Granier et al. 2000). In urban areas, the majority of CO sources are produced as exhausts of internal combustion engines, especially by motor vehicles. For natural emissions, several studies (Bates et al. 1995; Khalil and Rasmussen 1984) report that forest fire emissions account for more than 20% of the total global CO budget. However, the absolute magnitude of individual sources is still uncertain since biomass burning emissions vary seasonally and interannually (van der Werf et al. 2006). Understanding CO sources also places constraints on emissions of other pollutants that are released during combustion process such as PM, VOCs, and a range of toxic gases (Andreae and Merlet 2001; Kopacz et al. 2010).

Long-term datasets of global CO columns have been measured continuously by a number of space-borne sensors including the Measurements Of Pollution In The Troposphere (MOPITT) onboard EOS-Terra in 2000, the Atmospheric Infrared Sounder (AIRS) onboard EOS-Aqua in 2002, SCIAMACHY onboard ENVISAT in 2002, the Atmospheric Chemistry Experiment Fourier Transform Spectrometer (ACE-FTS) onboard SCISAT-1 in 2003, the Tropospheric Emission Spectrometer (TES) onboard EOS-Aura in 2004, and the Infrared Atmospheric Sounding Interferometer (IASI) onboard METOP in 2006. Figure 2.2 shows the image of total CO columns retrieved from MOPITT satellite during February 2014. Several studies have thoroughly evaluated and validated CO measurements from MOPITT satellite using in situ CO vertical profiles measured from aircraft over a variety of geographical regions and in multiple field campaigns (Deeter et al. 2013, 2010, 2007; Emmons et al. 2009, 2007, 2004). Since the MOPITT product is the longest and the most extensively validated satellite dataset for CO observations, many

studies have used the MOPITT product to validate CO retrievals from other satellite products such as AIRS (Warner et al. 2007), TES (Luo et al. 2007), SCIAMACHY (Buchwitz et al. 2007; de Laat et al. 2010b), and ACE-FTS (Clerbaux et al. 2008). Some studies also investigated interannual and seasonal variations of CO columns both over land and ocean (Edwards et al. 2006, 2004; Yurganov et al. 2010, 2008, 2005). Worden et al. (2013) performed an intercomparison of the MOPITT CO product with the AIRS, TES, and IASI products using the available data during the period 2000-2011. The results show that all the products have reasonable agreement in term of seasonal variability and mean total column averages for the Northern Hemisphere. The satellite observations also present the decreasing decadal trends of total columns CO in Europe, Eastern USA, and Eastern China during the study period. de Laat et al. (2006) used a chemistry transport model simulation to evaluate SCIAMACHY CO total columns. The results show that the global distributions of modeled and observed CO columns have similar spatial patterns; a north-south gradient, low CO over mountains, and high CO over emission regions. In term of quantitative comparison, the seasonality of modeled and observed CO columns agrees very well showing that SCIAMACHY CO observations can be used to evaluate CO emission inventories. Gloudemans et al. (2009) investigated five-year interannual variability of CO retrieved from SCIAMACHY during 2003-2007. They presented three highlighted examples. First is the Asian outflow of pollution over northern Pacific. Both chemistry transport model and satellite observations show high levels of CO columns during local winter due to minimum OH concentrations during that time. Moreover, CO peaks revealed in 2005 and 2007 causing by high biomass burning from Southern Asia. The second example is the biomass burning outflow over the Indian Ocean originating from Indonesia. Higher levels of CO were presented in 2006 from both observed and modeled columns comparing to other years. These results coincide with warm phases of El Niño which led to an extended period of biomass burning activities in Indonesia. The third example is biomass burning in Amazonia over an active deforestation during the dry season. The results in these three cases are similar with MOPITT observations and CO emissions. de Laat et al. (2010a) conducted global evaluation of MOPITT and SCIAMACHY CO columns during 2004-2005. They found that both satellites present qualitatively similar seasonality of CO columns. At mid and high latitudes, maximum CO columns occur during local winter and early spring for both Northern and Southern

Hemisphere. For tropical areas, CO columns increase due to the seasonal biomass burning emissions. Recent studies applied inverse modeling to derive quantitative constraints on emissions by using satellite observations. Kopacz et al. (2010, 2009) applied an adjoint inverse modeling method to constrain Asian and global source emissions of CO using retrieved CO columns from MOPITT, AIRS, SCIAMACHY, and TES satellites.

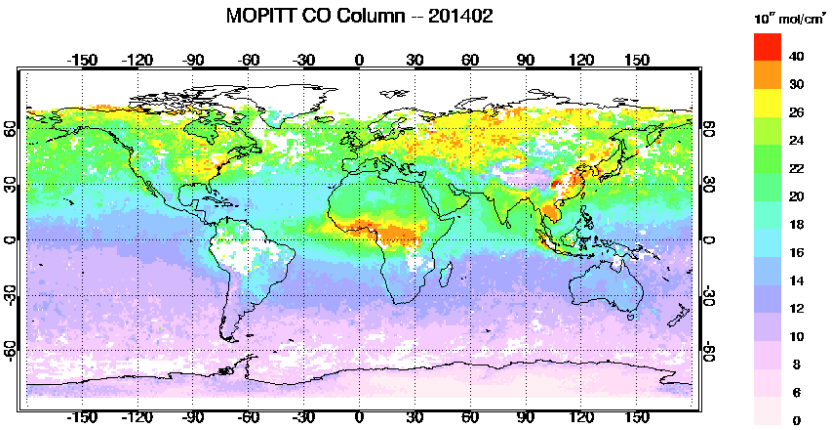

Figure 2.2 Image of total CO columns retrieved from MOPITT V5 TIR/NIR satellite
Data source: NCAR (http://www.acd.ucar.edu/mopitt/visualize.shtml)

2.3 Aerosol

Particulate matter (PM) or aerosol refers to a mixture of solid particles and liquid droplets suspended in the air including dust, dirt, soot and smoke. These particles can be suspended in the air from a few seconds to several months and vary greatly in shape, size, chemical composition and concentration depending on its origin such as geographic location and time. Some particles are primary particles which are emitted directly from both natural and anthropogenic sources. The largest natural sources of particles are volcanoes, wind-blown dust, forest and grassland fires, sea spray, etc. The largest anthropogenic sources are burning biomass for cooking/heating and land clearing, burning of fossil fuel in combustion engines in automobiles and power plants, industrial activities (grinding, crushing, etc.), re-suspended road dust, construction, and waste disposal. Some particles are secondary particles which are formed in the atmosphere by the chemical reactions of emitted gaseous precursors such as SO_2, NO_x, and VOCs. Aerosols can influence the

climate in two different ways. They affect the Earth's radiative balance by scattering and absorbing radiation (the direct effect) and by changing properties of clouds (the indirect effects) (CCSP 2009; Zhang et al. 2005). These direct and indirect aerosol effects are considered to be one of the largest uncertainties in current global climate models for predicting different atmospheric phenomenon. However, aerosols are highly variable spatially and temporally, so these effects and their impact are difficult to measure and assess (Panicker et al. 2010).

Since 1999 NASA has launched a series of satellite sensors which have been used as the inference of ground-level PM concentrations by retrieved Aerosol Optical Depths (AODs). AODs are the integral of the light extinction by aerosol scattering and absorption from the ground up to the top of the atmosphere. AOD measurements are dimensionless ranging from 0 to 4 (typically between 0 to 1). In particular, AODs derived from the Moderate Resolution Imaging SpectroRadiometer (MODIS) onboard EOS-Terra and -Aqua have been used to investigate the correlations with surface PM measurements. Figure 2.3 shows the image of AODs retrieved from MODIS-Terra satellite during March 6, 2014 - March 13, 2014. The validation of satellite aerosol retrievals have been widely conducted through Aerosol Robotic Network (AERONET), which is a worldwide ground-based network of automatic sun photometers and data archive providing spectral AODs as well as aerosol microphysical properties (Holben et al. 1998). Schaap et al. (2008) used AERONET sun photometer to validate MODIS AOD products over Europe, and found a good temporal correlation between these two variables. Retalis et al. (2010) also found that MODIS AOD data are within the expected accuracy comparing with AERONET measurements in Cyprus. Many more studies (Jiang et al. 2007; Mishchenko et al. 2010; Schaap et al. 2008) have used sun photometer in order to support the validation of satellite AOD products.

Using both imagery and statistical analysis from satellite AOD retrievals enable the determination of the regional sources of air pollution events, the general type of pollutants (smoke, haze, dust), the intensity of the events, and their motion (Engel-Cox et al. 2004). Most of the studies have developed empirical relationships between satellite AOD retrievals and surface PM measurements (Chu et al. 2003; Engel-Cox et al. 2006; Engel-

Cox et al. 2004; Liu et al. 2007; Pelletier et al. 2007; Wang and Christopher 2003). Koelemeijer et al. (2006) reported that the relationship between AODs and $PM_{2.5}$ varies with region, generally being higher in the eastern United States than either Europe or the western United States where there is more dust aloft. Gupta et al. (2007) used 4 years of MODIS AODs retrieved from Terra and Aqua satellites to compare with surface $PM_{2.5}$ mass concentrations in Sydney, Australia. The analysis shows that MODIS AODs are able to catch up the peaks of surface $PM_{2.5}$ during bushfire events. High correlations between MODIS AODs and $PM_{2.5}$ are observed when the air quality is in sensitive/unhealthy category indicating that satellite data were valuable for poor air quality conditions. They also found that the uncertainties in MODIS AODs are high for small AODs values. Barladeanu et al. (2012) performed the comparative analysis between in situ measurements of surface PM_{10} concentrations and AODs from satellite retrievals over Romania. They found that the correlation coefficients varied between 0.6-0.9 depending on the type of stations.

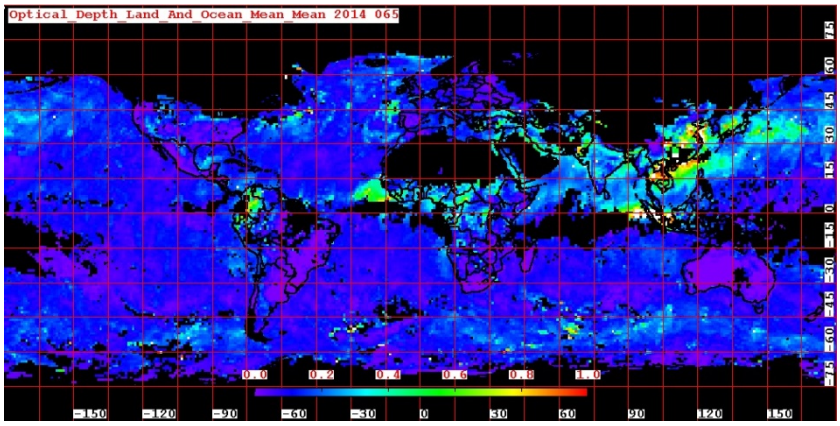

Figure 2.3 Image of AODs retrieved from MODIS-Terra satellite
Data source: LAADS (http://ladsweb.nascom.nasa.gov/)

As mentioned earlier that retrieved AODs are quantitative values measured of the integrated columnar aerosol load from the ground up to the top of the atmosphere, whereas the PM mass concentration is a quantitative measure of the particulate mass concentration at the ground surface (Dinoi et al. 2010). For this reason, the relationship of AODs-PM is expected to be affected by local meteorological conditions, and their correlations may vary

widely in different regions and different seasons. Gupta et al. (2006) examined the relationship between MODIS AODs and ground measurements of $PM_{2.5}$ over different locations across the global urban areas. The analysis shows that AOD-$PM_{2.5}$ relationship strongly depends on meteorological parameters such as ambient relative humidity, cloud cover, and mixing height. Dinoi et al. (2010) developed regression relationship between daily PM_{10} mass concentrations and MODIS AODs during 2006-2008 over Southeastern Italy. Stronger relationships of PM_{10}-AODs are obtained when AODs values are divided by mixing layer height and ground wind speed, and when the analysis is restricted to clear-sky MODIS AODs measurements. Research shows that the AODs-PM correlations also depend on the concurrence in time and location of satellite observations and surface monitoring. For example, Gupta and Christopher (2008) performed an analysis of 7 years MODIS AOD data and ground measurement of $PM_{2.5}$ over Southern United States. The correlation increased from 0.52 to 0.62 when hourly $PM_{2.5}$ data were used instead of daily mean $PM_{2.5}$ data to compare with MODIS AODs. They used three different box sizes of 0.5° × 0.5°, 0.4° × 0.4°, and 0.3° × 0.3° pixels for satellite AOD data around the ground station for the comparison with $PM_{2.5}$. The results show that changing box size produced less than ± 0.03 difference in mean AOD values for 90% of observations. The results in this study are similar with Guo et al. (2009) whose analysis was carried on in Eastern China.

Many more of recent studies derived AODs over Asia using MODIS data for air quality study (Guo et al. 2011; He et al. 2012; Kim et al. 2007; Xin et al. 2011). Kumar et al. (2007) developed an empirical relationship between $PM_{2.5}$ and AODs over Delhi metropolitan and found a significant positive association between these two variables. The analysis shows that a 1% change in AODs explains around 0.52% and 0.39% change in $PM_{2.5}$ monitored within ± 45 minutes and ± 75 minutes of satellite overpass time. Tsai et al. (2011) used ground-based measurements to assess MODIS AODs in Taiwan showing that high correlations between AODs and $PM_{2.5}$ normalized by boundary layer height can be obtained in autumn (~0.88-0.93), while high correlations can be obtained in winter (~0.76-0.87) and spring (~0.77-0.80) by normalized by haze layer height. Sukitpaneenit and Kim Oanh (2014) explored the use of MODIS AODs and MOPITT CO to monitor air pollutants in Northern Thailand during the forest fire episodes. They found the association

between MODIS AODs, MODIS fire hotspots, MOPITT CO, and surface PM_{10} and CO mass concentrations showing that satellite data are useful in monitoring the regional transport of forest fire plumes. Several other satellite sensors also provide AODs products such as OMI and NASA's Multi-angle Imaging SpectroRadiometer (MISR) onboard EOS-Terra satellite.

Chapter 3 Inter-Comparison of Satellite Products

3.1 Satellite data collection

There are 3 types of satellite air pollution monitoring products considered in this study which are NO_2 columns, CO columns, and AODs.

1) NO_2 columns

Long-term data of NO_2 columns (1996-2012) used in this study were retrieved from version 2.3 product of GOME, SCIAMACHY, and GOME-2 sensors, and version 2.0 product of OMI sensor. These satellite products were retrieved by KNMI/NASA (Royal Netherlands Meteorological Institute) for OMI, and by BIRA/IASB (Belgian Institute for Space Astronomy) for GOME, SCIAMACHY, and GOME-2 which can be downloaded from the website of the Tropospheric Emission Monitoring Internet Service (TEMIS) project (http://www.temis.nl).

2) CO columns

Long-term data of CO columns (2000-2012) were retrieved from two satellite products. The first one is retrieved from version 5.0, level-3 product of MOPITT (Thermal Infrared Radiances) sensor which is published through the website of the NASA Langley Research Center (https://eosweb.larc.nasa.gov/project/mopitt/mopitt_table). The second one is retrieved from version 7.4 product of SCIAMACHY (Near Infrared Radiances) sensor which is published through the website of TEMIS project.

3) AODs

Long-term data of AODs (2000-2012) were retrieved from collection 5.1, level-2 aerosol product of MODIS-Terra and MODIS-Aqua sensors. MODIS AOD data were acquired from NASA's Goddard Earth Sciences Distributed Active Archive Center (DAAC) through the website of NASA's Goddard Space Flight Center (GSFC) (http://ladsweb.nascom.nasa.gov/).

The details of all the satellite products applied in this study are summarized in Table 3.1. The satellite data used in this study were retrieved as monthly data for NO_2 columns, CO columns, and AODs, and as daily data for AODs during 1996-2012. Long-term period observations were analyzed in term of both spatial distribution and point-by-point over Asian region. For the latter one, the analysis was focused mostly on the capital cities of the countries in SEA, China, and Japan, and also the cities that produced high emissions. Figure 3.1 presents the map location of the considered areas in this study. Table 3.2 provides more details of latitude and longitude for the selected cities. In case of point-by-point analysis, since the spatial resolutions of each satellite are not equal hence, 0.5° × 0.5° search radius centering at the interested cities was applied for extracting and averaging all satellite pixels that fall within this search radius.

Table 3.1 Data collection of satellite products applied in this study

Parameter	Sensor	Platform	Ground pixel res. (km)	Overpass local time (LT)	Collecting period
NO_2 columns (10^{15} molecules/cm^2)	GOME	ERS-2	320 × 40	10:30	1996-2003
	SCIAMACHY	ENVISAT	60 × 30	10:00	2002-2012
	OMI	Aura	24 × 13	13:45	2004-2012
	GOME-2	MetOp	80 × 40	9:30	2007-2012
CO columns (10^{18} molecules/cm^2)	MOPITT	Terra	22 × 22	10:30	2000-2012
	SCIAMACHY	ENVISAT	120 × 30	10:30	2003-2008
AODs	MODIS	Terra	10 × 10	10:30	2000-2012
	MODIS	Aqua	10 × 10	13:30	2002-2012

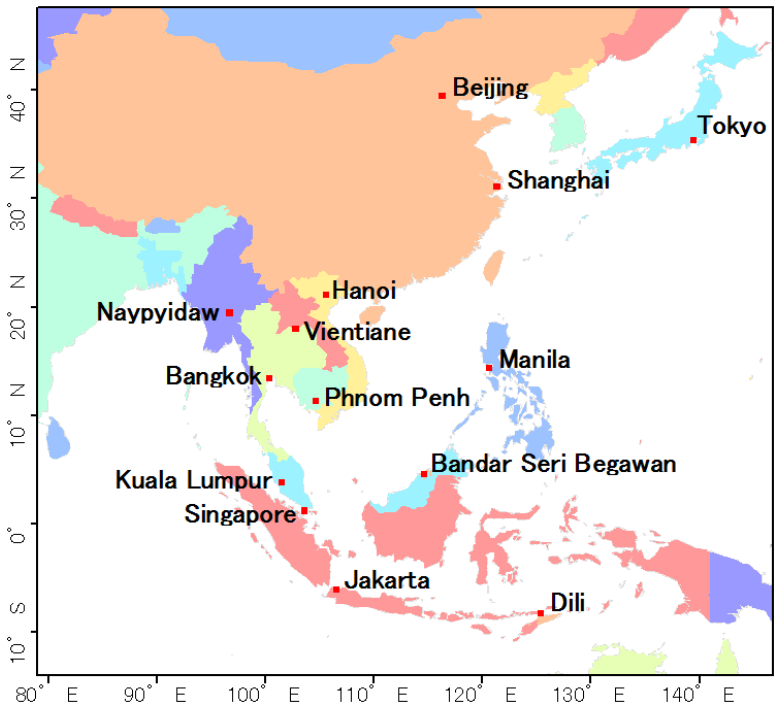

Figure 3.1 Map locations of the cities considered in this study

Table 3.2 Latitude and longitude of the cities considered in this study

Country	City	Latitude	Longitude
China	Beijing	39.54° N	116.24° E
China	Shanghai	31.13° N	121.28° E
Japan	Tokyo	35.41° N	139.41° E
Vietnam	Hanoi	21.01° N	105.51° E
Burma	Naypyidaw	19.45° N	96.06° E
Laos	Vientiane	17.57° N	102.36° E
Philippines	Manila	14.35° N	120.59° E
Thailand	Bangkok	13.43° N	100.28° E
Cambodia	Phnom Penh	11.33° N	104.55° E
Brunei	Bandar Seri Begawan	4.53° N	114.56° E
Malaysia	Kuala Lumpur	3.08° N	101.41° E
Singapore	Singapore	1.17° N	103.50° E
Indonesia	Jakarta	6.12° S	106.50° E
East Timor	Dili	8.33° S	125.34° E

3.2 Satellite products of NO_2

Since this study adopted several satellite products to perform long-term analysis of the pollutants, the consistency between the satellite products were then investigated. Different satellite datasets were compared using the concurrent time periods and point locations. Fourteen cities including capital cities of the countries in SEA and some cities in Japan and China were chosen to retrieve monthly tropospheric NO_2 columns data from GOME, SCIAMACHY, OMI, and GOME-2. Scatter plots of monthly mean tropospheric NO_2 columns from four satellites at all the interested cities and linear regression were applied for identifying a relationship between each satellite. In this case, SCIAMACHY datasets are used as reference since their measurements have the overlap time period with other satellite observations (GOME, OMI and GOME-2). Figure 3.2 shows the comparisons of GOME, OMI, and GOME-2 versus SCIAMACHY, and OMI versus GOME-2. All the satellite inter-comparisons show good agreements with the correlation coefficients larger than 0.85. The relationship between GOME-2 and SCIAMACHY gives the highest correlation coefficients of 0.91. For the correlation of GOME and SCIAMACHY, the correlation coefficient is 0.87. The main reason for a good consistency is due to their similar overpass time (GOME-2: 09:30LT, SCIAMACHY: 10:00LT, GOME: 10:30LT). However, the levels of tropospheric NO_2 columns from GOME-2 and GOME measurements are also lower than those from SCIAMACHY (with the ratio of NO_2 columns from GOME-2 to SCIAMACHY of 0.64, and GOME to SCIAMACHY of 0.62). This is owing to the lower resolutions of GOME-2 (GOME-2: 80 × 40 km^2) and GOME (GOME: 320 × 40 km^2) compared to SCIAMACHY (SCIAMACHY: 60 × 30 km^2) instrument that smooth out the concentrations of the pollutant from the local emissions which in this case focused in urban locations. Since the comparisons in this case were considered at 0.5° × 0.5° grid size, in order to confirm the effect of the difference between satellite horizontal resolutions, further comparative analysis between GOME and SCIAMACHY satellites at 3.0° × 0.5° grid size covering the GOME pixel was performed and presented in Figure 3.3. The result shows that GOME NO_2 levels were still lower than SCIAMACHY NO_2 levels, but the ratio of NO_2 columns from GOME to SCIAMACHY increased to 0.84 (from 0.62 at 0.5° × 0.5° grid size). This result highlights that the coarser resolution of GOME instrument did smooth out the pollutant concentrations in the urban

area. For OMI and SCIAMACHY, they also show good correlation with the correlation coefficient of 0.88. Even though, OMI and SCIAMACHY have a difference in spatial coverage but both of them have fine resolutions (OMI: 13 x 24 km^2) that are able to reveal the characteristic of urban and industrial scales as mentioned in Zyrichidou et al. (2009). Thus, the main reason of the discrepancy in this case is due to the difference in the local equator crossing time (OMI: 13:45LT). The inter-comparison of OMI and SCIAMACHY indicates that OMI has lower measurements of tropospheric NO_2 columns compared with SCIAMACHY (with the ratio of NO_2 columns from OMI to SCIAMACHY of 0.55). Since during rush hour in the morning, tropospheric NO_2 is significantly produced from the transportation especially in urban area, then the measurement of SCIAMACHY during this period is subsequently high. On the other hand, in the afternoon the photolysis rate is higher than in the morning causing the loss of NO_2 and resulting in the low measurement of tropospheric NO_2 during the overpass time of OMI instrument. The comparison between OMI and GOME-2 also provides good correlation with the correlation coefficient of 0.90. This is because both of them are the new generation of space borne measurements with high spatial resolutions. The levels of tropospheric NO_2 columns retrieved from OMI also appear to be smaller than those retrieved from GOME-2 (with the ratio of NO_2 columns from OMI to GOME-2 of 0.66) due to the same reason with the comparison with SCIAMACHY. In addition, difference in algorithms for the retrieval of pollutant information and the effects of instrument noise errors are also the reasons for the discrepancy. Table 3.3 summarizes the correlation coefficients of the inter-comparison between satellite products for each cities considered in this study.

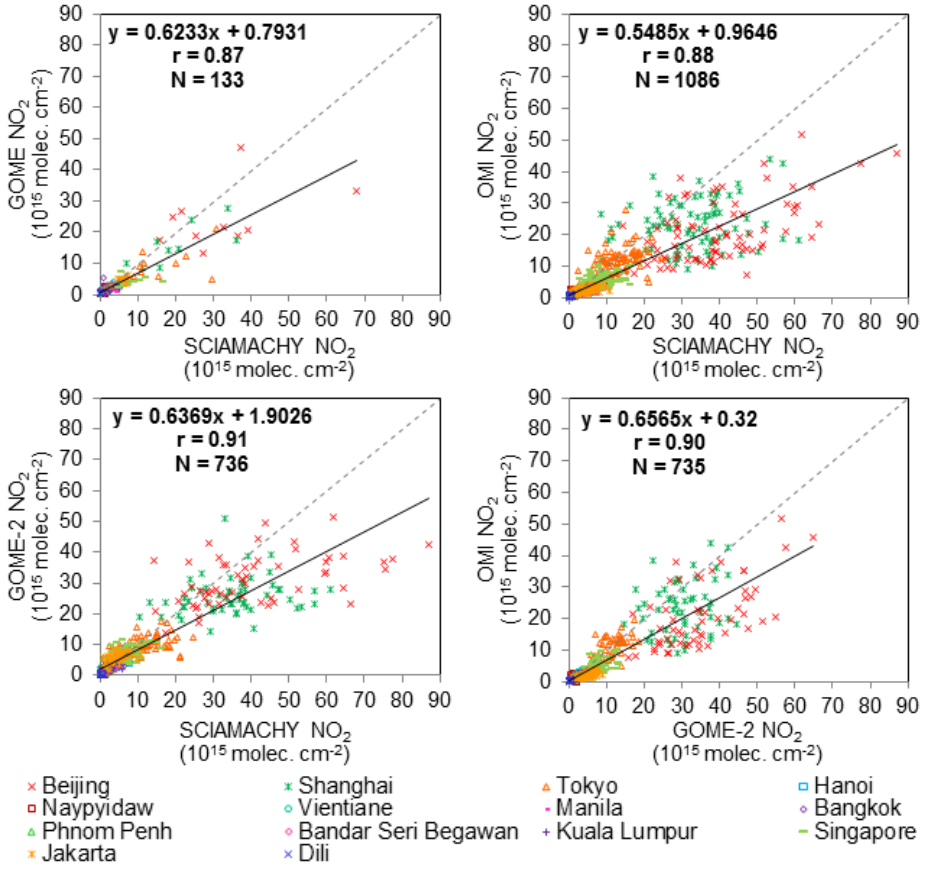

Figure 3.2 Satellite product inter-comparison of monthly tropospheric NO_2 columns at 0.5° × 0.5° grid size

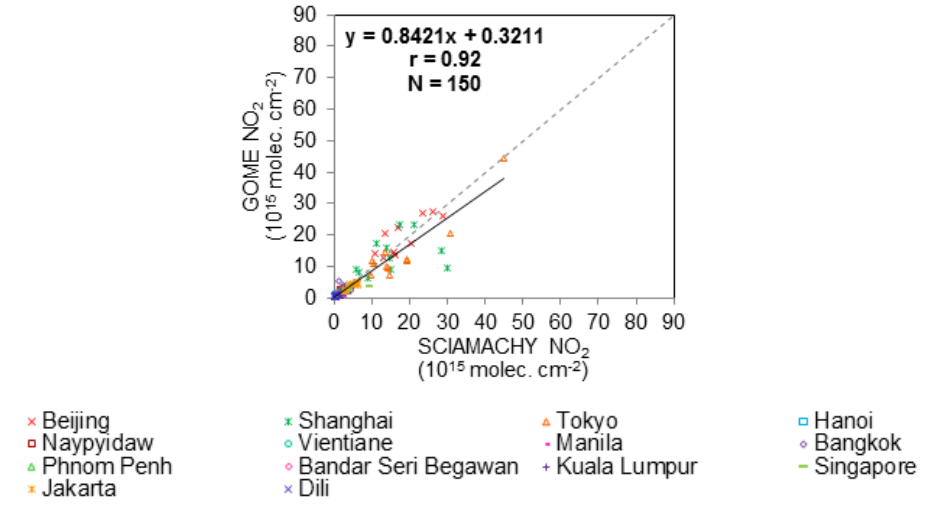

Figure 3.3 GOME versus SCIAMACHY inter-comparison of monthly tropospheric NO_2 columns at 3.0° × 0.5° grid size

Table 3.3 Summary of correlation coefficients (r) of inter-comparison between satellite products

r / City	NO_2				CO	AOD
	GOME vs. SCIMACHY (2002-2003)	OMI vs. SCIMACHY (2004-2012)	GOME-2 vs. SCIMACHY (2007-2012)	GOME-2 vs. OMI (2007-2012)	MOPITT vs. SCIMACHY (2003-2008)	MODIS-Terra vs. -Aqua (2002-2012)
Beijing	0.43	0.44	0.40	0.51	0.57	0.93
Shanghai	0.49	0.21	0.24	0.28	0.39	0.80
Tokyo	0.40	0.42	0.36	0.58	0.39	0.93
Hanoi	0.53	0.58	0.60	0.32	0.36	0.87
Naypyidaw	0.21	0.60	0.52	0.55	0.55	0.82
Vientiane	0.88	0.79	0.66	0.75	0.72	0.87
Manila	0.18	0.17	0.19	0.52	0.36	0.73
Bangkok	0.81	0.85	0.86	0.89	0.65	0.81
Phnom Penh	0.90	0.60	0.68	0.62	0.56	0.80
Bandar Seri Begawan	0.50	0.30	0.48	0.29	0.35	0.77
Kuala Lumpur	0.92	0.54	0.45	0.57	0.46	0.89
Singapore	0.70	0.33	0.42	0.19	0.32	0.74
Jakarta	0.84	0.59	0.56	0.66	0.52	0.83
Dili	0.43	0.42	0.41	0.60	0.36	0.78
All cities	0.87	0.88	0.91	0.90	0.58	0.92

Figure 3.4 gives long-term time series of tropospheric NO_2 columns retrieved from different satellite instruments, i.e., GOME (1996-2003), SCIAMACHY (2002-2012), OMI (2004-2012), and GOME-2 (2007-2012) for several interested cities such as Shanghai, Bangkok, and Jakarta during the period 1996-2012. For the other cities, the time series are provided in Appendix B.1. Figure 3.4 shows that each satellite is generally in agreement with each other, especially in term of seasonal variability. Observed data from OMI (the green triangle symbol) provide the clearest seasonal cycle. This is due to the finest resolution of OMI instrument compared with other instruments as mentioned earlier. Moreover, during the period of OMI operating time, OMI data also present the lowest levels of NO_2 columns since OMI overpass time is in the afternoon.

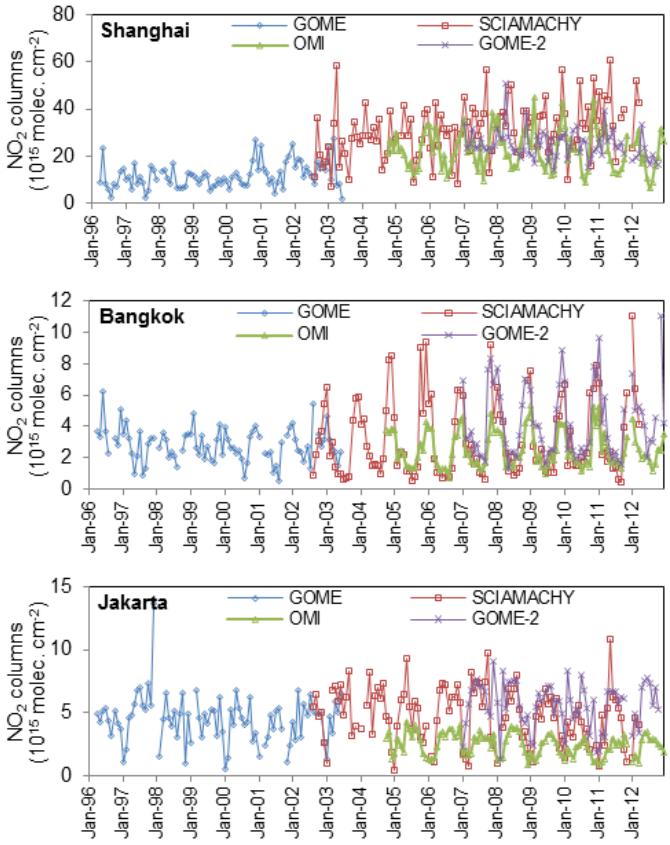

Figure 3.4 Time series of tropospheric NO_2 columns for Shanghai, Bangkok, and Jakarta

3.3 Satellite products of CO

The inter-comparison of satellite products of CO columns was examined for MOPITT and SCIAMACHY instruments. The datasets of monthly mean total CO columns were collected at all the cities considered in this study in order to investigate the consistency between these two satellites by using scatter plot and linear regression. Figure 3.5 shows that the correlation coefficient of CO columns retrieved from MOPITT and SCIAMACHY during 2003-2008 for all the cities is around 0.58. Correlation coefficients for each city are provided in Table 3.3. The reason for the large discrepancy between these two satellites is first due to the difference in spatial resolutions (SCIAMACHY: 120 × 30 km^2, MOPITT: 22 × 22 km^2). Secondly, MOPITT obtains CO information from the thermal infrared (TIR) band near 4.7 μm, whereas SCIAMACHY obtains from the short-wave infrared (SWIR) band near 2.3 μm. The advantage of the SWIR measurement is that it is sensitive to the entire troposphere while the TIR MOPITT instrument is mostly sensitive to the middle and upper troposphere. However, information in the lower troposphere can be derived from TIR measurement where there is sufficient temperature contrast between surface and free troposphere, especially during daytime observations over land. The advantage of the TIR measurement is that the instrument of noise error is generally less that 20% whereas the error of SWIR measurement can be larger (10-100%). Additional reason making the discrepancy between MOPITT and SCIAMACHY measurements is that SCIAMACHY provides CO information only above the clouds causing the missing columns below the clouds, but MOPITT provides only cloud-free data (de Laat et al. 2010a; de Laat et al. 2006; Worden et al. 2013). Figure 3.6 presents time series of total CO columns retrieved from MOPITT (2000-2012) and SCIAMACHY (2003-2008) instruments for several cities. From the graphs, both MOPITT and SCIAMACHY are able to observe the seasonal variation of CO columns. However, MOPITT provides clearer seasonal cycle lines due to the better spatial resolution. For this reason, the next analysis considered only the CO columns retrieved from MOPITT satellite. The long-term time series of CO columns for the other cities are provided in Appendix B.2.

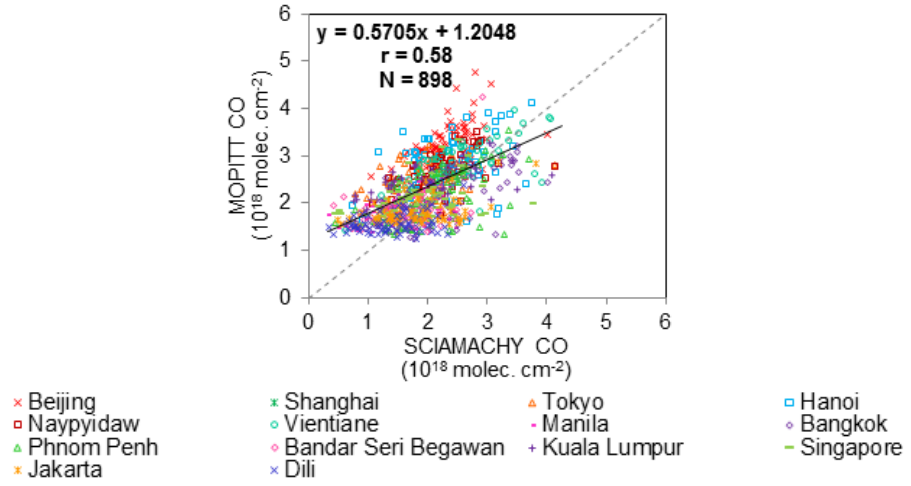

Figure 3.5 Satellite product inter-comparison of monthly total CO columns at 0.5° × 0.5° grid size

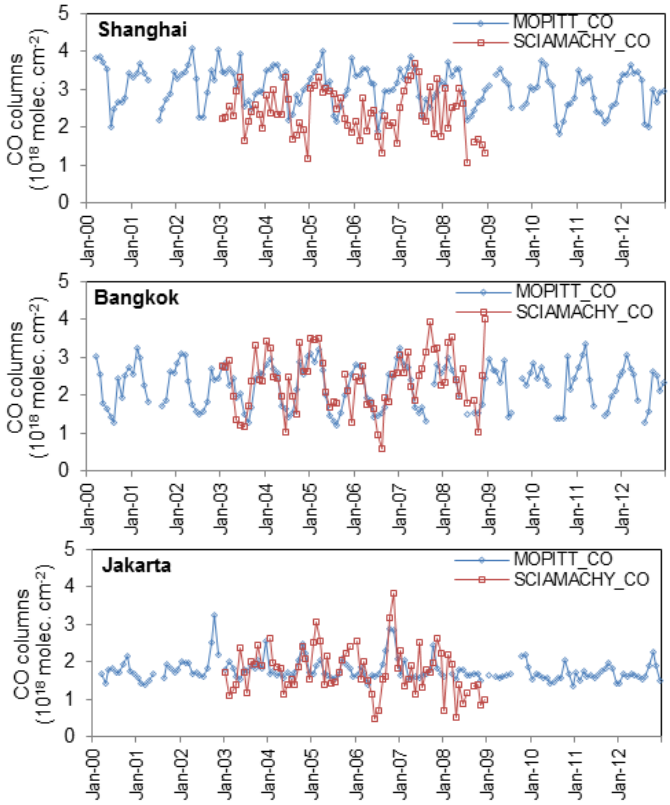

Figure 3.6 Time series of total CO columns for Shanghai, Bangkok, and Jakarta

3.4 Satellite products of AOD

The comparison of the satellite AOD products between MODIS-Terra and MODIS-Aqua satellites was performed during the period of 2002-2012 by collecting monthly averaged AOD data from all the interested cities. Figure 3.7 shows the scatter plot of AODs retrieved from MODIS-Terra and MODIS-Aqua. The regression analysis reveals good agreement for these two satellites with the correlation coefficient around 0.92. The correlation coefficients for each city are summarized in Table 3.3. From Table 3.3, the analysis for each city shows good correlation with the correlation coefficients larger than 0.73. The discrepancy between these two measurements is due to the difference in satellite overpass time, typically around 10:30LT for Terra and 13:30LT for Aqua. Figure 3.8 gives examples of long-term time series for AODs retrieved from MODIS-Terra (2000-2012) and MODIS-Aqua (2002-2012) for several interested cities. Based on this analysis, MODIS-Terra and MODIS-Aqua present no very significant difference. Both satellite measurements are able to observe clear seasonal variation with the similar monthly mean magnitudes of AODs varying from region to region. These results are similar with Wang et al. (2010) concluding that there was no significantly consistent negative or positive bias between Terra and Aqua AODs, though there may be a diurnal cycle near aerosol emission regions. Appendix B.3 presents more time series of AODs for the other interested cities. More details of daily AODs analysis between these two measurements are provided in Chapter 6.

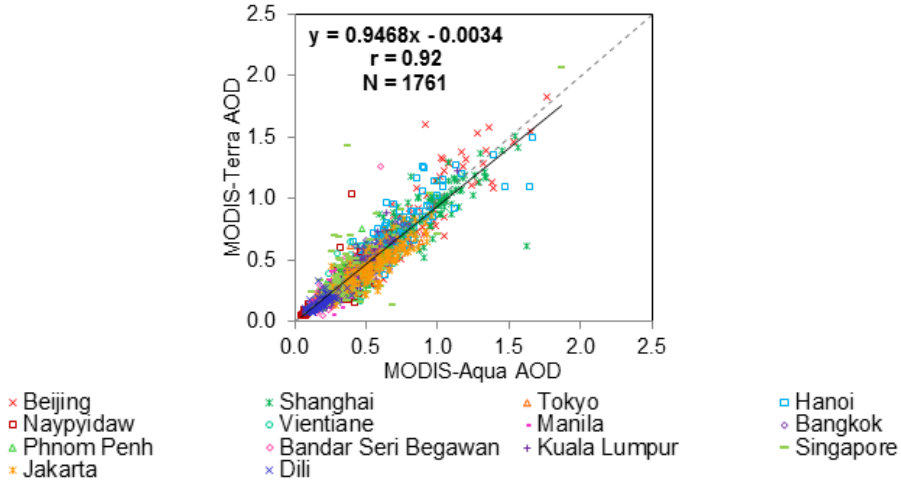

Figure 3.7 Satellite product inter-comparison of monthly AODs at 0.5° × 0.5° grid size

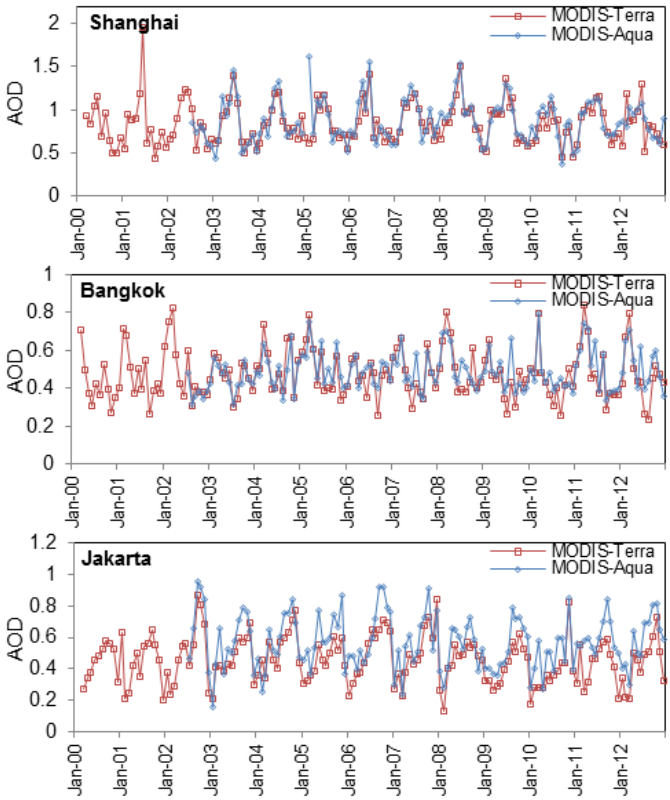

Figure 3.8 Time series of AODs for Shanghai, Bangkok, and Jakarta

Chapter 4 Long-Term Analysis for Gaseous Air Pollutants and Particulate Matter over Asia

4.1 Long-term trend of atmospheric pollutants retrieved from satellites

Since the first objective of this study is to investigate the capability of the satellite instruments to observe spatial and temporal variability of atmospheric pollutants such as NO_2, CO and aerosols over Asian region, long-term data of tropospheric NO_2 columns (retrieved from GOME, SCIAMACHY, OMI, and GOME-2), total CO columns (retrieved from MOPITT), and AODs (retrieved from MODIS-Terra) were collected to investigate the spatial distribution and annual trend of these pollutants during the period 1996 – 2012.

4.1.1 Long-term trend of NO_2 columns

For long-term analysis of NO_2 columns, Figure 4.1a shows the spatial distributions of yearly averaged tropospheric NO_2 columns over Asia for year 1996 (GOME), 2001 (GOME), 2005 (SCIAMACHY), and 2010 (SCIAMACHY), respectively. As illustrated in Figure 4.1a, significant increasing levels of tropospheric NO_2 columns can be clearly observed from year 1996 to 2010, especially above eastern part of Chinese regions. China is one of the world's fastest growing economies today. The enhancement of economic activities associates with large populated cities, large industrial areas, and large thermal power plants based on coal combustion (van der A et al. 2006; Ghude et al. 2009, 2008). These activities are the major sources of NO_x emissions which are contributed mainly from industrial and transportation sectors (Streets et al. 2003). Figure 4.1a also depicts other hotspot cities of tropospheric NO_2 over East Asia and SEA, such as Seoul, Tokyo, Taipei, Hong Kong, Hanoi, Bangkok, Singapore and Jakarta. Figure 4.1b presents the spatial distribution of long-term increasing trends (% per 16 years) of tropospheric NO_2 columns during the period 1996 - 2012. The monthly data of GOME product during 1996-2002, SCIAMACHY product during 2003-2011, and GOME-2 product during 2012 were used to calculate the linear trend of NO_2 columns. Since the absolute values of GOME and

GOME-2 are lower than SCIAMACHY as presented in the previous chapter (Chapter 3.2), the GOME and GOME-2 data were adjusted to be comparable with SCIAMACHY data by using regression equations in Figure 3.2. Sharp positive trends can be observed over East China. The results in this case are similar with van der A et al. (2008) reporting that a large positive trend of tropospheric NO_2 observed by GOME and SCIAMACHY during 1996 – 2006 is clearly visible in East China especially in the megacities as Beijing (~11% per year) and Shanghai (~29% per year). He et al. (2007) also found a sharp increase of tropospheric NO_2 columns over Beijing in order of 23.1 % per year (reference year 2000) by using GOME and SCIAMACHY measurements from 2000 to 2005. The long-term time series of tropospheric NO_2 columns plotted in Figure 3.3 (Chapter 3) also demonstrate that NO_2 columns retrieved from GOME, SCIAMACHY, OMI, and GOME-2 satellites have built up at high levels during 1996-2012 over Shanghai.

More analysis has focused on the capital cities of the countries in SEA and also some cities in Japan and China by using satellite data retrieved from GOME, SCIAMACHY, and GOME-2 in order to examine the increasing trend of tropospheric NO_2 columns over these cities along the study period. It should be noted that the calculation of the percent increase in this case only based on GOME, SHIAMACHY and GOME-2 satellites since OMI observation has a different local equator crossing time (13:00-14:00) from other observations (09:30-10:30) which may pull down the trend due to the reducing levels of NO_2 in the afternoon. Table 4.1 summarizes the mean values and the trends of tropospheric NO_2 columns during the period of 1996-2012 for the selected 14 cities. As presented in Table 4.1, the trends of tropospheric NO_2 columns for some cities are not quite clear whether they were increasing or decreasing during 1996 - 2012. However, for China, Shanghai and Beijing cities have the highest percent increasing trends with the percent increase around 10.9 and 7.3 % per year (ref. year 1996) implying an approximate 174.5 and 117.3 % increase within 16 years, respectively. For SEA, the cities that give high increasing trend are Hanoi, Singapore, and Kuala Lumpur with the percent increase per 16 years of 121.1, 105.6 and 77.4, respectively. Moreover, the results in Table 4.1 also show that Beijing has the highest mean value of tropospheric NO_2 columns during the period 1996 – 2012 with the average concentration of 33.7×10^{15} molecules/cm^2, followed

by Shanghai and Tokyo with the average concentration of 27.5×10^{15} and 16.0×10^{15} molecules/cm^2, respectively.

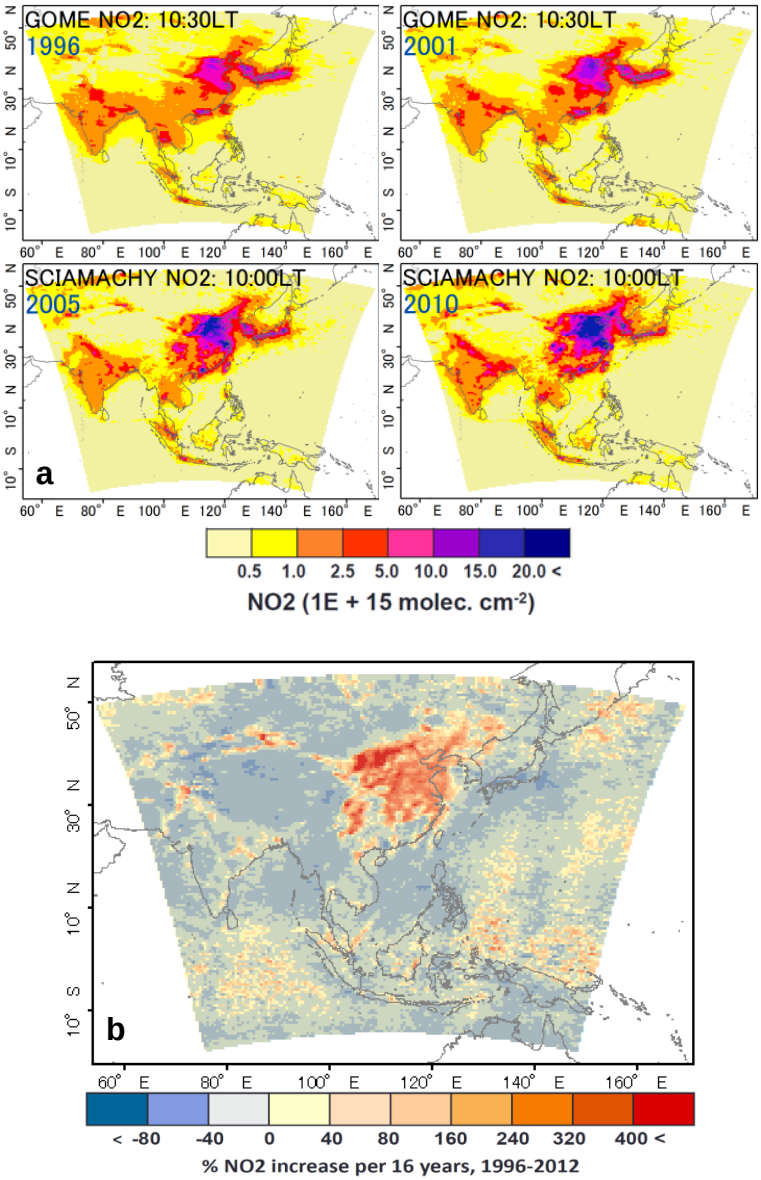

Figure 4.1 Spatial distributions of tropospheric NO_2 columns retrieved from GOME and SCIAMACHY (a), and Spatial distribution of percent increasing trend per 16 years of tropospheric NO_2 columns (b)

Table 4.1 Mean values and standard deviations of tropospheric NO_2 columns during 1996-2012, and rate of increase (%)

Country	City	Mean 10^{15}molecules/cm^2 (1996-2012)	s.d. (1996-2012)	Mean 10^{15}molecules/cm^2 (Ref. 1996)	% increase 16yr^{-1}	%increase yr^{-1}
China	Beijing	33.74	14.65	21.50	117.33	7.33
China	Shanghai	27.47	11.88	13.84	174.54	10.91
Japan	Tokyo	16.01	6.85	17.13	-26.20	-1.64
Vietnam	Hanoi	3.34	1.34	2.02	121.08	7.57
Burma	Naypyidaw	1.63	0.97	2.22	-58.15	-3.63
Laos	Vientiane	2.36	1.24	2.84	-38.05	-2.38
Philippines	Manila	3.29	1.04	3.74	-13.76	-0.86
Thailand	Bangkok	4.13	2.07	3.93	18.94	1.18
Cambodia	Phnom Penh	1.55	0.67	1.25	47.52	2.97
Brunei	Bandar Seri Begawan	1.05	0.57	0.87	34.62	2.16
Malaysia	Kuala Lumpur	2.68	1.07	2.03	77.38	4.84
Singapore	Singapore	7.96	3.16	5.11	105.58	6.60
Indonesia	Jakarta	5.94	2.41	6.63	-9.69	-0.61
East Timor	Dili	0.57	0.30	0.54	-27.92	-1.75

Figure 4.2a and Figure 4.2b present the available data of coal and petroleum consumptions for some countries in this study area. In China, coal consumption has increased from ~ 1470 million short tons in 1996 to ~ 3830 million short tons in 2011, which is around 250% increase within 15 years. For the countries in SEA such as Singapore, Burma, Malaysia, Indonesia and Vietnam, the positive trend of coal consumption have been observed to increase by approximately 2000, 840, 710, 600 and 470% over 15 years during 1996 – 2011, respectively. Even through these countries have higher increasing trend of coal consumption compared to China, the total amount of coal consumption in China still tremendously larger than other countries in East Asia and SEA. Furthermore, China also has the highest increasing trend (190% per 15 years) and total amount of petroleum consumption (9.8 million barrels per day, 2011) compared to others countries. This implies that China is the main contributor of NO_x emissions over these regions as reflected in the spatial distributions of tropospheric NO_2 columns in Figure 4.1a.

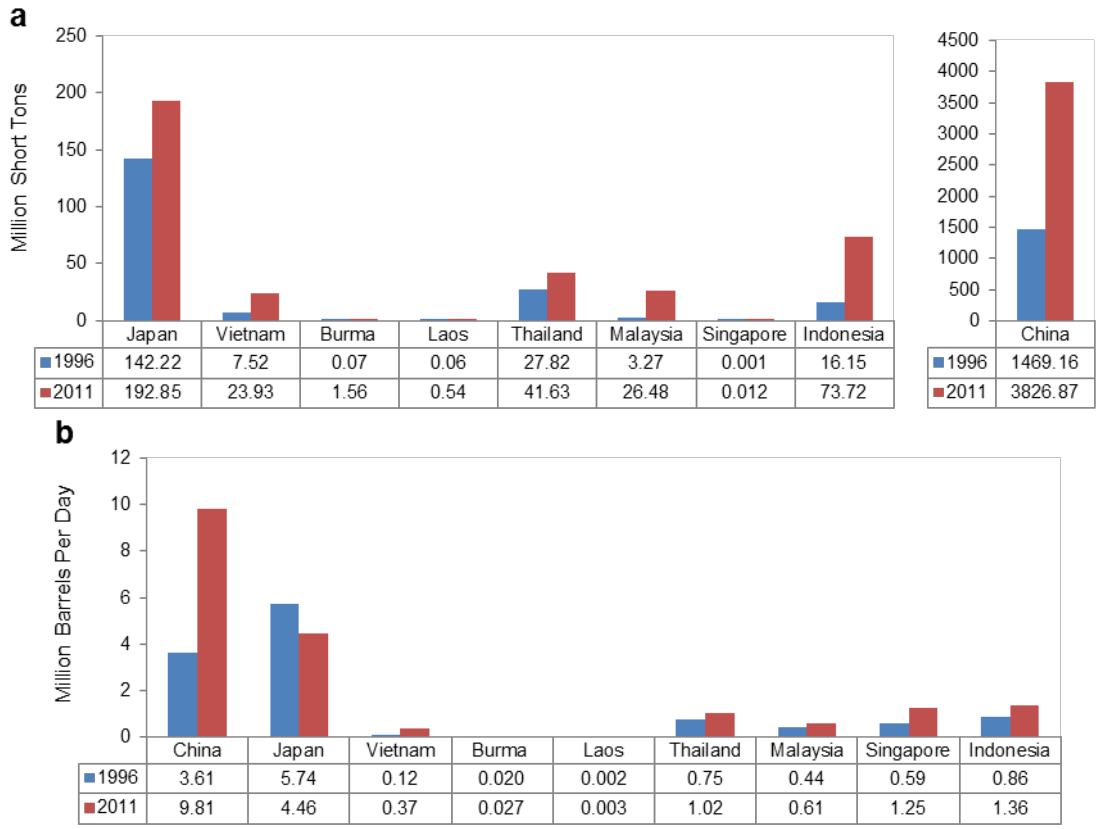

	Japan	Vietnam	Burma	Laos	Thailand	Malaysia	Singapore	Indonesia
1996	142.22	7.52	0.07	0.06	27.82	3.27	0.001	16.15
2011	192.85	23.93	1.56	0.54	41.63	26.48	0.012	73.72

	China
1996	1469.16
2011	3826.87

	China	Japan	Vietnam	Burma	Laos	Thailand	Malaysia	Singapore	Indonesia
1996	3.61	5.74	0.12	0.020	0.002	0.75	0.44	0.59	0.86
2011	9.81	4.46	0.37	0.027	0.003	1.02	0.61	1.25	1.36

Figure 4.2 Total coal (a) and petroleum (b) consumptions over selected countries

Data source: EIA (U.S. Energy Information Administration)

4.1.2 Long-term trend of CO columns

Figure 4.3a presents the spatial distribution of CO columns retrieved from MOPITT satellite for year 2001, 2005, and 2010. Chinese regions, especially in CEC, have the highest abundance of CO columns compared to other regions in Asia. Figure 4.3b illustrates the spatial distribution of long-term trends (% per 12 years) of CO columns during the period 2000-2012.

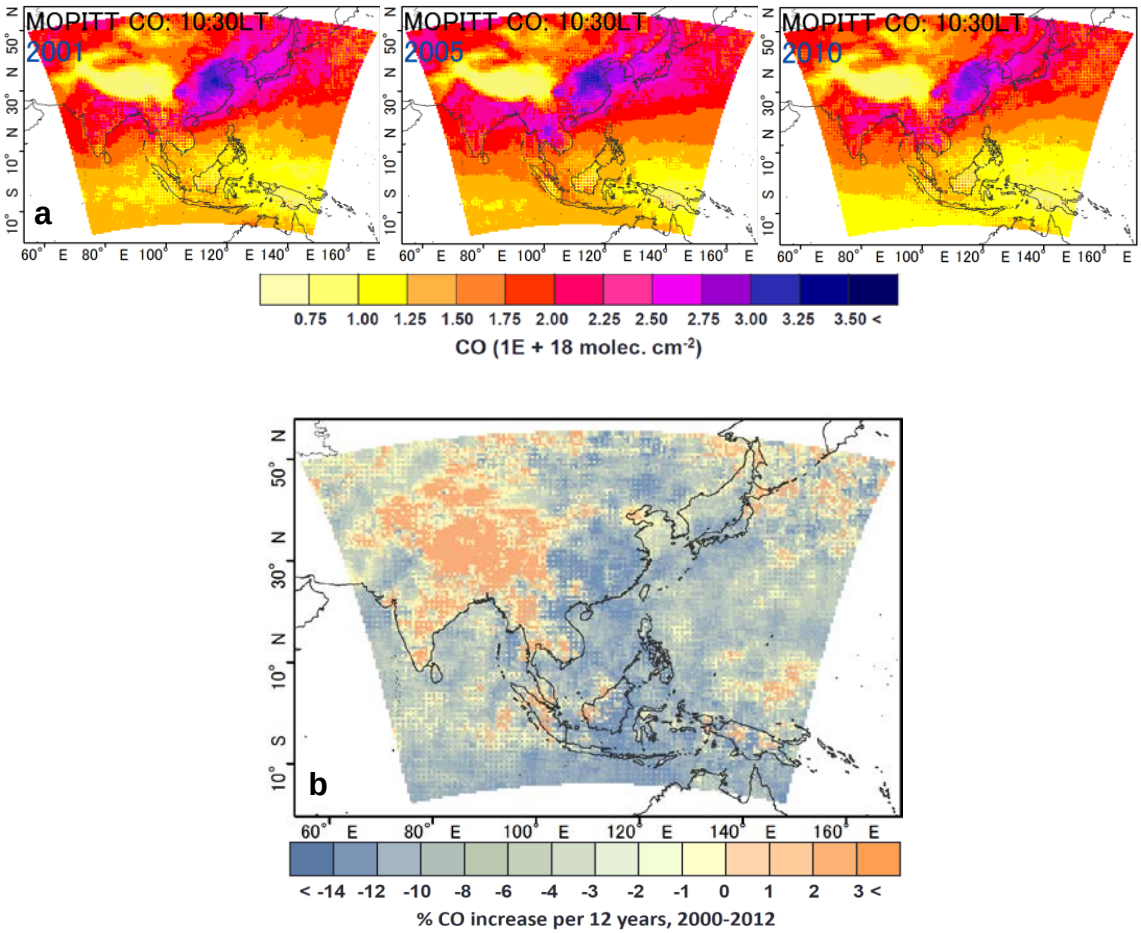

Figure 4.3 Spatial distributions of total CO columns retrieved from MOPITT (a), and Spatial distribution of percent increasing trend per 12 years of total CO columns (b)

The long-term trend of MOPITT CO columns during this period is quite constant, most of the areas show slightly decreasing trend with the mean value around -5.5% per 12 years. However, the spatial distribution in year 2005 illustrates that CO columns are higher than in other years, especially in the regions of Indonesia and Malaysia. This is due to the effect of warm phase El Niño that extends dry season during this year and led to an increase in biomass burning period (Gloudemans et al. 2009). There are also other detected hotspots of CO columns in SEA such as in Northern part of Thailand, Burma and Laos where biomass burning is the key activities in this area.

4.1.3 Long-term trend of AODs

In term of aerosol loads, Figure 4.4a presents the spatial distribution of AODs retrieved from MODIS-Terra satellite for year 2001, 2005 and 2010. The spatial distribution of AODs reveals the largest amount of AODs over CEC and some parts of Indian regions. Similar with the case of CO columns, several hotspots of AODs are also detected by the satellite over the same areas in SEA due to the high emissions from biomass burning. Furthermore, higher level of AODs can be observed over the region of Indonesia in 2005 compared with other years owing to the warm phase El Niño. The similar spatial distribution of CO columns and AODs indicates that satellite instruments are capable to observe surface emissions and can be used to study air quality; especially in this case during biomass burning period. Figure 4.4b illustrates the spatial distribution of long-term trends (% per 12 years) of AODs during the year 2000-2012. There is no significant increasing trend of AODs during this period. Most of the areas reveal slightly decreasing trend with the mean value around -6.5% per 12 years. Some studies over United States (Gupta and Christopher 2008b, 2008a) also indicate that air quality has improved from 2000 to 2006 according to the observation of AODs. However, AODs loads vary significantly across space and time depending on various sources, meteorological conditions, as well as long-range transboundary transport.

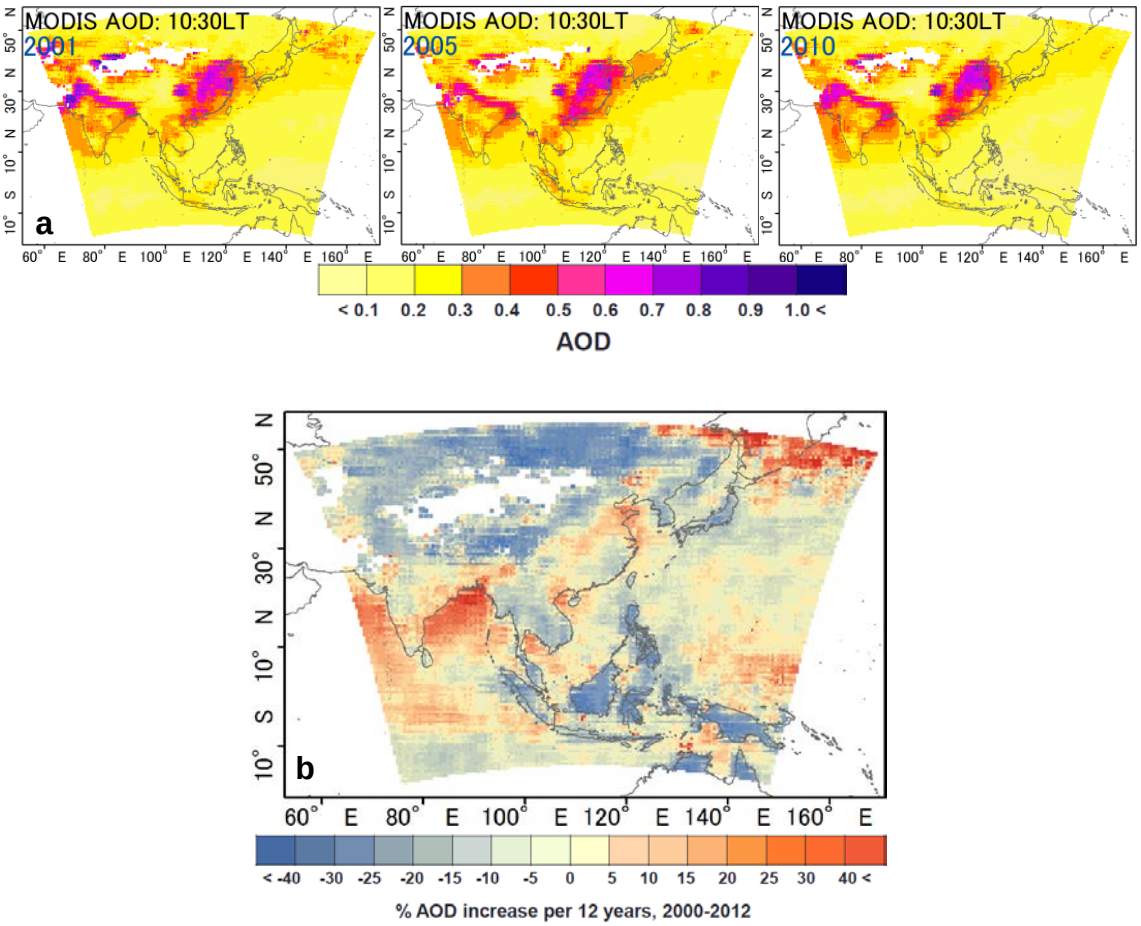

Figure 4.4 Spatial distributions of AOD retrieved from MODIS-Terra (a), and Spatial distribution of percent increasing trend per 12 years of AOD (b)

4.2 Seasonal variability for different latitude zones

The availability of more than ten years of satellite columnar observations allows for investigating the characteristic of interannual and seasonal variability and possible global changes in the pollutant concentrations. In this section, the characteristics of seasonal variation of NO_2 columns, CO columns and AODs were analyzed.

4.2.1 Seasonal variability of NO_2 columns

Figure 4.5 illustrates spatial distributions of monthly averaged tropospheric NO_2 columns retrieved from SCIAMACHY satellite during 2005-2012 for January to December. Chinese region especially in CEC area has the highest levels of NO_2 columns in every

month compared to other countries. For the SEA, the regions of Thailand, Malaysia and Indonesia present the dominant levels. The characteristic of seasonal cycle of NO_2 columns reveals differently at different regions. More analysis has performed by plotting time series of monthly NO_2 columns retrieved from OMI satellite during 2005-2012 for the cities over different latitude zones; mid-latitude, upper part of low-latitude, and near Equator zones, which is presented in Figure 4.6. Overall, satellite instruments are able to observe seasonal cycle of the pollutants. Figure 4.6a shows the time series of tropospheric NO_2 columns over the cities in mid-latitude zone such as Beijing, Shanghai, and Tokyo. In this area, the maximum levels of NO_2 columns were observed during wintertime (November-March), while the minimum levels were observed during summertime (July-September). This is due to the longer chemical lifetime of NO_2 during the winter related to lower OH concentration (produced by solar radiation) and also higher anthropogenic emissions (especially from heating). The results in this case are similar with He et al. (2007), Ma et al. (2006), and Uno et al. (2007) which also studied on the seasonal variability of tropospheric NO_2 over China. In case of SEA region, time series of NO_2 columns for the cities located in the upper part of low-latitude zone are presented in Figure 4.6b. Figure 4.6b shows the seasonal variability of NO_2 columns for Hanoi, Naypyidaw, Vientiane, Bangkok, and Phnom Penh cities. The seasonal cycle in this area is similar with mid-latitude zone which has the maximum levels in winter season (November – January) and minimum levels in summer/rainy season (June – August). Some cities also found another high peak of NO_2 columns during biomass burning season (February – April). However, for the cities that located near Equator zone as presented in Figure 4.6c for Bandar Seri Begawan, Kuala Lumpur, Jakarta and Dili cities, the maximum abundances of NO_2 columns was found in the different time period compared with the cities in the upper latitude zone. For equatorial region, this area generally has a tropical rainforest climate with relatively constant temperature throughout the year. The only variation is the amount of rainfall which determines the lifetime of NO_2 by the period of rainy and dry seasons. During rainy season, western monsoon brings the main rains, which is one of the causes of low concentration of NO_2 columns by the reaction with rainfall during this period of December-March (Beverland et al. 1998; Ghude et al. 2008; Paramee et al. 2005). On the contrary, eastern monsoon brings the driest weather during June-September causing the maximum levels of NO_2 columns during these months.

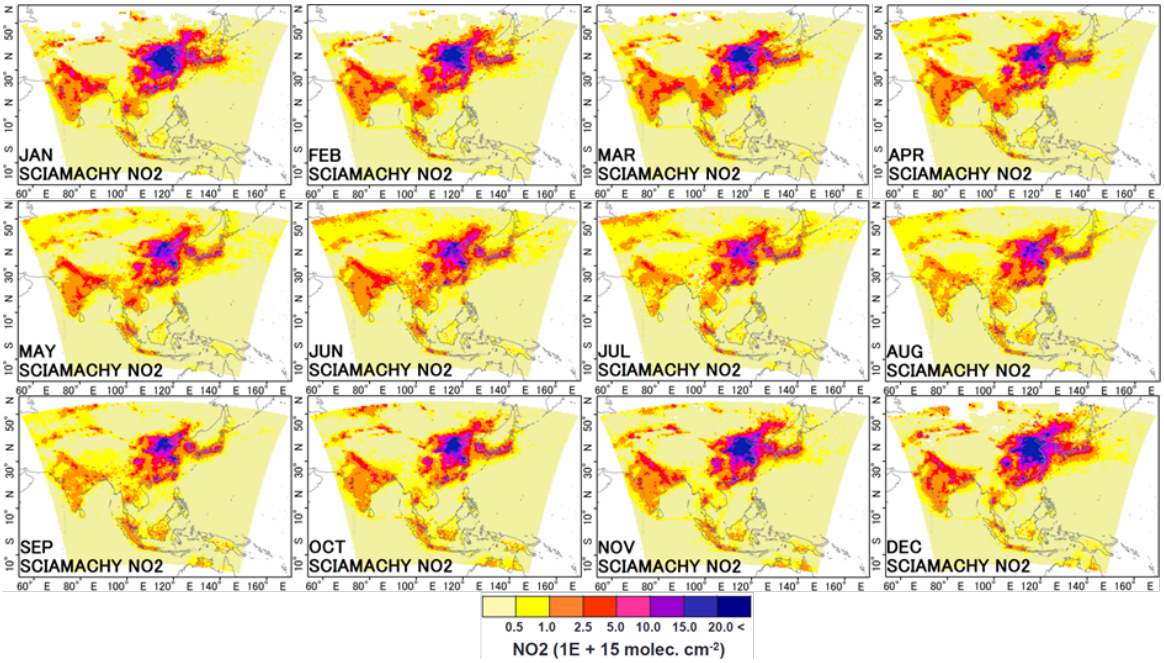

Figure 4.5 Spatial distributions of monthly averaged tropospheric NO_2 columns retrieved from SCIAMACHY satellite from January-December

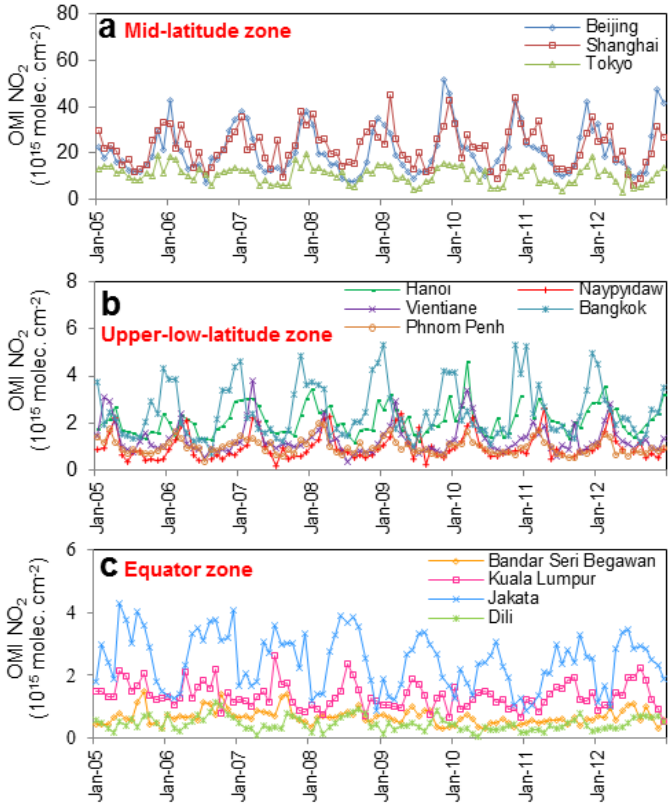

Figure 4.6 Time series of NO_2 columns retrieved from OMI for the cities located in mid-latitude (a), upper-low-latitude (b), and Equator (c) zones

4.2.2 Seasonal variability of CO columns

Figure 4.7 illustrates spatial distribution of monthly averaged CO columns retrieved from MOPITT satellite during 2005–2012 for January to December. From Figure 4.7, it is quite clear that CEC and some parts of Northern Thailand, Vietnam, Laos, and Burma are the main contributors of CO columnar loads which were built up at high concentration during December to May. July appears to be the period that has the lowest concentration of CO columns considering all the regions in Asia. Figure 4.8a-c presents time series of CO columns plotted for the cities over different latitude zones during 2000–2012. For the cities in mid-latitude zone, i.e., Beijing, Shanghai, and Tokyo (Figure 4.8a), the seasonal cycle of CO columns reveals to be similar with NO_2 columns that depend on the seasonality of OH concentrations. Both NO_2 and CO abundances start being higher during wintertime. However, the seasonal maximum of CO columns tends to stay last longer than NO_2 columns for a couple months (December-May) due to the longer lifetime and the accumulation of CO in the atmosphere. Moreover, there are high biomass burning activities in south China and Taiwan during March-May, and in central China, Korea and Japan during May-July, which are also the cause of high CO columns during this period. (Streets et al. 2003). The transboundary transport of CO plum from China to the downwind area such as Korea and Japan can be detected by MOPITT satellite during March-May as shown in Figure 4.7. Similar pattern of seasonal variability is also found in other cities located in low-latitude zone. The largest concentrations of CO columns for the cities in upper part of SEA (Figure 4.8b) were found in the period of January-April when there are high emissions from biomass burning activities. In addition, Figure 4.7 illustrates that long-range transport of CO during forest fire season from east-northeast Indian region (Venkataraman et al. 2006) toward Burma, central and northern parts of Thailand, Laos, and then Vietnam can be observed from February to April due to the prevailing northwesterly winds, which enhances intensive emission source already existing in this area. For the cities that located near Equator (Figure 4.8c), the seasonal cycle of CO columns is not very clear; however, for most of the cities the maximum peak showed up during biomass burning period of September-November as also illustrated in Figure 4.7.

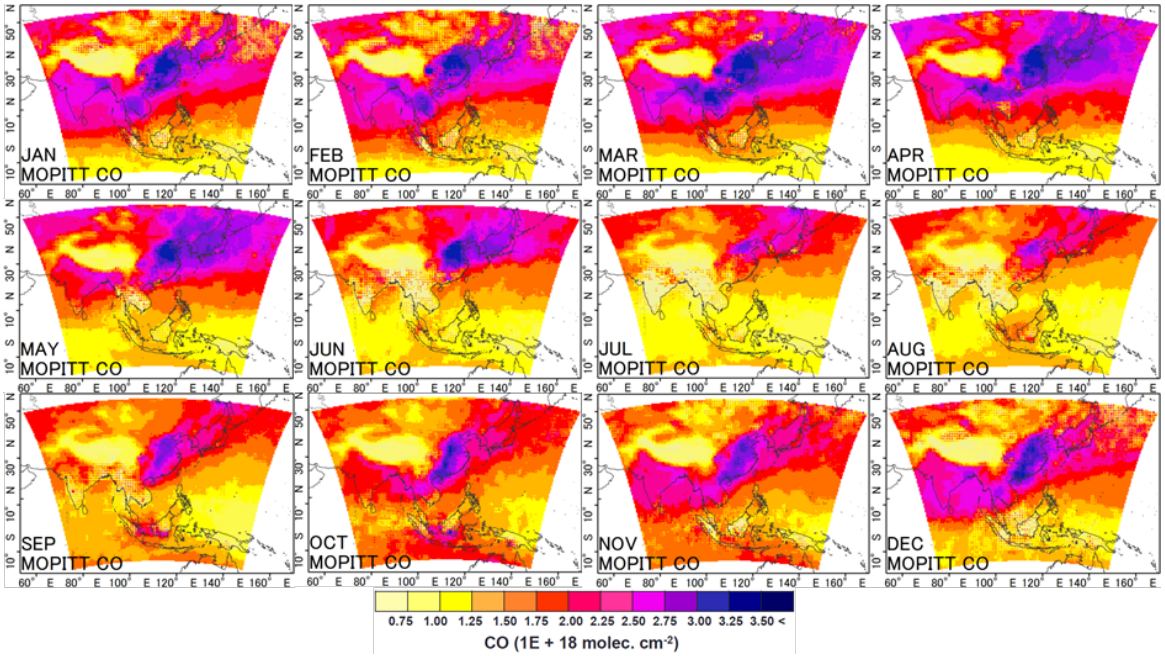

Figure 4.7 Spatial distributions of monthly averaged total CO columns retrieved from MOPITT satellite from January-December

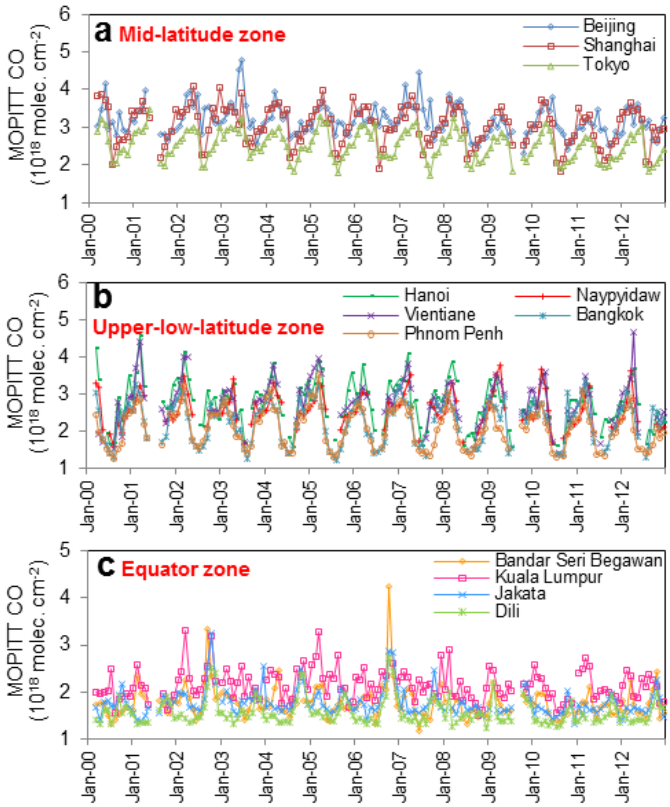

Figure 4.8 Time series of CO columns retrieved from MOPITT for the cities located in mid-latitude (a), upper-low-latitude (b), and Equator (c) zones

4.2.3 Seasonal variability of AODs

Figure 4.9 shows the spatial distribution of monthly averaged AODs retrieved from MODIS-Terra satellite during 2005–2012 for January to December. Similar to NO_2 and CO columns, the seasonal spatial distribution of AODs reveals the highest abundance of AODs over CEC in every month compared to other regions in Asia. Indian region also shows high levels of AODs during May to August; however, this region is beyond the scope of this study, and hence it will not be discussed here. The transboundary transport of aerosol from China that pass toward CEC, Korea and then Japan can be observed during March, April, and May as illustrated in Figure 4.9 which is coincident with the observation of CO columns presented in Figure 4.7. For the regions in SEA, high amounts of AODs were presented during February to April over Thailand, Burma, Laos, and Vietnam, and during September to November over Indonesia due to high biomass burning emissions.

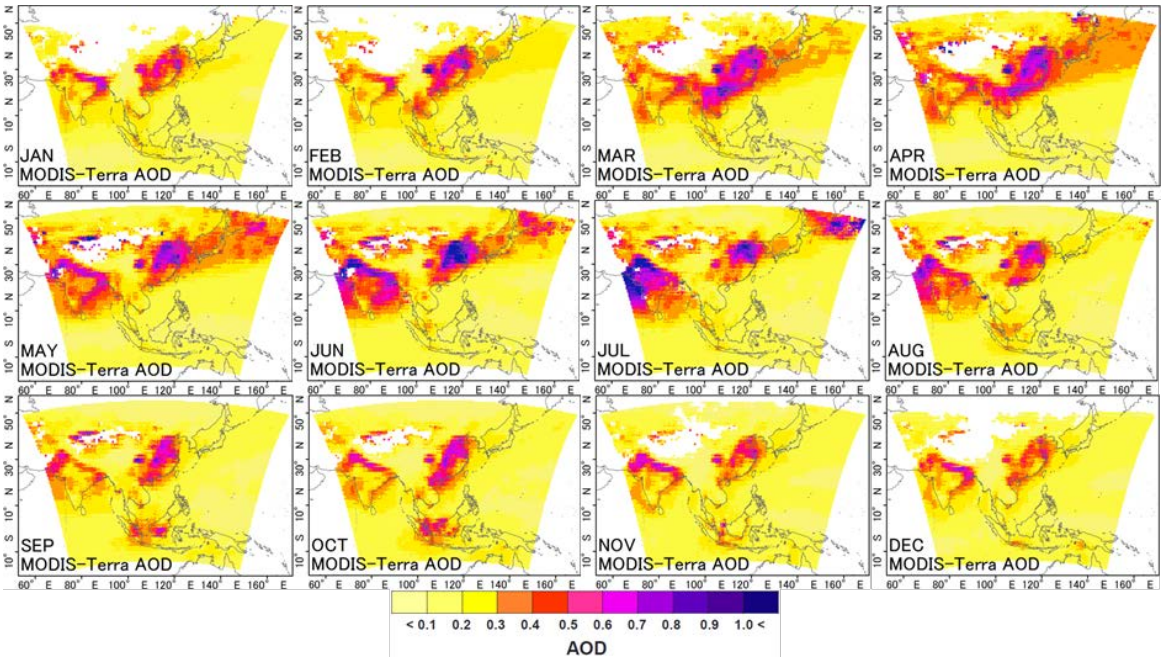

Figure 4.9 Spatial distributions of monthly averaged AOD retrieved from MODIS-Terra satellite from January-December

Figure 4.10a-c present time series of AODs in different latitude zones during 2000-2012. The MODIS data of AODs present maximum seasonal values during spring and summer (May-July) for the cities in mid-latitude zone as shown in Figure 4.10a for Beijing, Shanghai and Tokyo. The maximum levels of AODs in these regions are consistent with the seasonal biomass burning (March – July). Besides, dust storm originating in the deserts of Mongolia, northern China and Kazakhstan that hits China in springtime (March, April, May and may delay trips) results in a higher load of aerosol over China, Korea and Japan. As mentioned in previous section that this area has high anthropogenic emissions especially from China, these emissions can lead to nitrate aerosols, sulfate aerosols and carbonaceous aerosols which also contribute to high AODs (Sun et al. 2013; Zhang et al. 2010). For the upper part of Southeast Asian cities, Figure 4.10b shows the maximum AODs peak during March-April and the second small peak during September-October which also matches with the biomass burning period in this area. In case of the cities located near Equator zone (Figure 4.10c), the seasonal cycle of AODs is different from the cities in the upper part of SEA. The peaks of AODs normally occur during dry season of August-October. It is noteworthy that there is a coincidence of a peak during October 2005 and 2006 between the time series of AODs and CO columns over the cities that located near Equator zone. The results in this study are similar with the results in (Gloudemans et al. 2009). They found that CO columns retrieved from SCIAMACHY satellite have large peaks during spring 2005 and autumn 2006 over Indonesia. With the comparison with El Niño-Southern Oscillation (ENSO) precipitation index (ESPI), they suggested that peaks of CO columns during this period coincide with El Niño events as also mentioned in the previous section.

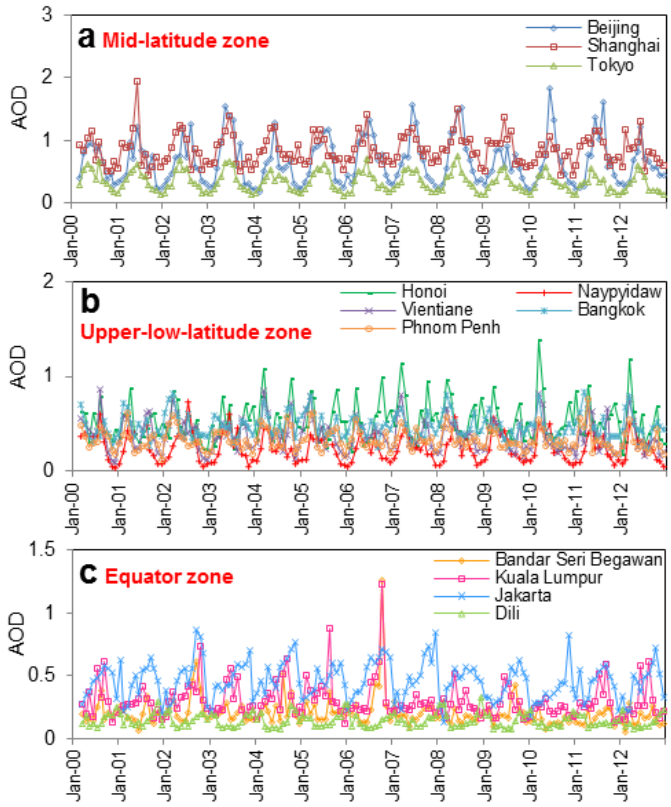

Figure 4.10 Time series of AODs retrieved from MODIS-Terra for the cities located in mid-latitude (a), upper-low-latitude (b), and Equator (c) zones

Chapter 5 Comparison of Surface Measurements and Satellite Observations

5.1 Surface data collection

Surface data in this study were derived from two monitoring sources; (1) The Acid Deposition Monitoring Network in East Asia (EANET), and (2) Pollution Control Department (PCD), Thailand.

1) EANET

In case of EANET data source, the datasets of NO_2 and PM_{10} concentrations were obtained from 4 stations at Bangkok (Thailand), Xiang Zhou (China), Hongwen (China), and Banryo (Japan) during the period of 2001-2008. The sampling sites are located in urban area using automatic dry deposition monitoring methods to collect the ground-level pollutants.

2) PCD

For PCD data source, NO_2, CO and PM_{10} concentrations were obtained from 15 stations over Bangkok, Rayong and Chiangmai provinces during the period of 1996-2012. The reference methods applied for collecting NO_2, CO and PM_{10} are Chemiluminesence, Non-Dispersive Infared Detection, and Gravimetric High Volume, respectively. Bangkok is the capital city of Thailand with a population of over eight million (12.6% of the country's population). The city is the economic center of the country's investment and development coupled the high concentration of vehicles and also factories in the city and metropolitan area. Rayong is placed in the east coast of Thailand. The city is the location of the largest industrial estate in Thailand, in which petrochemical and related productions are major industries. Chiangmai is located in the North of Thailand. Air pollution from urban activities and seasonal vegetation fires is the major issue in this area. The city is also

affected by smoke haze from intensive biomass burning in neighboring Burma and Laos. Since these three cities have their own characteristic of atmospheric pollutants from different sources, long-term satellite measurements were derived to investigate the capability of the satellite instruments to observe the annual trend and seasonal variability of these pollutants.

Datasets of satellite NO_2 columns, CO columns and AODs were compared with surface datasets of NO_2, CO and PM_{10} concentrations, respectively, at the concurrent locations and time periods. Since retrieved satellite information is provided as grid, whereas the ground measurements are represent only a small spot in the area. Hence, inter-comparisons between the satellite-based and ground-based measurement are not straightforward. In case of EANET data source, four 0.5° × 0.5° grid boxes were set around four station sites. All the satellite pixels that fall within the grid boxes were averaged and then compare with ground-based data at each station. For PCD data, three 0.5° × 0.5° grid boxes were set around Bangkok, Rayong and Chiangmai cities. The ground-based data of all monitoring stations that fall within these grid boxes were grouped and averaged together for each city (10 stations in Bangkok, 3 stations in Rayong, and 2 stations in Chiangmai) to compare with satellite-based data falling within the same grid sizes. Figure 5.1 shows the location of EANET and PCD sites. Table 5.1 and 5.2 give the latitude and longitude of the ground monitoring stations and the locations of grid boxes over EANET and PCD sites, respectively.

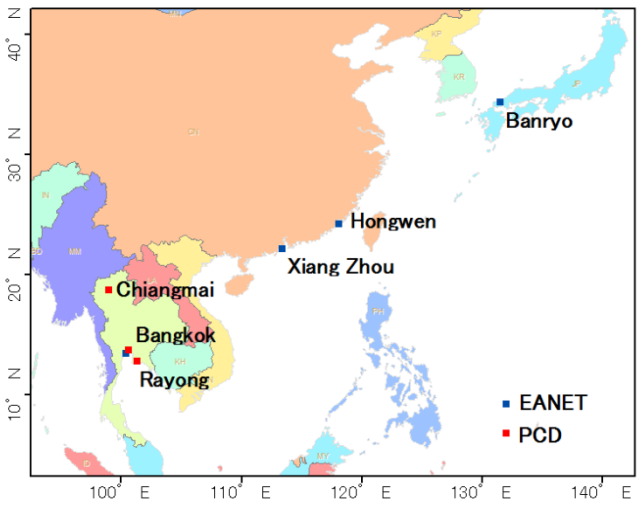

Figure 5.1 Locations of EANET and PCD monitoring sites

Table 5.1 Locations of EANET monitoring stations and grid boxes covering the stations

No.	Station name (City)	Country	Latitude	Longitude	Ht. above sea level	0.5° × 0.5° Grid box (Latitude, Longitude)
1	Bangkok	Thailand	13.46° N	100.32° E	2 m	(13.25-13.75° N, 100.25-100.75° E)
2	Xiang Zhou	China	22.16° N	113.34° E	40 m	(21.75-22.25° N, 113.25-113.75° E)
3	Hongwen	China	24.28° N	118.08° E	50 m	(24.25-24.75° N, 117.75-118.25° E)
4	Banryo	Japan	34.41° N	131.48° E	53 m	(34.25-34.75° N, 131.25-131.75° E)

Table 5.2 Locations of PCD monitoring stations and grid boxes covering the stations

No.	Station name	City	Latitude	Longitude	0.5° × 0.5° Grid box (Latitude, Longitude)
1	Health Promotion Hospital Maptaput	Rayong	12.71° N	101.17° E	(12.60-13.10° N, 101.00-101.50° E)
2	Field Crop Research Center	Rayong	12.74° N	101.14° E	
3	Ta Sit Provincial Administrative	Rayong	13.06° N	101.22° E	
4	Ratburana Post Office	Bangkok	13.67° N	100.49° E	(13.50-14.00° N, 100.30-100.80° E)
5	Thai Meteorological Department Bangna	Bangkok	13.67° N	100.51° E	
6	Mathayomwatsing School	Bangkok	13.68° N	100.45° E	
7	Nonsi Witthaya School	Bangkok	13.71° N	100.55° E	
8	Bansomdejchaopraya Rajabhat University	Bangkok	13.73° N	100.49° E	
9	Bodindecha Sing Singhaseni School	Bangkok	13.77° N	100.60° E	
10	Public Relations Department	Bangkok	13.78° N	100.54° E	
11	National Housing Stadium Huaykwang	Bangkok	13.78° N	100.57° E	
12	National Housing Authority Klongchan	Bangkok	13.78° N	100.65° E	
13	Chandrakasem Rajabhat University	Bangkok	13.82° N	100.58° E	
14	Yupparaj Wittayalai School	Chiangmai	18.79° N	98.99° E	(18.50-19.00° N, 98.70-99.20° E)
15	Chiangmai City Hall	Chiangmai	18.84° N	98.97° E	

5.2 Validation of satellite observations

This part aims to provide quantitative comparisons between ground-based monitoring of NO_2 and PM_{10} in one hand, and satellite-based monitoring of NO_2 columns and AODs, respectively in the other hand in order to assess the capability of satellite instruments for observing surface concentrations of the pollutants. Monthly surface NO_2 and daily surface PM_{10} data in this study were derived from Bangkok, Xiang Zhou, Hongwen, and Banryo stations processed by EANET during the period 2001–2008.

Figure 5.2 illustrates the scatter plots of surface NO_2 measurements versus tropospheric NO_2 columns from GOME, SCIAMACHY, OMI, and GOME-2 satellites in term of monthly average at Bangkok, Xiang Zhou, Hongwen, and Banryo stations, respectively. The summary of the correlation coefficients between ground-based and satellite-based datasets is given in Table 5.3. The results from four stations reveal similar outcome. The correlations between satellite- and ground-based NO_2 monitoring are in better agreement in case of OMI and GOME-2 with the correlation coefficients of 0.61 - 0.74 and 0.62 – 0.71, respectively, while GOME and SCIAMACHY present weaker relationships with the correlation coefficients of 0.40 - 0.56 and 0.45 – 0.55, respectively. The reasons of the results in this case can be explained by the horizontal resolution of the satellite instruments. Since OMI and GOME-2 have finer spatial resolutions than GOME and SCIAMACHY, they are able to provide more precise detection of the characteristic of the pollutants in the local scale than those with low spatial resolutions. However, for SCIAMACHY case, even it has similar resolution and overpass time with GOME-2 but it presents smaller correlation. This is probably due to the better detector of GOME-2 instrument since GOME-2 is the new generation of satellite observation as mentioned earlier in the previous chapter (Chapter 3). Moreover, many researches has studied on the comparison between satellite-borne and ground-based tropospheric NO_2 measurements and proved that their relationships can be varied by location influenced by land surface, seasonal cycle, climate effects, and meteorological parameters such as cloud, fog, wind speed and aerosol loading. Therefore, the discrepancy in this case can be also explained by the effects of these parameters.

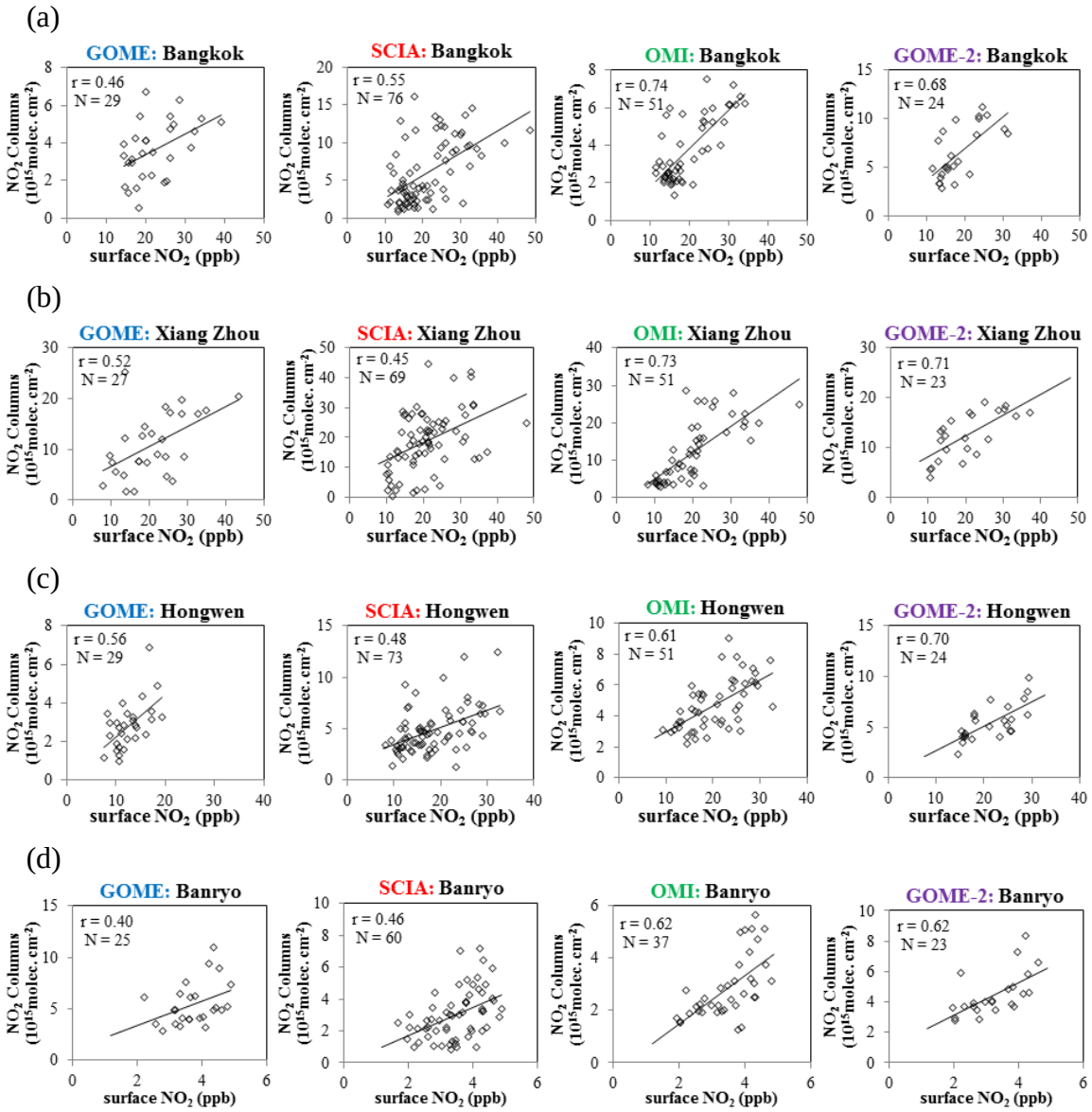

Figure 5.2 Scatter plots of surface NO_2 concentrations versus tropospheric NO_2 columns at Bangkok (a), Xiang Zhou (b), Hongwen (c), and Banryo (d) stations

Figure 5.3 presents the scatter plot between daily surface PM_{10} mass concentrations and satellite AODs retrieved from MODIS-Terra and MODOS-Aqua at Bangkok, Xiang Zhou, Hongwen, and Banryo stations, respectively. The results show that the relationships of AODs-PM_{10} vary by locations with the highest correlation coefficient in Xiang Zhou. However, the correlations from all sites are generally low with the correlation coefficients of 0.33 - 0.59 and 0.38 - 0.62 for surface PM_{10} mass versus AODs from MODIS-Terra and MODIS-Aqua, respectively. Table 5.3 summarizes the correlation coefficients between

ground-based and satellite-based datasets for all stations. Note that AODs do not directly represent PM_{10} mass concentrations since AODs refer to the radiation extinction due to the interaction of aerosol loads from the ground up to the top of the atmosphere. Therefore, several factors can influence the relationship. First, AODs seem to be more sensitive to fine particles and sulfates than nitrates and dust (Kim Oanh 2012). Second, meteorological parameters such as cloud, relative humidity, boundary layer height, etc. also affect the correlations (Gupta et al. 2006; Tsai et al. 2011). Third, the algorithm of AODs retrievals perform differently over different land surface (Engel-Cox et al. 2004). For these reasons, more analysis on the effect of these factors is needed to improve the correlation between surface PM_{10} and AODs, which is provided in Chapter 6.

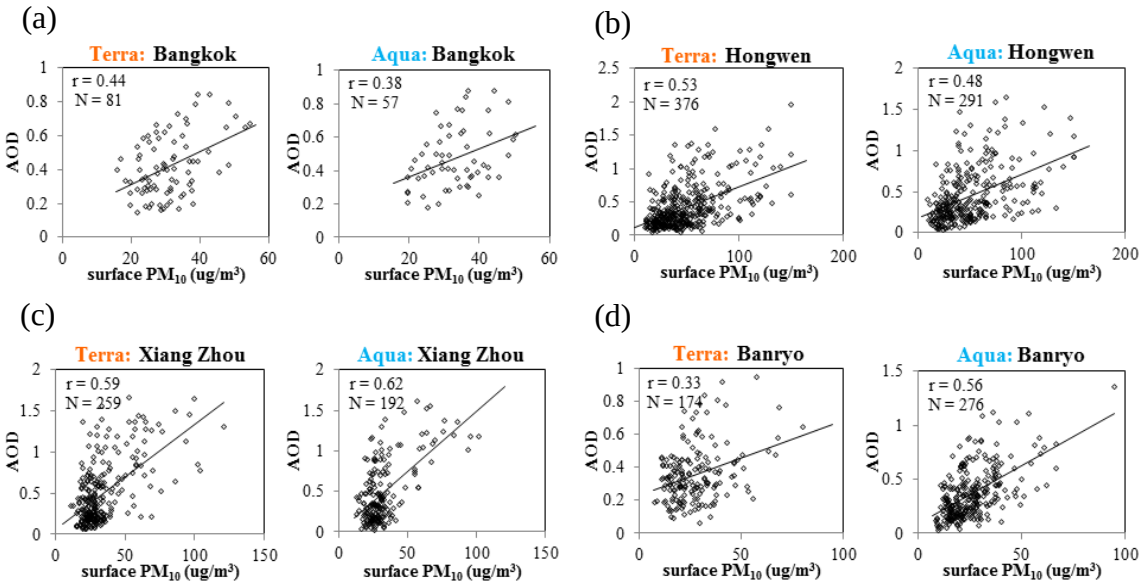

Figure 5.3 Scatter plots of surface PM_{10} concentrations versus AODs at Bangkok (a), Xiang Zhou (b), Hongwen (c), and Banryo (d) stations

Table 5.3 Summary of correlation coefficients (r) between satellite-based (S) and ground-based data (G) from EANET

Site name	NO_2(S)-NO_2(G)								AOD(S)-PM_{10}(G)			
	GOME		SCIAMACHY		OMI		GOME-2		MODIS-Terra		MODIS-Aqua	
	r	N	r	N	r	N	r	N	r	N	r	N
Bangkok (Thailand)	0.46	29	0.55	76	0.74	51	0.68	24	0.44	81	0.38	57
Xiang Zhou (China)	0.52	27	0.45	69	0.73	51	0.71	23	0.59	259	0.62	192
Hongwen (China)	0.56	29	0.48	73	0.61	51	0.70	24	0.53	376	0.48	291
Banryo (Japan)	0.40	25	0.46	60	0.62	37	0.62	23	0.33	174	0.56	276

5.3 Long-term time series of surface measurements and satellite observations

In order to investigate the capability of the satellite instruments to observe long-term trend and seasonal variability of surface pollutants, surface monitoring data were derived from PCD, Thailand during 1996 to 2012 for NO_2 mass concentrations and during 2000 to 2012 for CO and PM_{10} mass concentrations. Figure 5.4-5.6 give the long-term comparison of the monthly satellite data and surface monitoring of NO_2, CO and PM_{10} concentrations, respectively over Thailand in Bangkok, Chiangmai and Rayong cities. It can be seen that satellite observations can generally capture the seasonal trend of these pollutants, especially in case of NO_2 and CO. For NO_2 columns in case of Bangkok and Rayong (Figure 5.4a, b), the maximum values of both satellite NO_2 columns and surface NO_2 concentration appear in winter month of November-February as expected due to the longer lifetime of NO_2 and also high anthropogenic emissions (e.g., mobile and industrial sources) while the maximum values in Chiangmai (Figure 5.4c) shows during February-April due to the high degree of biomass burning activities in Chiangmai during this period.

For CO columns, Figure 5.5 shows good seasonal consistence between MOPITT CO columns and surface CO concentrations. The results of seasonal analysis of CO columns and surface CO are similar with NO_2 columns and surface NO_2 for all Bangkok (Figure 5.5a), Rayong (Figure 5.5b), and Chiangmai (Figure 5.5c) cases. However, in case of Bangkok and Rayong cities the maximum period of CO columns (November to March)

tend to stay a bit last longer than surface CO concentration (November to February). This is probably caused by the elevated CO that transported from the suburban area due to the high rice straw burning activities in March.

In case of AODs, even the seasonal trend of AODs shown in Figure 5.6 is not in good consistence with PM_{10} as previous cases of NO_2 and CO columns, satellite AODs can catch the temporal variation of PM_{10}, especially in Chiangmai. In Bangkok (Figure 5.6a), ground monitoring data of PM_{10} give high concentrations during dry period of October-March with the peak in December and January, but the maximum peak of AODs appears during February-April and the second peak during October-November. Since PM_{10} data are derived from point source, but AODs are the spatial average of the integrated columnar aerosol loads from the ground up to the top of the atmosphere, the possible bias can be owing to the influence of the transport of PM from suburban area during paddy fields burning season in February-April and August-December. Tsai et al. (2011) also demonstrated that elevated PM has a large impact on the relationship of AODs and PM. In case of Chiangmai (Figure 5.6c), both AODs and PM_{10} concentrations reveal the highest peak during February-April. The peaks of AODs and PM_{10} concentrations in Chiangmai occur at the same period as forest fires which generally have the largest burned area in dry season of January-April (highest in March-April) (Bonnet et al. 2006). The seasonal variability of AODs and PM_{10} in Rayong (Figure 5.6b) is similar with Bangkok that gives high degree of AODs and PM_{10} concentrations during February-April and December-January, respectively. However, the correlation coefficient of AODs and PM_{10} in Rayong is relatively small ($r = 0.24$-0.35) comparing with other cases in Bangkok and Chiangmai ($r = 0.47$-0.50 and 0.52-0.55, respectively). Table 5.4 summarizes the correlation coefficients of the comparison between satellite retrievals and the concentration of surface pollutants. Most of the results show that the relationships of satellite and ground data are generally in better agreement for Bangkok and Chiangmai cities than for Rayong cities. Rayong is located along the coastline with abundant rainfall. Meteorological variation such as cloud, fog, and wind speed can be the cause of lower correlation of satellite and ground data as also presented in Chu et al. (2002) that over the coastal regions, there are large errors on MODIS AOD products. Moreover, the correlation coefficients of the comparisons of satellite data versus NO_2 concentrations ($r = 0.23$-0.89) and CO

concentrations (r = 0.51-0.71) provide rather good correlation than PM_{10} concentration (r = 0.24-0.55) for all cities. This result is similar with the comparison between satellite data and surface data collected from EANET stations in the previous section. Moreover, in case of NO_2 the comparison of OMI satellite data and surface NO_2 also gives higher correlation coefficient compared to other satellites due to its finer spatial resolution (Zyrichidou et al. 2009b).

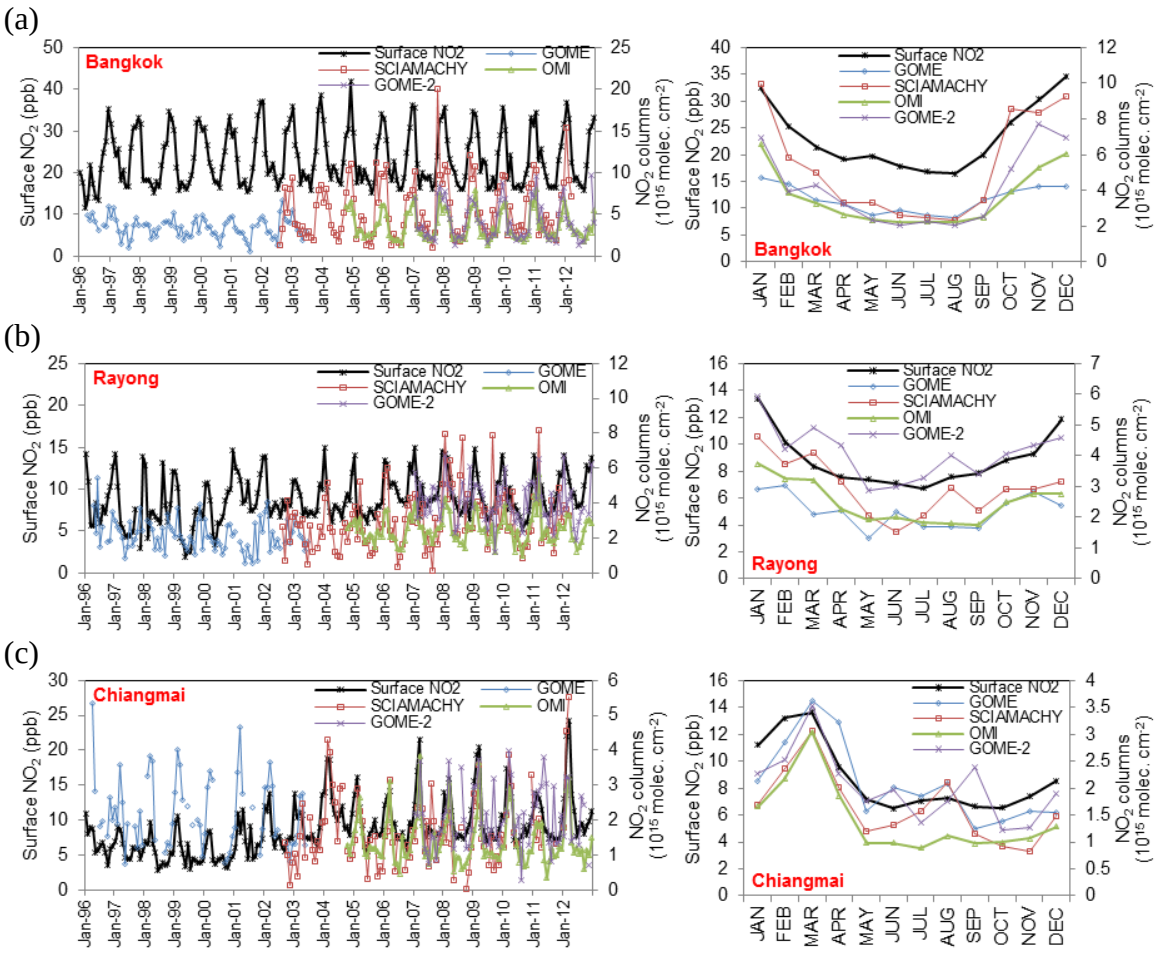

Figure 5.4 Long-term comparisons of surface NO_2 concentrations and satellite NO_2 columns over Bangkok (a), Rayong (b), and Chiangmai (c)

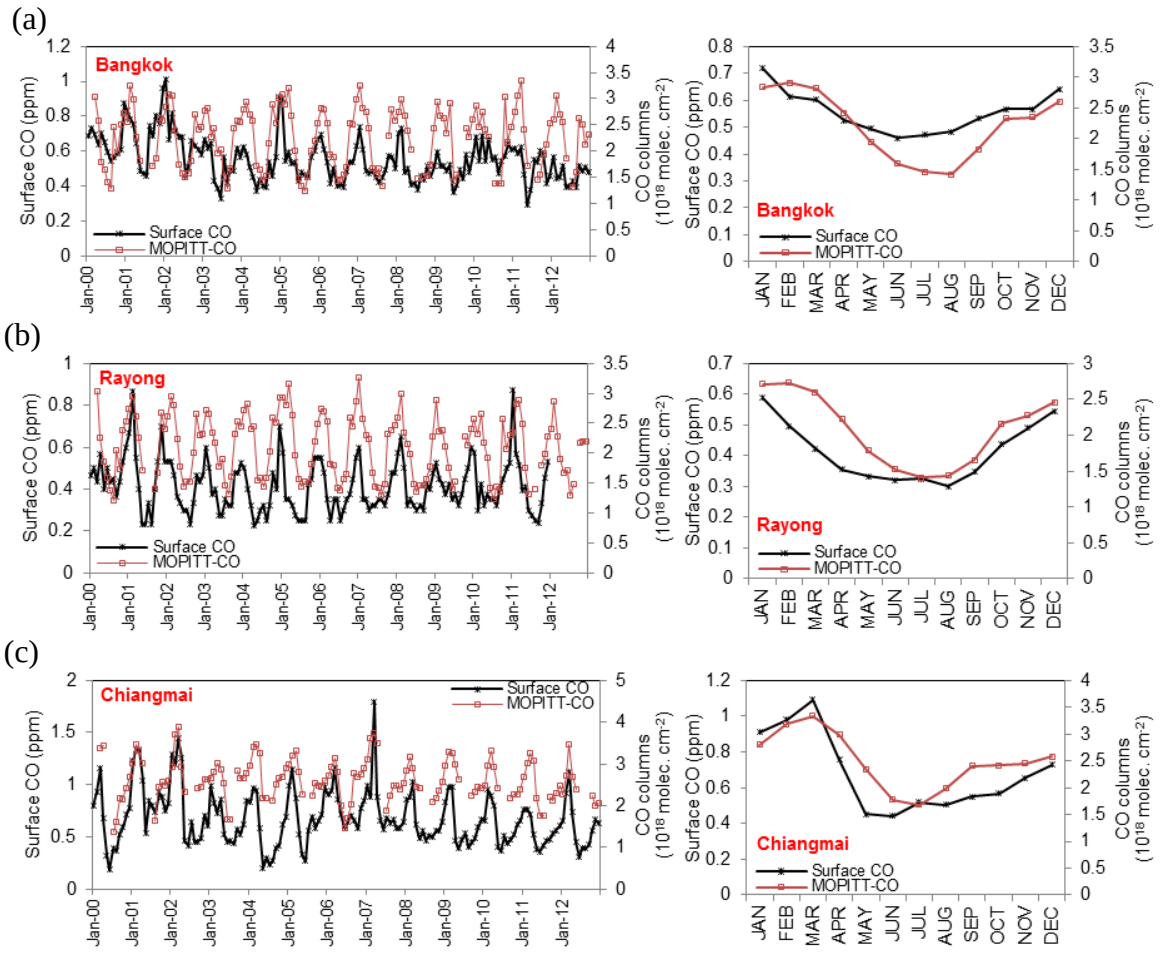

Figure 5.5 Long-term comparisons of surface CO concentrations and MOPITT CO columns over Bangkok (a), Rayong (b), and Chiangmai (c)

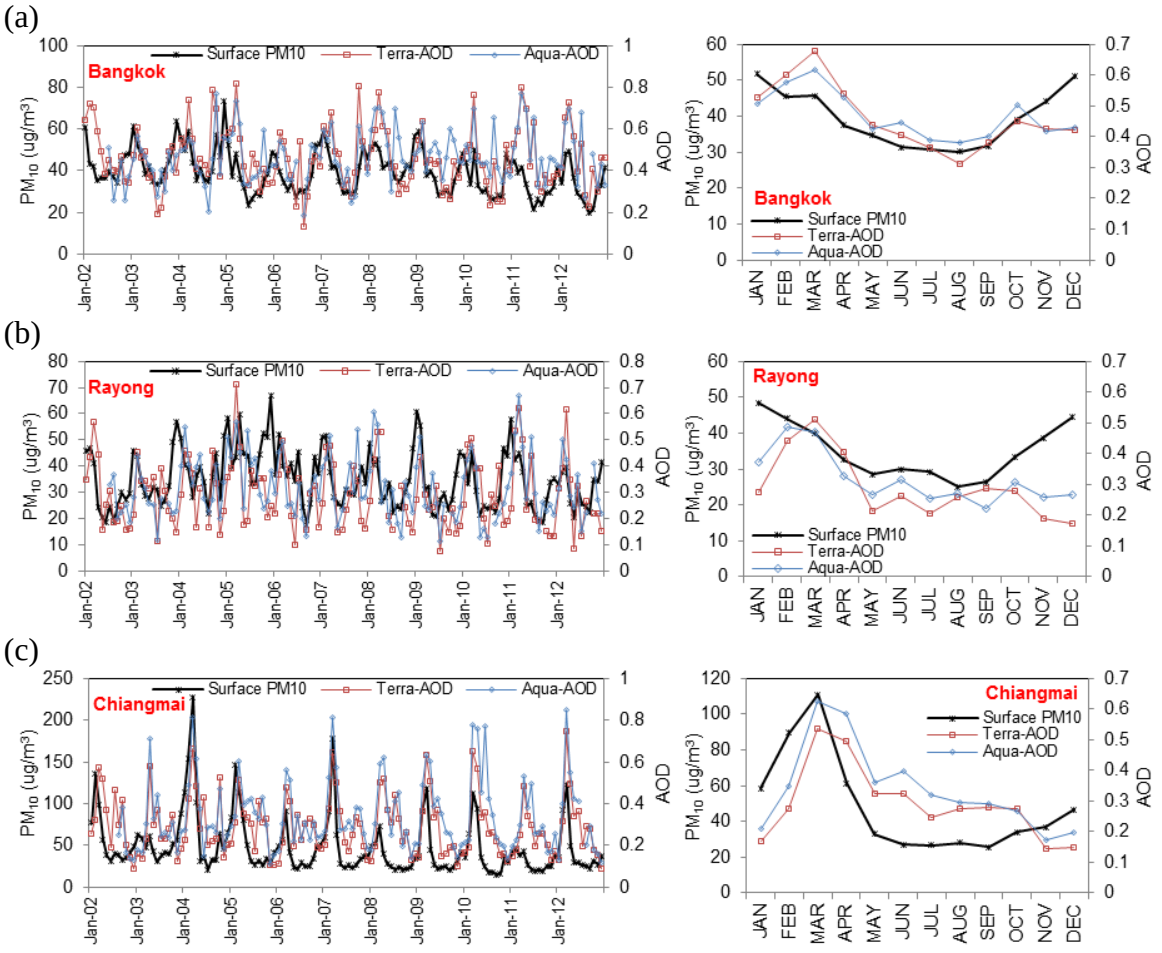

Figure 5.6 Long-term comparisons of surface PM_{10} concentrations and MODIS AODs over Bangkok (a), Rayong (b), and Chiangmai (c)

Table 5.4 Summary of correlation coefficients (r) between satellite-based (S) and ground-based data (G) from PCD

City	NO_2(S)-NO_2(G)								CO(S)-CO(G)		$AOD(S)-PM_{10}(G)$			
	GOME		SCIAMACHY		OMI		GOME-2		MOPITT		MODIS-Terra		MODIS-Aqua	
	r	N	r	N	r	N	r	N	r	N	r	N	r	N
Bangkok	0.54	83	0.79	116	0.89	99	0.86	71	0.51	142	0.50	132	0.47	124
Rayong	0.23	83	0.46	114	0.68	99	0.53	71	0.62	146	0.24	126	0.35	122
Chiangmai	0.48	63	0.74	94	0.84	99	0.56	67	0.71	126	0.52	132	0.55	124

Chapter 6 Development of Regression Model for PM Mass Estimation

As mentioned earlier in previous section that satellite AODs do not directly represent surface PM_{10} concentrations. Several factors can influence the relationship between them. This section focused more on satellite retrievals of AODs in order to improve the correlation of AODs-PM_{10} by developing the linear regression models between AODs and surface PM_{10} with the correction of meteorological parameters and then apply such models to estimate surface PM_{10} mass concentrations and validate with surface monitoring data.

6.1 Model development process

To develop regression model between satellite AODs and surface PM_{10} mass concentrations, the methodology comprises of 4 steps as follows.

1) Comparative analysis of AODs and surface PM_{10} mass

This part intended to develop linear regression models by using five-year datasets (2008-2012) of AODs-PM_{10} relationship. AODs used in this analysis were retrieved from MODIS-Terra and MODIS-Aqua satellites as daily data. The considered areas were three provinces of Thailand; Chiangmai, Bangkok, and Rayong. The hourly surface PM_{10} concentrations were collected from 15 stations of PCD, Thailand (as presented in Table 5.2, Chapter 5), from 2008 to 2012. Three 0.5° × 0.5° grid boxes were set around interested cities. All the ground-based data falling within these grid sizes were grouped and averaged together, and then compared with the satellite-based data falling within the same grid sizes. Figure 6.1 shows the locations of 15 PCD stations and the location of three 0.5° × 0.5° grid boxes.

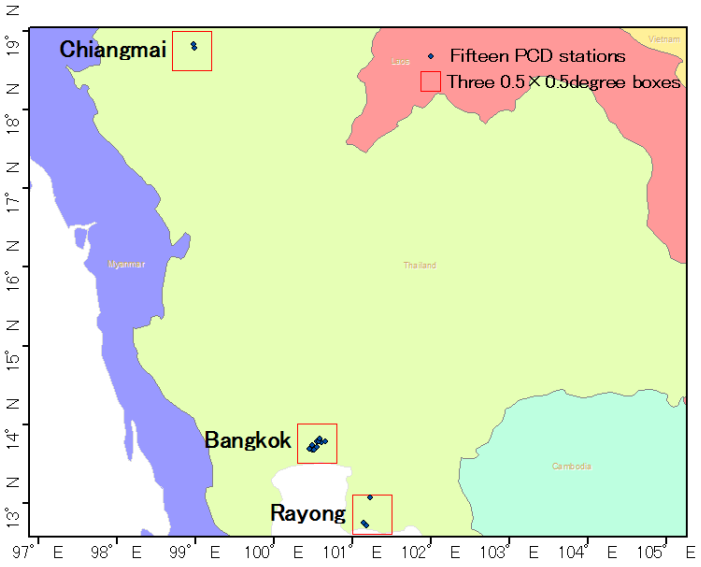

Figure 6.1 Locations of PM_{10} monitoring stations and grid of AOD retrievals

MODIS AODs were monitored at different space and time subject to progressive orbits while PM monitoring was taken at different time intervals. In order to take temporal variability into account, the criteria for collecting surface PM_{10} data was set to compare with satellite AODs at their overpass time. Three-hour of PM_{10} data were collected and averaged from 09:00LT to 12:00LT and from 12:00LT to 15:00LT covering the period of MODIS-Terra and MODIS-Aqua overpass times over the study area (Terra ~10:30LT and Aqua ~13:30LT), respectively. In addition, 24-hour averaged PM_{10} data were also applied to compare with averaged AODs data of MODIS-Terra and MODIS-Aqua.

2) Cloud screening process

The accuracy of satellite retrievals to estimate ground mass concentrations depends on the strength of the regression relationship between retrieved AODs and PM mass concentration, which can depend on the accuracy of retrieved AODs and other factors such as the study area, aerosol load and type, aerosol vertical profiles, and meteorological parameters. Several studies (Engel-Cox et al. 2004; Gupta et al. 2006; Dinoi et al. 2010) indicated that cloud contamination in MODIS AODs significantly affects the AODs-PM correlation. In this study, cloud screening process was adopted in order to investigate the variations of the correlations between surface PM_{10} mass concentrations and MODIS AODs in the different classes of cloudiness in term of cloud fraction (CF). The CF data in

this study were derived from the same satellite product of AODs; collection 5.1, level-2 aerosol product of MODIS-Terra and MODIS-Aqua sensors, during the period of 2008-2012.

3) Analysis for the effect of other meteorological parameters

As AOD is a quantitative measure of the integrated columnar aerosol load, from the ground up to the top of the atmosphere, whereas PM mass is a quantitative measure of the particulate mass concentration at the ground surface. Thus, the relationship between PM mass concentrations and AODs is expected to depend on meteorological condition (Dinoi et al. 2010). In case of ambient relative humidity (RH), it can significantly affect the AODs-PM relationship by changing the light scattering properties of the aerosol due to the hygroscopic property of the particles. The higher the relative humidity, the larger the portion of the light is scattered and then the larger AODs (Zhang and Hoff 2009). Surface wind speed (WS) and temperature (T) also play a crucial role in aerosol generation and dispersion. They determine the level of the turbulence in the atmosphere. When the turbulence is low, satellite sensors will observe almost the same amount of aerosol mass as observed by ground instruments. On the contrary, when the level of the turbulence is high, ground instruments will observe smaller amount of aerosol mass while satellites still observe the same amount. Moreover, higher T also accelerates photochemical reaction which may change the composition of PM and then affect the relationship between satellite AODs and surface PM mass concentrations.

In this section, the role of the RH, WS, and T on the AODs-PM_{10} relationship was investigated in order to get a better understanding of the robustness of AODs-PM_{10} relationship and to improve the overall accuracy of the estimations of surface PM_{10} mass from satellite observations. RH, WS, and T measurements in this study were obtained from 15 stations of PCD, Thailand from 2008 to 2012 as hourly data. These parameters were averaged as 3-hour average during 09:00LT-12:00LT and 12:00LT-15:00LT, and as 24-hour average corresponding to the overpass time of MODIS AOD observations. Finally, data analysis was conducted by using simple linear regression and multiple linear regression to analyze the relationship of AODs-PM_{10} and the effect of meteorological

parameters as presented in Model 1 and Model 2, respectively, where b_0 is an intercept, and b_1, b_2, b_3 and b_4 are regression coefficients. Table 6.1 summarizes the data used for this analysis.

$$PM_{10} = b_0 + b_1\,(AOD) \qquad \text{(Model 1)}$$

$$PM_{10} = b_0 + b_1\,(AOD) + b_2\,(RH) + b_3\,(WS) + b_4\,(T) \qquad \text{(Model 2)}$$

b_0: Intercept

$b_{1\text{-}4}$: Regression coefficient

PM_{10}: Surface PM_{10} mass concentration ($\mu g/m^3$)

AOD: Aerosol Optical Depth

RH: Relative Humidity (%)

WS: Wind Speed (m/s)

T: Temperature (°C)

Table 6.1 Data applied for the regression analysis of AODs-PM_{10}

Satellite AODs (2008-2012)	PCD PM_{10} (2008-2012)	Cloud Fraction (CF) (2008-2012)	Meteorological Data (2008-2012)
10:30LT (MODIS-Terra)	Averaged 9-12:00LT	Without cloud screen CF ≤ 4/10 CF ≤ 1/10	Relative Humidity Wind Speed Temperature
13:30LT (MODIS-Aqua)	Averaged 12-15:00LT		
Averaged 10:30/13:30LT	Averaged 24-hour		

4) Model evaluation and comparison

The development of linear regression models to estimate surface PM_{10} mass concentrations used 5-year database of AODs, PM_{10}, RH, WS, and T during 2008-2012. To evaluate the validity of the regression model, Model 1 and Model 2 were used to estimate surface PM_{10} mass concentrations over Chiangmai, Bangkok, Rayong, and other cities in northern Thailand around Chiangmai city for the pre- and post- year of the database used in the model; in this case are year 2007 and 2013. The estimated surface PM_{10} mass concentrations were then compared with those collected from PCD, Thailand during the same periods.

6.2 Comparative analysis of AODs and surface PM_{10} mass

MODIS AOD data were comparably analyzed with surface PM_{10} mass concentrations during the 5-year period of 2008-2012 over Thailand to investigate its applicability to monitor surface air quality. The first column of Figure 6.2a-c show the scatter plots of 3-hour averaged surface PM_{10} mass concentrations during 9:00-12:00LT and 12:00-15:00LT versus collocated in space of daily AOD data retrieved from MODIS-Terra (10.30LT overpass time) and MODIS–Aqua (13:30LT overpass time), respectively using the process as previously stated in the methodology (all the ground- and satellite-based data falling within 0.5° × 0.5° grid boxes centering at interested cities were averaged and compared together) for Chiangmai, Bangkok, and Rayong cities. In this case, the analysis was separated into two seasons, dry season (November-April) and wet season (May-October). The blue diamond symbol with the linear black solid line represents the data analysis conducted for dry season, whereas the red triangle symbol with the linear black dash line represents those for wet season. The results in Figure 6.2a-c demonstrate that during dry and wet seasons the comparative analysis gives different correlation of AODs-PM_{10} as can be seen from the linear regression lines. For Chiangmai, the relationship of AODs-PM_{10} provides more promising results during dry period than wet period for both Terra and Aqua retrievals. The correlation coefficients during dry period (r_D) for Terra was 0.61 and for Aqua was 0.69 while the correlation coefficients during wet period (r_W) were 0.30 and 0.33 for Terra and Aqua, respectively. The reason for large discrepancy between dry and wet seasons is probably due to the lower concentration of surface PM_{10} mass during wet season. As mentioned earlier in several studies (Gupta et al. 2006, 2007) that the correlations between AODs and surface PM mass are generally performed better in sensitive/unhealthy environment because of the high uncertainties in small MODIS AOD values, which in this case there are high amount of particle emissions from the biomass burning activities in Chiangmai, especially during dry period of February-March. For Bangkok and Rayong, the overall correlation coefficients of AODs-PM_{10} are generally low ranging from 0.19-0.44 for dry season and 0.31-0.51 for wet season with slightly higher correlations for AODs retrieved from Aqua satellite. The reason for the lower correlations in Bangkok and Rayong could be due to smaller values of AODs and PM_{10}

mass concentrations compared to Chiangmai city in the dry season. Further, in the central part of Thailand, rice straw field burning commonly happen during dry season of November-December and mainly in March-April (Tipayarom and Kim Oanh 2007). Therefore, another possible reason for the weak correlations of AODs-PM_{10} is probably caused by the effect of elevated aerosols that transported from the other sources in suburban areas outside the considered grid boxes of Bangkok and Rayong cities. This can also be the reason for the mildly higher correlations in the wet season compared to dry season since the levels of AODs in dry and wet seasons are not quite different for these two cities. However, this is only the preliminary analysis. A number of variables are also found to be taking into account to improve the AODs-PM correlation which is discussed in the next step.

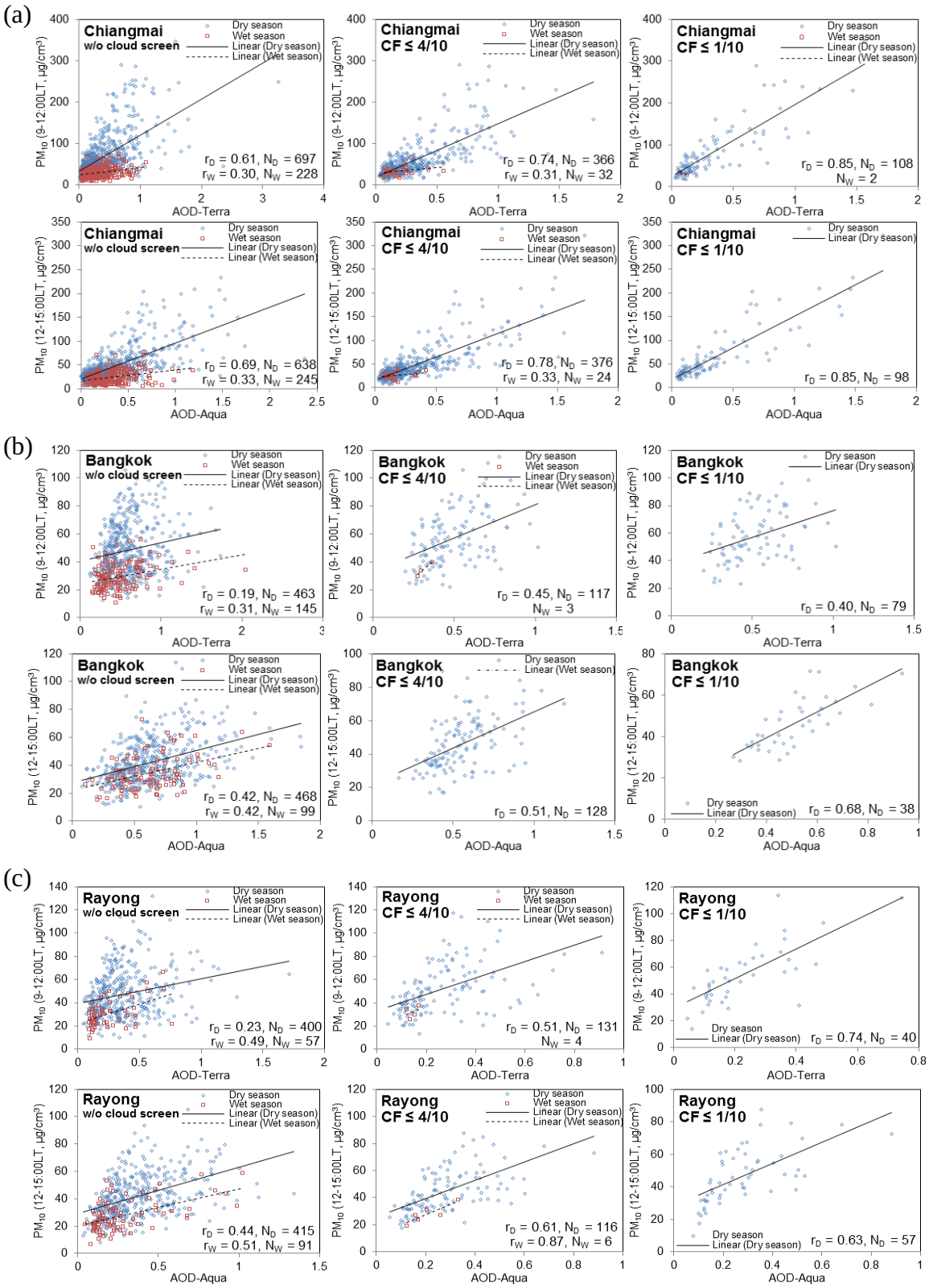

Figure 6.2 Scatter plots of AODs-PM_{10} at different cloud factor over Chiangmai (a), Bangkok (b), and Rayong (c)

6.3 Cloud screening process

Many studies (Dinoi et al. 2010; Koelemeijer et al. 2006; Schaap et al. 2009) have shown that additional cloud screening would help to improve the correlation of AODs and surface PM mass. In this study, cloud data were derived from level-2 Cloud Fraction (CF) product of MODIS-Terra and MODIS-Aqua land only algorithm to investigate the impact of cloud contamination on the AODs-PM_{10} relationship. AOD data were grouped in different class of CF as CF $\leq$ 4/10 and CF $\leq$ 1/10 and plotted against surface PM_{10} mass concentrations over Chiangmai, Bangkok, and Rayong as depicted in the second and third columns of Figure 6.2a-c, respectively. Overall, the AOD-PM_{10} correlation become stronger when adopted cloud screening procedure which presented in the higher correlation coefficients when the analysis is restricted to more clear-sky day for all the considered cities. The results illustrated in Figure 6.2a-c are summarized in Table 6.2 for the regression equations, correlation coefficients (r), and number of the data (N) at three different cloudiness levels (without cloud screen, CF $\leq$ 4/10, and CF $\leq$ 1/10) for MODIS-Terra and –Aqua observations during both dry and wet seasons. The r values under the clear-sky condition of CF $\leq$ 1/10 increase significantly compared to AODs-PM_{10} correlation without cloud screen procedure. For example, in Rayong city during dry season the Terra/AODs-PM_{10} correlation is quite low under the cloudy-sky condition (without cloud screen) with the r value of 0.23, but become stronger to 0.51 under CF $\leq$ 4/10 and reach the maximum of 0.74 under CF $\leq$ 1/10. Similar results are also found in other cities. In addition to the r values, the slopes of the linear regression equations become steeper and the intercepts become smaller after excluding cloud-contaminated AOD values, which mean that AODs measured in clear-sky day become more sensitive to surface PM mass measurements. This outcome is similar with Dinoi et al. 2010 when the analysis was conducted in southeastern Italy during 2006-2008.

Table 6.2 Relationship of AODs and surface PM_{10} mass at different class of cloudiness

City	Parameter	Season	w/o cloud screen			CF ≤ 4/10			CF ≤ 1/10		
			Equation	r	N	Equation	r	N	Equation	r	N
Chiangmai	AOD(Terra)-PM_{10}(9-12:00LT)	Dry	PM_{10} = 87.1 AOD + 32.8	0.61	697	PM_{10} = 129.4 AOD + 19.0	0.74	366	PM_{10} = 171.4 AOD + 24.3	0.85	108
		Wet	PM_{10} = 18.6 AOD + 24.5	0.30	228	PM_{10} = 27.6 AOD + 28.0	0.31	32	-	-	2
	AOD(Aqua)-PM_{10}(12-15:00LT)	Dry	PM_{10} = 75.7 AOD + 20.7	0.69	638	PM_{10} = 98.1 AOD + 15.3	0.78	376	PM_{10} = 124.2 AOD + 20.7	0.85	98
		Wet	PM_{10} = 23.4 AOD + 17.0	0.33	245	PM_{10} = 23.1 AOD + 22.6	0.33	24	-	-	-
Bangkok	AOD(Terra)-PM_{10}(9-12:00LT)	Dry	PM_{10} = 13.5 AOD + 40.2	0.19	463	PM_{10} = 48.4 AOD + 32.9	0.45	117	PM_{10} = 38.6 AOD + 37.4	0.40	79
		Wet	PM_{10} = 10.3 AOD + 24.5	0.31	145	-	-	3	-	-	-
	AOD(Aqua)-PM_{10}(12-15:00LT)	Dry	PM_{10} = 23.4 AOD + 27.3	0.42	468	PM_{10} = 43.2 AOD + 22.1	0.51	128	PM_{10} = 56.4 AOD + 16.1	0.68	38
		Wet	PM_{10} = 19.9 AOD + 22.0	0.42	99	-	-	-	-	-	-
Rayong	AOD(Terra)-PM_{10}(9-12:00LT)	Dry	PM_{10} = 21.1 AOD + 39.5	0.23	400	PM_{10} = 70.4 AOD + 33.4	0.51	131	PM_{10} = 110.1 AOD + 29.5	0.74	40
		Wet	PM_{10} = 32.9 AOD + 22.5	0.49	57	-	-	4	-	-	-
	AOD(Aqua)-PM_{10}(12-15:00LT)	Dry	PM_{10} = 33.6 AOD + 29.2	0.44	415	PM_{10} = 67.0 AOD + 26.0	0.61	116	PM_{10} = 63.0 AOD + 28.7	0.63	57
		Wet	PM_{10} = 26.9 AOD + 20.2	0.51	91	PM_{10} = 74.8 AOD + 12.4	0.87	6	-	-	-

It is noteworthy that the number of the AOD data becomes tremendously smaller after adopted cloud screening process. For dry season, the number of the available AOD data dropped by the factor around 1.5-4 from CF ≤ 10/10 to CF ≤ 4/10 and by the similar factor from CF ≤ 4/10 to CF ≤ 1/10. For wet season, the available AOD data dropped by the factor around 7-10 from CF ≤ 10/10 to CF ≤ 4/10 for Chiangmai, but almost reach zero at CF ≤ 4/10 for Bangkok and Rayong. This is due to the quite cloudy weather in Bangkok and Rayong throughout the year (CF = 7/10 ± 3/10 for dry season, CF = 9/10 ± 1/10 for wet season) compared to Chiangmai (CF = 5/10 ± 3/10 for dry season, CF = 9/10 ± 2/10 for wet season). Since the cloud screening process provide reasonably better AODs-PM_{10} correlations, further analysis was considered only the AOD data on clear-sky day with CF ≤ 1/10.

6.4 Effects of other meteorological parameters

A number of researches have provided evidences showing that meteorological variables play a crucial role in the robustness of the regression relationship between AODs and surface PM mass such as RH, WS, T, and mixing height (MH) (van Donkelaar et al. 2006; Gupta et al. 2006; Koelemeijer et al. 2006; Pelletier et al. 2007; Tian and Chen 2010; Wang et al. 2010).

In principle, the concentration of PM mass is measured in a dry condition while the measurement of AODs is conducted in an actual ambient environment. Therefore, the relationship of AOD-PM is expected to be dependent on the ambient RH. Air humidity accounts for changing the light-scattering properties of the aerosol due to its hygroscopic property. The higher the RH, the larger the size of hygroscopic particles and hence the larger the portion of light is scattered which results in the overestimation of AOD value (Zhang et al. 2009). In addition to the RH, planetary boundary layer (PBL) height or MH also plays a crucial role determining the volume in which the turbulence is active and available for the pollutants to disperse. The development of MH is related to WS, T, and RH. In general, a thinner MH corresponds to a higher aerosol density near the surface which represents almost the same amount of aerosol observed by the satellites. On the other hand, ground samplers detect a lower aerosol density for a thicker MH, but the

satellites still observe the same. Surface WS also plays another important role for aerosol generation and dispersion in horizontal direction (Dinoi et al. 2010). In term of surface T, higher T accelerates photochemical conversion of gaseous to secondary aerosol species, especially the production of sulfate which results in an overall increase of fine particle mass concentration in the atmosphere (Dawson et al. 2007; Liu et al. 2009). Since sulfate is known as a hygroscopic aerosol which is able to enhance the light-scattering properties of the aerosol, the MODIS algorithm seem to be more sensitive to fine particles and sulfates than to nitrate and dust (Engel-Cox et al. 2004; Wang and Martin 2007). In this way, the increase of sulfate aerosols may also affect the AODs-PM relationship.

This study aims to improve the correlation of AODs-PM_{10} by developing multiple linear regression models using retrieved satellite AODs with the consideration of meteorological effects and then use such models to estimate surface PM_{10} mass concentrations. The accuracy of such models depends on the strength of AODs-PM_{10} correlation which is also dependent on local meteorological parameters. The linear regression models in this section were then developed by using 5-year (2008-2012) data of satellite AODs retrieved from MODIS-Terra and MODIS-Aqua as well as meteorological parameters obtained from ground monitoring stations including surface RH, WS, and T over Chiangmai, Bangkok, and Rayong. These meteorological parameters can be basically monitored elsewhere which is suit for the MODIS near real-time AOD products to estimate surface PM mass concentrations. Table 6.3 summarizes 5-year data of RH, WS, and T during dry and wet season from 2008 to 2012 for Chiangmai, Bangkok, and Rayong. RH values in Bangkok and Rayong are commonly higher than Chiangmai for both during dry and wet season due to the closer city locations to the coastal areas. The WS data in Bangkok and Rayong present lower levels compared to Chiangmai due to the characteristic of urban and industrial areas with the presence of high-rising buildings. According to the more northern latitude and higher elevation of Chiangmai city, the temperature levels in Chiangmai are normally cooler than the other two cities.

Table 6.3 Meteorological parameters during dry and wet seasons for Chiangmai, Bangkok, and Rayong

City	RH (%, 2008-2012)						WS (m/s, 2008-2012)						T (ºC, 2008-2012)					
	Dry			Wet			Dry			Wet			Dry			Wet		
	Avg±SD	Max	Min	Avg±SD	Max	Min	Avg±SD	Max	Min	Avg±SD	Max	Min	Avg±SD	Max	Min	Avg±SD	Max	Min
Chiangmai	64.8±9.5	93.0	40.0	76.8±7.1	95.0	46.0	1.9±0.5	4.3	0.9	2.0±0.4	4.2	0.9	26.1±3.1	33.4	17.8	28.2±1.5	34.1	24.0
Bangkok	69.6±8.1	92.0	47.0	78.0±6.5	97.0	57.0	1.3±0.2	2.0	0.7	1.8±0.2	1.9	0.7	28.9±2.0	33.6	18.7	29.4±1.4	34.4	25.0
Rayong	75.8±7.5	93.0	46.0	80.7±4.8	94.0	60.0	1.6±0.6	4.0	0.3	1.6±0.5	3.3	0.5	28.2±1.4	32.3	22.5	28.8±1.2	32.4	23.9

The development of the regression models between satellite AODs and surface PM_{10} mass concentration was performed following the structure as described earlier in model development process. Two type of regression models were developed and compared for each city in this study. First, simple linear regression model (Model 1) was developed by fitting between AODs and surface PM_{10} mass concentrations. Second, multiple linear regression model (Model 2) was developed to investigate the improvement of the model performance due to the meteorological parameter correction. Since the AOD data on clear-sky day with CF $\leq$ 1/10 provide the highest AODs-PM_{10} correlations, the development of Model 1 and 2 were then considered only when CF $\leq$ 1/10 which in this case is for dry season. The datasets of AODs retrieved from MODIS-Terra/Aqua with the coincident in space and time of surface PM_{10} mass concentration and meteorological parameter (RH, WS, and T) were fitted in the models to calculate model coefficients. Table 6.4 summarizes model fitting results for Model 1 and 2. The overall results for all the cities show that both Model 1 and 2 performances are statistically significant with the *p* value < 0.001. In Chiangmai as indicated by adjusted r^2 values, the Model 1 and 2 are able to explain 72-78% (r = 0.85-0.88) and 73-81% (r = 0.86-0.90) of the variability in surface PM_{10} mass concentrations, respectively. However, the adjusted r^2 values of Model 2 did not increase much compared to Model 1 for both AODs retrieved from Terra and Aqua satellites implying that correcting the model by meteorological parameters, i.e. surface RH, WS, and T, may not significantly improve the predictive performance of the model. In case of Bangkok and Rayong, the adjusted r^2 values are generally low compared to Chiangmai city. The Model 1 and 2 explain 15-43% and 42-57%, respectively for Bangkok and 38-54% and 42-62%, respectively for Rayong of the temporal variability in surface PM_{10} mass concentrations. However, including meteorological data in Model 2 for Bangkok reasonably enhanced model performance by an increase of adjusted r^2 of 27%, 13%, and 34%, respectively for the analysis of AOD(Terra)-PM_{10}(9-12:00LT), AOD(Aqua)-PM_{10}(12-15:00LT), and AOD(Terra-Aqua)-PM_{10}(24hrs).

All the fitting results in Table 6.4 show the negative coefficients for RH and T. This supports the idea that incorporating these two parameters in the model helps correcting the overestimation of surface PM_{10} mass concentrations caused by the hygroscopic properties of the aerosols. In case of WS, since this study averaged 3-hour and 24-hour data of

surface PM_{10} mass concentrations concurrent with the overpass time of the satellite, surface WS is expected to influence on the AODs-PM relationship. Increasing level of WS can affect surface PM measurement by diluting PM mass concentration, thus the regression coefficient of WS is expected to be negative. From the model fitting results in Table 6.4 although positive coefficients appeared for WS in some case of the Model 2, these parameters were found to be not significant with the *p* value > 0.1 (Appendix C). Further analysis is then needed to focus on the significance of each parameter in the model. In addition, the effect of WS on AODs-PM correlation also depends on wind direction; whether the locations of the interested grids are in upwind or downwind of the pollutant emission sources, which is not included in this case study.

Table 6.4 Comparison of model fitting results for Model 1 and 2

City	AOD-PM_{10}	Regression Model at CF ≤ 1/10	r	adjusted r^2	*p* value
Chiangmai	AOD(Terra)-PM_{10}(9-12:00LT)	Model 1: PM_{10} = 24.30 + 171.42 (AOD)	0.85	0.72	3.12E-32
		Model 2: PM_{10} = 232.66 + 153.80 (AOD) - 1.71 (RH) - 14.93 (WS) - 2.77 (T)	0.89	0.79	2.17E-35
	AOD(Aqua)-PM_{10}(12-15:00LT)	Model 1: PM_{10} = 20.71 + 124.22 (AOD)	0.85	0.73	2.72E-29
		Model 2: PM_{10} = 109.32 + 128.01 (AOD) - 0.68 (RH) + 1.08 (WS) - 2.28 (T)	0.86	0.73	1.54E-30
	AOD(Terra-Aqua)-PM_{10}(24hrs)	Model 1: PM_{10} = 36.49 + 121.94 (AOD)	0.88	0.78	1.18E-104
		Model 2: PM_{10} = 100.24 + 110.43 (AOD) - 0.77 (RH) - 5.07 (WS) - 0.22 (T)	0.90	0.81	6.99E-110
Bangkok	AOD(Terra)-PM_{10}(9-12:00LT)	Model 1: PM_{10} = 37.35 + 38.64 (AOD)	0.40	0.15	2.53E-04
		Model 2: PM_{10} = 146.92 + 43.20 (AOD) - 0.39 (RH) - 27.80 (WS) - 1.94 (T)	0.66	0.42	8.12E-09
	AOD(Aqua)-PM_{10}(12-15:00LT)	Model 1: PM_{10} = 16.14 + 56.42 (AOD)	0.68	0.43	2.26E-10
		Model 2: PM_{10} = 36.05 + 51.35 (AOD) - 0.51 (RH) + 1.31 (WS) - 0.12 (T)	0.75	0.56	7.09E-10
	AOD(Terra-Aqua)-PM_{10}(24hrs)	Model 1: PM_{10} = 36.94 + 48.49 (AOD)	0.48	0.23	1.04E-08
		Model 2: PM_{10} = 154.65 + 50.53 (AOD) - 0.87 (RH) - 40.94 (WS) - 0.8 (T)	0.76	0.57	3.58E-22
Rayong	AOD(Terra)-PM_{10}(9-12:00LT)	Model 1: PM_{10} = 29.46 + 110.14 (AOD)	0.74	0.54	3.69E-08
		Model 2: PM_{10} = 129.57 + 113.99 (AOD) - 0.93 (RH) - 4.55 (WS) - 1.27 (T)	0.81	0.62	8.30E-08
	AOD(Aqua)-PM_{10}(12-15:00LT)	Model 1: PM_{10} = 28.65 + 62.89 (AOD)	0.63	0.38	5.80E-07
		Model 2: PM_{10} = 37.12 + 67.68 (AOD) - 0.21 (RH) + 1.03 (WS) - 0.02 (T)	0.65	0.42	2.68E-08
	AOD(Terra-Aqua)-PM_{10}(24hrs)	Model 1: PM_{10} = 44.17 + 96.22 (AOD)	0.65	0.42	4.56E-09
		Model 2: PM_{10} = 155.72 + 90.96 (AOD) - 1.11 (RH) - 11.98 (WS) - 0.70 (T)	0.75	0.53	7.13E-10

6.5 Model evaluation and comparison

To evaluate the validity of the model performance, Model 1 and Model 2 were applied to estimate surface PM_{10} mass concentrations over Chiangmai, Bangkok, and Rayong during dry season of 2007 (6 months of January-April and November-December) and 2013 (4 months of January-April). The estimated results were then compared with surface PM_{10} mass concentrations collected from PCD, Thailand during the same periods. Figure 6.3-6.5 present the scatter plots of estimated versus measured 3-hour/24-hour PM_{10} mass concentrations over Chiangmai, Bangkok, and Rayong, respectively for year 2007. For year 2013, scatter plots were presented in Appendix D.1-3. Since the weather in Thailand is commonly cloudy, the validation was performed both without and with cloud screening process ($CF \leq 4/10$ and $CF \leq 1/10$). The overall results in these three cities show that when the validation was conducted at lower CF, the correlation coefficients of the estimated and measured values became higher for both Model 1 and 2 and for all time window analysis (9-12:00LT, 12-15:00LT, and 24-hour), which emphasizes the effect of the cloud screening process on AODs-PM_{10} relationship.

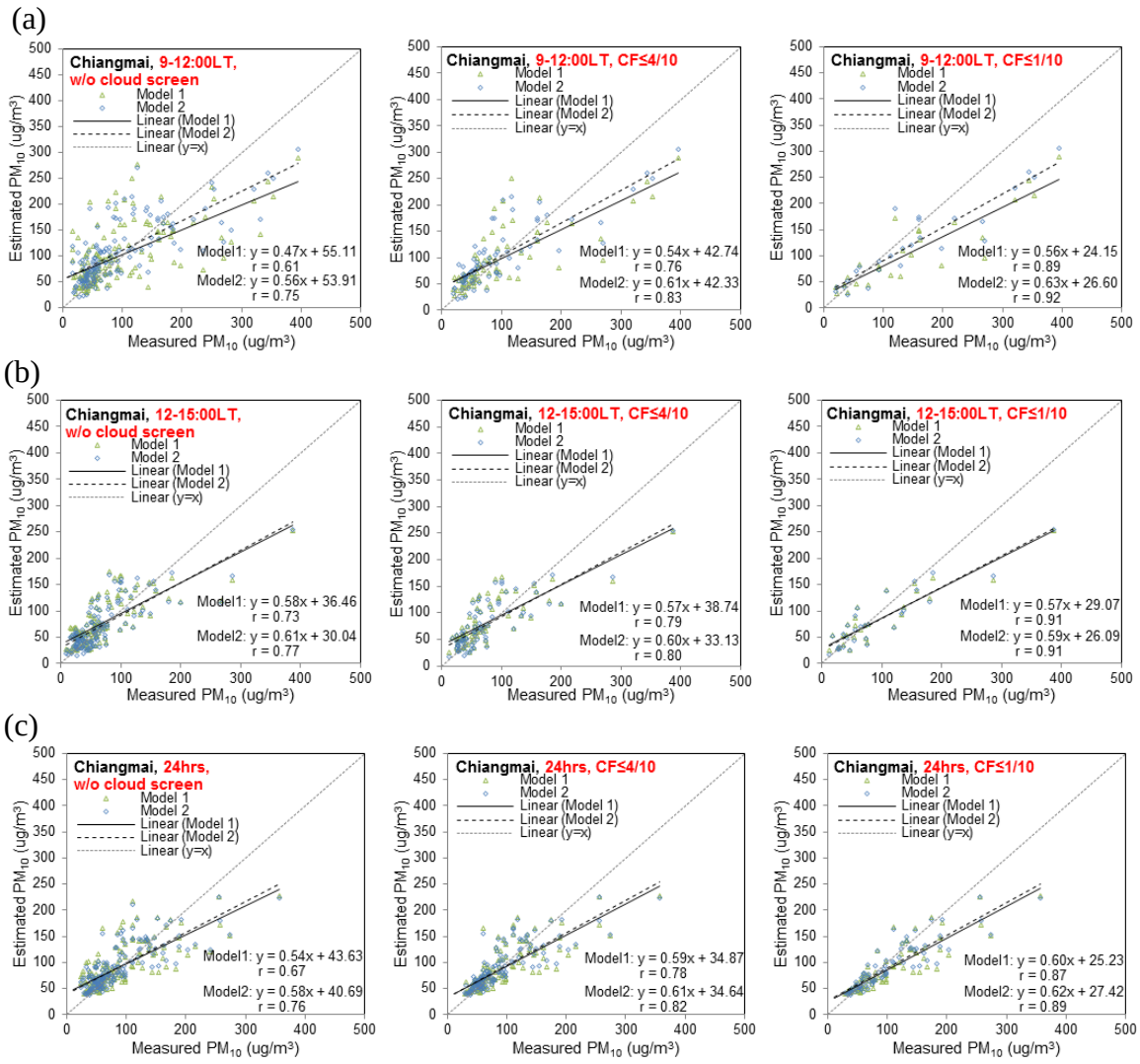

Figure 6.3 Scatter plots of estimated vs. measured PM_{10} concentrations over Chiangmai during dry season 2007 for 9-12:00LT (a), 12-15:00LT (b), and 24-hr (c) time windows

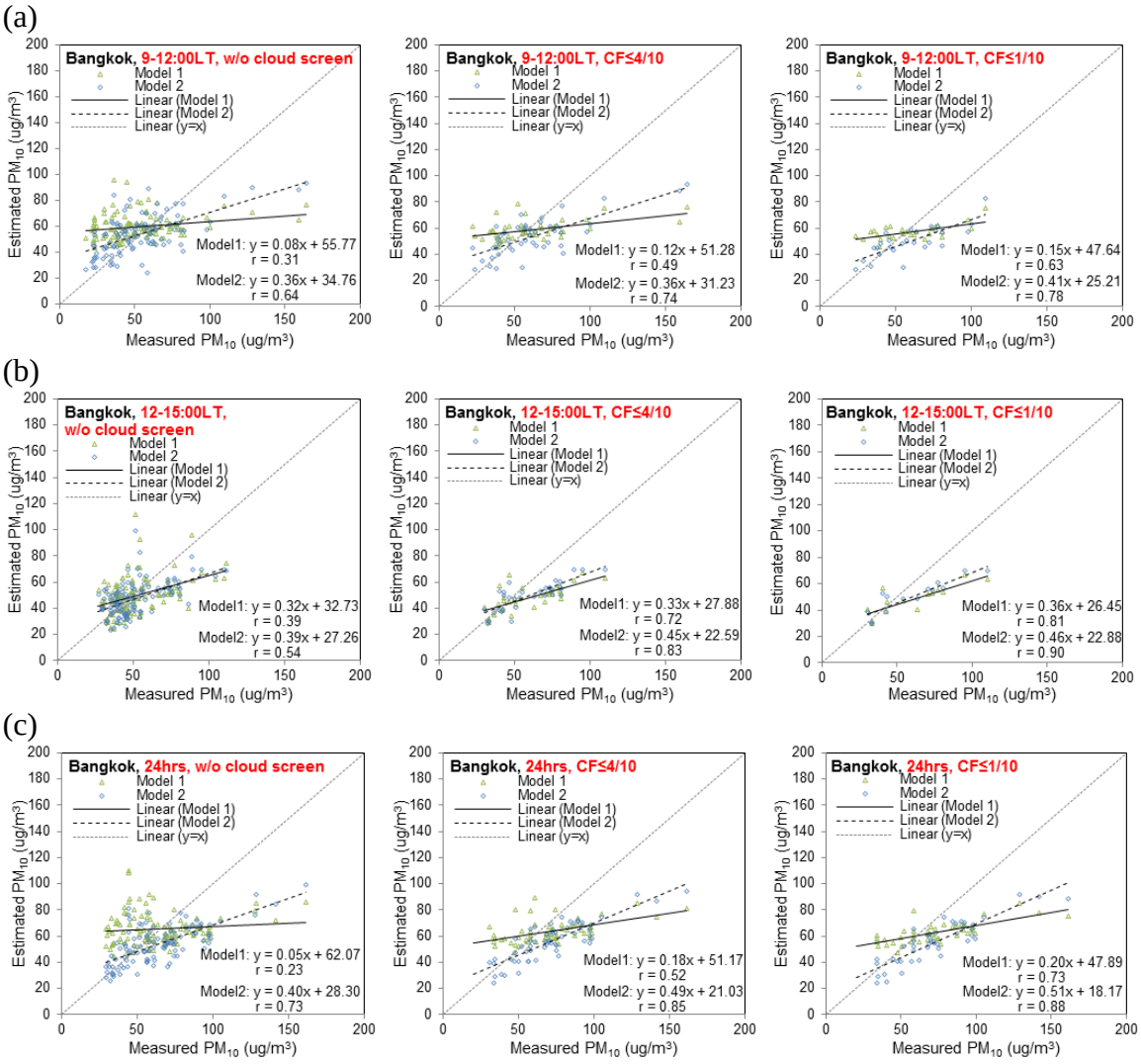

Figure 6.4 Scatter plots of estimated vs. measured PM_{10} concentrations over Bangkok during dry season 2007 for 9-12:00LT (a), 12-15:00LT (b), and 24-hr (c) time windows

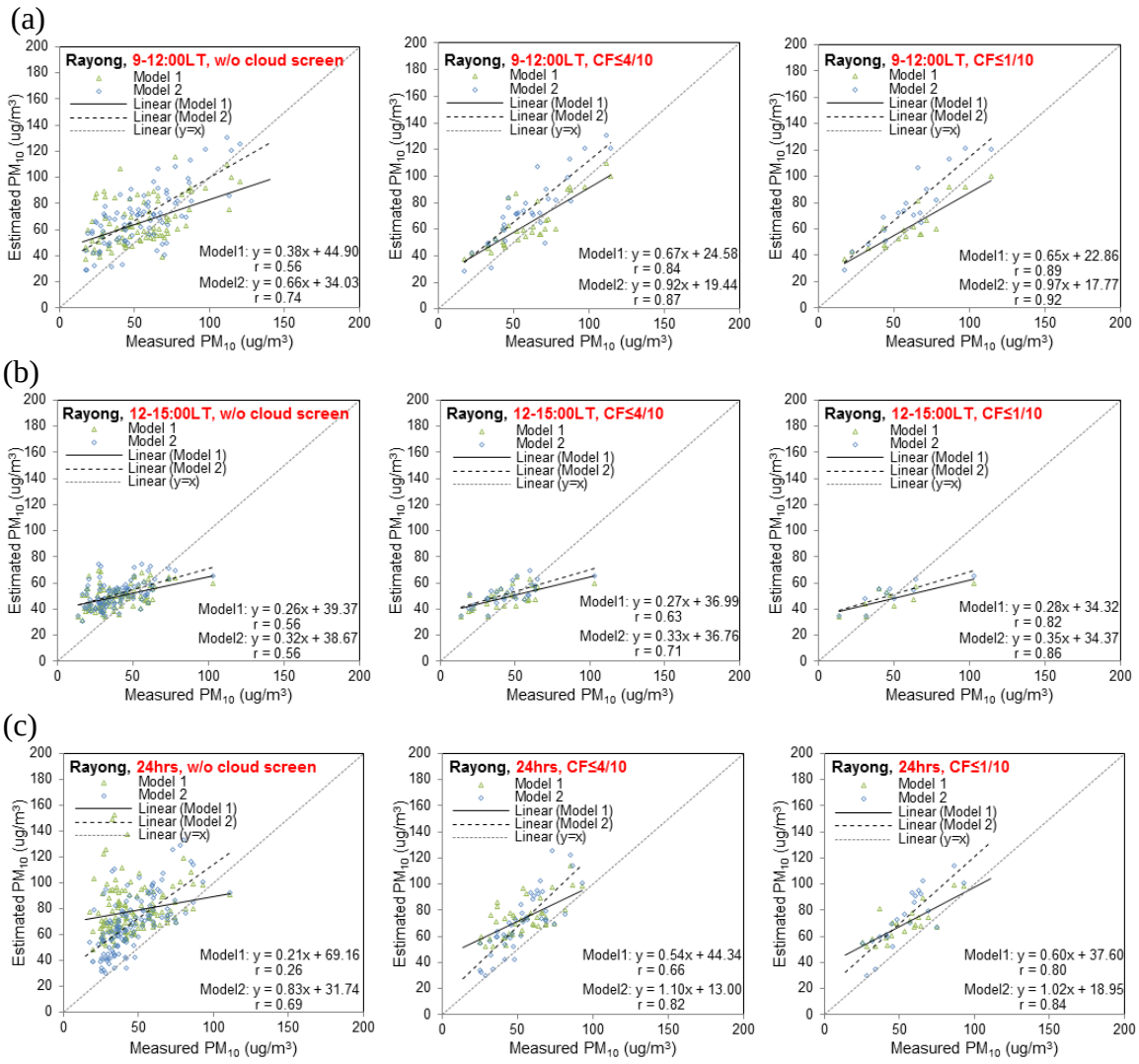

Figure 6.5 Scatter plots of estimated vs. measured PM_{10} concentrations over Rayong during dry season 2007 for 9-12:00LT (a), 12-15:00LT (b), and 24-hr (c) time windows

In case of Chiangmai (Figure 6.3), correcting the regression model by meteorological variables did not improve much the estimation of surface PM_{10} mass concentrations. The r values for Model 2 (r = 0.75-0.92) are mildly higher than Model 1 (r = 0.61-0.91). The first reason is probably due to the lower RH during dry season in Chiangmai (~ 65%) compared to Bangkok (~ 70%) and Rayong (~ 76%). As demonstrated in Day and Malm (2001) and Wang and Martin (2007) that the light-scattering properties of hygroscopic aerosol would not change significantly with RH when RH is less than around 70%, as a result modifying the regression model by including RH may not improve surface PM_{10} mass estimation in Chiangmai as much as in the other two cities. These results are similar with Tsai et al. 2011 that the RH values in their study were around 50-65%. Moreover, high levels of sulfate concentration are generally found in industrial areas (like Bangkok and Rayong), an increase in the production of sulfate aerosols due to high T may be not significant enough to affect the AODs-PM_{10} relationship in Chiangmai where there are more of residential areas. Figure 6.6a, b illustrate daily plots between estimated and measured 3-hour/24-hour PM_{10} mass concentrations without cloud screen of AODs during biomass burning period from 1st January to 31st March for year 2007 and 2013, respectively over Chiangmai city. The modeling results from both Model 1 and 2 are very well correlated with measured PM_{10} mass concentrations both in term of quantitative levels and diurnal variations. Nevertheless, during March 2007 the model seem to underestimate the measured ones. Chiangmai has been experienced air pollution haze episodes each year around February-April (highest in March) due to forest fires and agricultural burning. However, the most severe haze episodes were reported in March 2007 when the whole province was blanketed with haze for two weeks (Kim Oanh and Leelasakultum 2011). This could be the reason for the underestimation of PM_{10} mass concentrations during March 2007 since the modelling database did not include the information of this year. Table 6.5 and 6.6 summarize the results of model validation for year 2007 and 2013, respectively including correlation coefficient (r), an increase of r value of Model 2 compared to Model 1, mean ± 1 standard deviation (SD) of actual PM_{10} mass concentration, root-mean-square error (RMSE), and number of the data (N) at different class of cloudiness. All the results in Chiangmai present that the RMSE values of Model 2 are smaller than Model 1 and smaller than ± 1 SD.

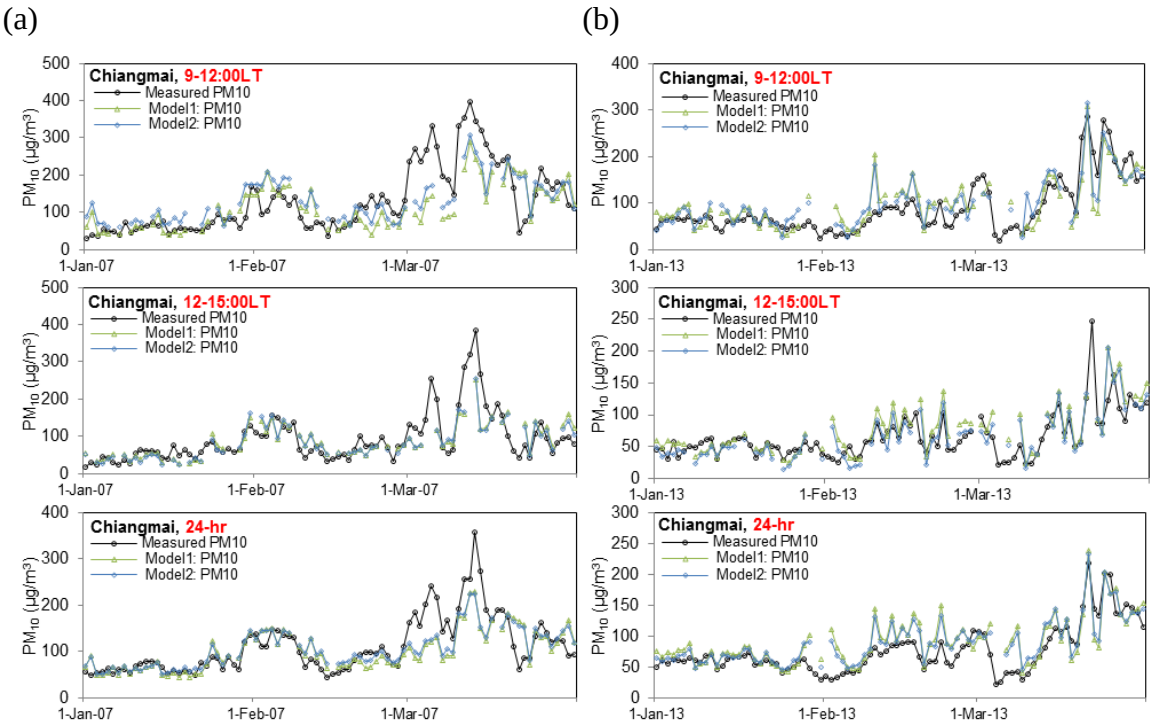

Figure 6.6 Daily plots of estimated and measured 3-hour/24-hour PM_{10} mass concentrations during biomass burning period for year 2007 (a) and 2013 (b)

For Bangkok and Rayong, the model performance for these two cities are not satisfying as much as for Chiangmai city, however, including meteorological variables in the model provided relatively better estimation results for all cases of Model 2 (Bangkok: r = 0.54-0.90, Rayong: r = 0.56-0.92) compared to Model 1 (Bangkok: r = 0.23-0.81, Rayong: r = 0.26-0.89). The regression lines of Model 2 provide steeper slope (closer to 1) and smaller intercept (closer to zero) implying that Model 2 are more sensitive to actual surface PM_{10} mass concentrations than Model 1. In addition, RMSE values of Model 2 are lower than Model 1 considering all class of cloudiness for both year 2007 and 2013. Most of the results in Figure 6.5 shows that Model 1 and 2 slightly overestimated actual values for Rayong city as can be seen from the data points scattering above the y=x line. For Bangkok, Figure 6.4 presents that the models slightly underestimated the actual ones when the values are approximately larger than 60 µg/m^3. Nevertheless, the RMSE values of both Model 1 and 2 in Bangkok and Rayong cities are generally smaller than ± 1 SD of measured PM_{10} mass concentrations. The results also show that when the validation was restricted to more clear-sky day, the effect of the other meteorological parameter (RH,

WS, and T) to improve the estimation became less; as presented in the increase of r values of Model 2 compared to Model 1 that reveal the smaller values when CF became lower. This is due to the stronger sensitivity of AODs to PM_{10} compared to other parameters when there is less cloud-contamination in AOD values. However, since Thai weather is usually cloudy, adopting clear-sky AODs as a representative of surface PM concentrations on the daily basis is considerably difficult. This analysis highlights the significance of the meteorological factors, i.e. RH, WS, and T, in order to obtain more frequent PM data with higher accuracy.

Since Model 1 and 2 over Chiangmai city provide the highest model performance compared to Bangkok and Rayong cities, further analysis used Model 1 and 2 of Chiangmai city to estimate surface PM_{10} mass concentrations over seven cities around Chiangmai in northern Thailand i.e., Chiangrai, Maehongson, Phayao, Nan, Lamphun, Lampang, and Phrae, during January-March 2013. The estimated results were then validated with the surface data from PCD stations. Figure 6.7 presents the locations of 0.5° × 0.5° grid boxes of the averaged satellite AOD data centering at each PCD station for each considered city around Chiangmai.

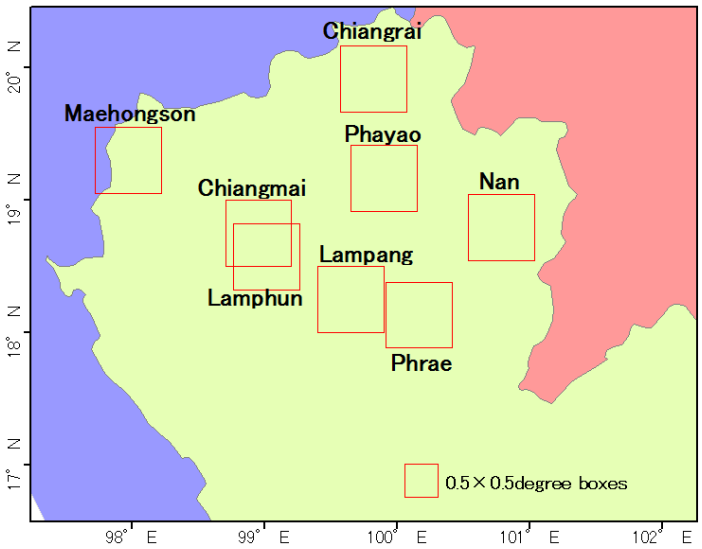

Figure 6.7 Lacations of AOD grid boxes centering at ground stations in northern Thailand

Table 6.5 The results of model validation for surface PM_{10} concentration estimations during 2007

City	Estimated vs. PCD Measured PM_{10} (2007)	Model	w/o cloud screen					CF ≤ 4/10					CF ≤ 1/10				
			r	r increase	mean±1SD (PCD PM_{10})	RMSE	N	r	r increase	mean±1SD (PCD PM_{10})	RMSE	N	r	r increase	mean±1SD (PCD PM_{10})	RMSE	N
Chiangmai	9:00-12:00LT	Model 1	0.61	0.14	94.0±77.2	61.5	142	0.76	0.07	97.2±81.9	54.8	73	0.89	0.03	154.6±108.7	79.9	26
		Model 2	0.75			53.8		0.83			47.9		0.92			64.2	
	12:00-15:00LT	Model 1	0.73	0.04	57.4±50.6	38.3	131	0.79	0.01	74.5±60.2	39.2	76	0.91	0.00	95.0±82.6	47.0	29
		Model 2	0.77			33.8		0.80			37.7		0.91			46.3	
	0:00-24:00LT	Model 1	0.67	0.09	69.9±51.4	42.2	162	0.78	0.04	87.3±53.7	34.3	131	0.87	0.02	101.9±63.0	37.2	78
		Model 2	0.76			36.7		0.82			31.6		0.89			33.9	
Bangkok	9:00-12:00LT	Model 1	0.31	0.33	47.8±25.5	26.8	108	0.49	0.25	64.4±35.4	32.7	48	0.63	0.15	58.6±22.6	19.2	27
		Model 2	0.64			19.9		0.74			25.7		0.78			18.0	
	12:00-15:00LT	Model 1	0.39	0.15	49.1±18.1	18.0	117	0.72	0.11	62.5±21.1	20.8	34	0.81	0.09	60.5±24.0	20.6	14
		Model 2	0.54			15.5		0.83			17.6		0.90			17.2	
	0:00-24:00LT	Model 1	0.23	0.50	57.7±25.1	26.1	108	0.52	0.33	71.6±25.6	23.7	64	0.73	0.15	73.3±27.7	25.0	49
		Model 2	0.73			18.7		0.85			21.7		0.88			23.4	
Rayong	9:00-12:00LT	Model 1	0.56	0.18	50.9±23.7	24.6	87	0.84	0.03	59.5±23.3	14.8	33	0.89	0.03	60.1±24.3	13.9	18
		Model 2	0.74			23.2		0.87			20.5		0.92			22.1	
	12:00-15:00LT	Model 1	0.56	0.00	37.9±16.3	18.6	94	0.63	0.08	44.7±18.1	16.7	30	0.82	0.04	49.0±23.2	25.1	10
		Model 2	0.56			19.0		0.71			16.6		0.86			23.0	
	0:00-24:00LT	Model 1	0.26	0.43	42.1±17.3	41.4	134	0.66	0.16	53.0±17.1	25.6	44	0.80	0.04	53.7±17.6	21.8	22
		Model 2	0.69			29.0		0.82			23.7		0.84			26.5	

Table 6.6 The results of model validation for surface PM_{10} concentration estimations during 2013

City	Estimated vs. PCD Measured PM_{10} (2013)	Model	w/o cloud screen					CF ≤ 4/10					CF ≤ 1/10				
			r	r increase	mean±1SD (PCD PM_{10})	RMSE	N	r	r increase	mean±1SD (PCD PM_{10})	RMSE	N	r	r increase	mean±1SD (PCD PM_{10})	RMSE	N
Chiangmai	9:00-12:00LT	Model 1	0.68	0.13	80.4±56.9	48.8	102	0.75	0.08	99.1±60.8	44.3	54	0.81	0.08	111.9±64.8	43.0	22
		Model 2	0.81			37.7		0.83			37.2		0.89			35.0	
	12:00-15:00LT	Model 1	0.72	0.04	58.7±30.7	35.5	98	0.88	0.00	64.4±29.5	21.5	58	0.93	0.01	65.4±26.2	14.6	16
		Model 2	0.76			27.4		0.87			19.0		0.94			15.6	
	0:00-24:00LT	Model 1	0.68	0.09	67.3±39.2	41.2	114	0.77	0.05	79.3±35.9	28.4	95	0.88	0.02	85.7±40.6	20.9	51
		Model 2	0.77			35.3		0.82			25.5		0.90			20.0	
Bangkok	9:00-12:00LT	Model 1	0.44	0.22	48.0±26.3	28.0	62	0.52	0.29	57.7±19.7	17.2	16	-	-	-	-	-
		Model 2	0.66			23.7		0.81			12.4		-			-	
	12:00-15:00LT	Model 1	0.50	0.07	36.8±16.6	24.2	72	0.83	0.04	41.1±14.9	11.7	16	-	-	-	-	-
		Model 2	0.57			21.6		0.87			10.9		-			-	
	0:00-24:00LT	Model 1	0.41	0.3	40.0±20.1	35.1	84	0.50	0.26	53.6±17.8	19.4	27	-	-	-	-	-
		Model 2	0.71			26.2		0.76			17.0		-			-	
Rayong	9:00-12:00LT	Model 1	0.51	0.19	55.8±29.3	36.7	44	0.57	0.21	60.4±22.5	28.0	14	-	-	-	-	-
		Model 2	0.70			31.2		0.78			22.3		-			-	
	12:00-15:00LT	Model 1	0.57	0.06	46.6±22.4	21.8	57	0.73	0.06	47.7±21.3	21.7	13	-	-	-	-	-
		Model 2	0.63			21.3		0.79			19.9		-			-	
	0:00-24:00LT	Model 1	0.41	0.24	51.0±27.8	44.2	72	0.52	0.20	60.8±28.0	33.3	19	-	-	-	-	-
		Model 2	0.65			32.3		0.72			24.9		-			-	

The daily plots of estimated and PCD measured PM_{10} mass concentrations over these seven cities are given in Figure 6.8 for the time window at 9:00-12:00LT and 12:00-15:00LT. For the time window at 0:00-24:00LT, the results are presented in Appendix E. From Figure 6.8, the estimated PM_{10} concentrations from both Model 1 and 2 are generally in good agreement with actual one, especially during biomass burning period in March. Most of the modeling results can capture the high episode of PM_{10} mass. Model 2 slightly provides better correlation coefficients and Model 1 for all the cities and all time windows. In addition, the RMSE values of the estimated PM_{10} mass concentrations from Model 2 compared to the actual one are smaller than from Model 1 for all cases except for Phrae city. Well correlated results in term of absolute level between the estimated PM_{10} mass concentrations and the actual one can be seen in Phayao, Nan, Lamphun, and Lampang, particularly at 12:00-15:00LT (during the overpass time of MODIS-Aqua) and 0:00-24:00LT time windows. However, there are still some overestimations during January-February for most of the results at 9:00-12:00LT time window (during the overpass time of MODIS-Terra). For Chiangrai, Maehongson, and Phrae, most of the modeling results seem to underestimate the actual PM_{10} mass, especially over Maehongson city where the highest concentration in March during the morning almost reached 700 $\mu g/m^3$ while the highest levels in the other cities were generally lower than 300 $\mu g/m^3$. Table 6.7 summarizes the comparison results of estimated and measured surface PM_{10} concentrations for all time windows over the seven cities. The correlation coefficients for all the cities are between 0.75-0.92 for Model 1 and 0.78-0.93 for Model 2 at all time windows. The RMSE values of both Model 1 and 2 are all smaller than ± 1 SD of the actual one. More details of the analysis are presented in the scatter plots of the estimated versus PCD measured PM_{10} in Appendix D.4. From the scatter plots, the results show that slopes of Model 2 are closer to 1 compared to Model 1. Moreover, the intercepts of Model 2 also closer to zero compared to Model 1. This analysis suggests that satellite AOD observations can provide the data of PM_{10} mass concentration, particularly during high episode of PM_{10} which in this case is during biomass burning period, and are able to be used as a proxy of surface PM_{10} mass after the careful validation, especially in the limited in situ availability. Furthermore, including meteorological parameters (RH, WS, and T) into the models also help improving the estimated results in term of both quantitative level and diurnal variation.

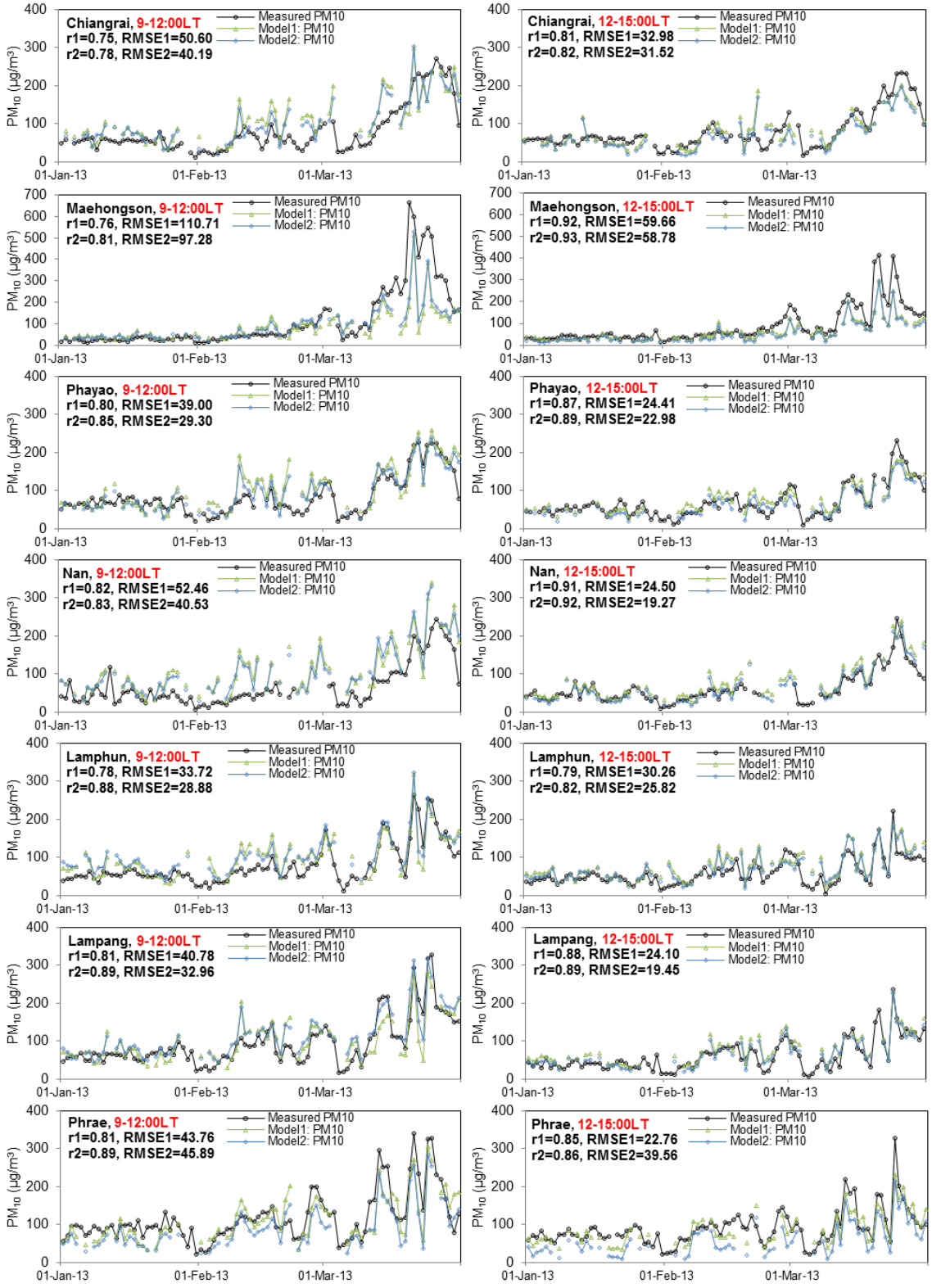

Figure 6.8 Daily plots of estimated and measured 3-hour PM_{10} mass concentrations during biomass burning period for year 2013 over northern Thailand

Table 6.7 The results of model validation for surface PM_{10} concentration estimations during 2013 over northern Thailand

Station name (City)	Latitude	Longitude	Estimated vs. PCD Measured PM_{10} (2013)	Model	r	mean±1SD (PCD PM_{10})	RMSE	N
Chiangrai	19.91°N	99.82°E	9:00-12:00LT	Model 1	0.75	80.03±61.62	50.60	64
				Model 2	0.78		40.19	
			12:00-15:00LT	Model 1	0.81	78.33±49.35	32.98	64
				Model 2	0.82		31.52	
			0:00-24:00LT	Model 1	0.77	79.44±51.35	36.55	80
				Model 2	0.81		30.18	
Maehongson	19.30°N	97.97°E	9:00-12:00LT	Model 1	0.76	110.76±143.16	110.71	73
				Model 2	0.81		97.28	
			12:00-15:00LT	Model 1	0.92	87.50±84.07	59.66	74
				Model 2	0.93		58.78	
			0:00-24:00LT	Model 1	0.84	88.22±93.39	60.06	87
				Model 2	0.88		56.08	
Phayao	19.16°N	99.90°E	9:00-12:00LT	Model 1	0.80	83.92±51.64	39.00	72
				Model 2	0.85		29.30	
			12:00-15:00LT	Model 1	0.87	67.47±42.56	24.41	61
				Model 2	0.89		22.98	
			0:00-24:00LT	Model 1	0.86	69.74±45.33	30.84	81
				Model 2	0.90		24.63	
Nan	18.79°N	100.78°E	9:00-12:00LT	Model 1	0.82	65.56±55.15	52.46	70
				Model 2	0.83		40.53	
			12:00-15:00LT	Model 1	0.91	61.91±42.28	24.50	66
				Model 2	0.92		19.27	
			0:00-24:00LT	Model 1	0.86	75.25±48.00	31.86	83
				Model 2	0.88		28.52	
Lamphun	18.57°N	99.01°E	9:00-12:00LT	Model 1	0.78	79.41±53.39	33.72	72
				Model 2	0.88		28.88	
			12:00-15:00LT	Model 1	0.79	59.33±35.43	30.26	75
				Model 2	0.82		25.82	
			0:00-24:00LT	Model 1	0.76	77.03±36.91	25.57	87
				Model 2	0.82		24.43	
Lampang	18.25°N	99.65°E	9:00-12:00LT	Model 1	0.81	93.76±62.81	40.78	73
				Model 2	0.89		32.96	
			12:00-15:00LT	Model 1	0.88	60.19±41.48	24.10	63
				Model 2	0.89		19.45	
			0:00-24:00LT	Model 1	0.86	79.49±42.51	24.29	83
				Model 2	0.91		20.62	
Phrae	18.13°N	100.16°E	9:00-12:00LT	Model 1	0.81	116.84±66.21	43.76	73
				Model 2	0.89		45.89	
			12:00-15:00LT	Model 1	0.85	89.81±47.50	22.76	67
				Model 2	0.86		39.56	
			0:00-24:00LT	Model 1	0.88	94.81±42.39	20.31	81
				Model 2	0.90		21.42	

Chapter 7 Comparison of Source Emissions and Satellite Observations

7.1 Source emission data collection

Pollution source inventories considered in this study are REAS and MACCity inventories. These two inventories were used to comparably analyze with satellite observations to investigate the ability of the satellite to observe surface emissions. The details of REAS and MACCity are provided as follows.

1) REAS emission inventory

Regional Emission inventory in Asia (REAS) is the inventory that integrates historical, present, and future emissions for the period 1980-2020 covering East, Southeast, and South Asia. It was constructed for historical emissions for 1980-2003, and predicted emissions for 2004-2009 on the basis of emissions in 2003 and 2010. For the future emissions in 2010 and 2020, they were projected on the basis of emissions in 2000 and emission scenarios. For China, three emission scenarios were also developed for year 2010 and 2020 in term (1) Policy Failed Case (PFC), (2) Reference (REF), and (3) Policy Success Case (PSC). REAS emissions were estimated based on fuel combustion sources and non-combustion sources as a part of anthropogenic activities including power sectors, industrial sectors, transport sectors, and other (mainly domestic) sectors. It mainly focused on the emissions of BC (black carbon), CO, NMVOCs (non-methane volatile organic compounds), NO_x, OC (organic carbon), and SO_2. More details on the development of REAS anthropogenic emission source are provided in Ohara et al. (2007). Moreover, CH_4 (methane) emissions from rice fields and livestock were also considered in REAS inventories. The details are provided in Yamaji et al. (2003) and Yan et al. (2003b, 2003a). These emission estimations were calculated in term of yearly average and distributed into a 0.5° × 0.5° grid using index database information such as population, positions of the large point sources, land cover, and land area.

2) MACCity emission inventory

MACCity emission dataset is a new extension of the ACCMIP and the RCPs emissions dataset as part of MACC (Monitoring Atmospheric Composition & Climate) and CityZen EU project. At first, in order to support the fifth IPCC-AR5 (Intergovernmental Panel for Climate Change Assessment Report 5), ACCMIP (Atmospheric Chemistry and Climate – Model Intercomparison Project) and RCP (Representative Concentration Pathways) emissions were developed on a decadal basis to provide a dataset of monthly, sectoral, gridded anthropogenic and biomass burning emissions during the historical period of 1850 – 2000 by using year 2000 as a reference year. For the future period, the extended emission dataset was developed by using RCP8.5 emission scenario for the year 2005 and 2010. This dataset was extended on a yearly basis for the period 1960-2010 for the anthropogenic emissions, and 1960-2008 for the biomass burning emissions in term of gridded monthly mean global sectoral emissions and was referred as MACCity. For ACCMIP MACCity anthropogenic inventory, emissions comprise of the emissions originating from energy use in stationary and mobile sources, industrial processes, domestic and agricultural activities. For ACCMIP MACCity biomass burning inventory, emissions consist of all emissions resulting from natural and man-made activities which are quantified for two sectors; forest and grassland/savanna. The spatial resolution of the MACCity emission dataset is 0.5° × 0.5° grid. Further description of MACCity emission datasets are provided in Diehl et al. (2012), Granier et al. (2011), Lamarque et al. (2010), and van der Werf et al. (2006).

3) Integration of satellite measurements and source emissions

The objective of this part is to comparably analyze the consistency between satellite observations and emissions of the pollutants. Satellite NO_2 columns were retrieved from GOME, SCIAMACHY, OMI, and GOME-2. Satellite CO columns retrieved from MOPITT. NO_x and CO emissions were derived from REAS (anthropogenic source) and MACCity (anthropogenic and biomass burning sources) inventories through ECCAD-Ether (Emissions of atmospheric Compounds & Compilation of Ancillary Data) database website from 1996 to 2008. Since the spatial resolutions of both emission inventories are

at 0.5° degree, the comparison between satellite and emission datasets were then set at 0.5° grid size covering the interested cities to facilitate the comparison between them. All the satellite data and emission data that fall within this grid size were averaged and compared together.

The analysis in this case was separated into two parts; yearly analysis and monthly analysis. For the first part, monthly data of MACCity emissions (NO_x and CO) and satellite retrievals (NO_2 and CO columns) were averaged in term of yearly average, and then compared together in order to study interannual variation and long-term evolution of the pollutant emissions. For REAS emissions, since the data format are originally provided in term of yearly average, both NO_x and CO emissions from REAS were directly compared with those from MACCity and satellite retrievals.

For the second part, MACCity NO_x and CO emissions were obtained in term of monthly average from both anthropogenic emissions and biomass burning emissions. Monthly NO_x and CO emissions were then compared with monthly satellite retrievals of NO_2 columns and CO columns, respectively in order to investigate the consistency of seasonal variation between them. Moreover, the MACCity anthropogenic emissions and biomass burning emissions were compared together to investigate the dominant emission in that area.

7.2 Long-term comparison of source emissions and satellite observations

7.2.1 Yearly analysis

1) satellite NO_2 columns versus NO_x emissions

In this section, REAS and MACCity NO_x emission inventories were derived in term of yearly data to study the evolution of NO_x emissions over the study areas during the period 1996–2008. Figure 7.1 presented the annual trend of REAS and MACCity NO_x emissions together with the tropospheric NO_2 columns data from GOME, SCIAMACHY and GOME-2 satellites. The averaged data of tropospheric NO_2 columns from these three satellites (black star symbol) were calculated based on yearly averages in order to

investigate the consistency with NO_x emissions. The measurements of OMI are not included in this part since OMI have the different satellite overpass time. Figure 7.1a-c gives examples of the results for Shanghai, Naypyidaw and Jakarta cities, respectively. The orange diamond symbol represents anthropogenic NO_x emissions from REAS inventory, the blue diamond symbol represents anthropogenic NO_x emissions from MACCity inventory, and the red circle symbol represents the sum of anthropogenic and biomass burning NO_x emissions (total NO_x emissions) from MACCity inventory.

Table 7.1 summarizes the % increasing trend over the study period for satellite NO_2 columns and NO_x emissions for all the cities. In case of China, both NO_x emissions from REAS and MACCity inventories and tropospheric NO_2 columns show increasing trends with the % increase over Shanghai city of 4.72, 4.61, and 14.94 per year, respectively, and over Beijing city of 3.70, 6.61, and 9.45 per year, respectively. The earlier study of Uno et al. (2007) over CEC region during 1996 to 2003 shows that REAS NO_x emissions and tropospheric NO_2 columns retrieved from GOME and simulated from CMAQ model have similar increasing trends, but GOME data give a steeper trend after the year 2000. Their results are similar with this study as presented in Figure 7.1a for Shanghai. From Table 7.1, the cities that have increasing trends of both total NO_x emissions and satellite NO_2 columns more than 2 % per year are Hanoi, Bangkok, Phnom Penh, and Kuala Lumpur. For the cities that have increasing trends less than 2 % per year are Manila, Bandar Seri Begawan, and Jakarta. The city that has decreasing trends of both total NO_x emissions and satellite NO_2 columns is Tokyo with the % decrease of -3.73 and -1.71 per year, respectively. In case of Naypyidaw city as presented in Figure 7.1b, even though the long-term trends of NO_x emissions and tropospheric NO_2 columns are demonstrated in opposite way, the interannual variability in some years presents the similar pattern between NO_2 columns and NO_x emissions from biomass burning activity which is dominant in that area. This suggests that for the further study, it should be considered more on interannual variation. Singapore city also reveals the opposite trend between NO_x emissions and NO_2 columns. From Table 7.1, Singapore presents a significant increasing trend of NO_2 columns with the % increase of 7.52 per year, while the trend of NO_x emissions from both REAS and MACCity are relatively constant. This indicates that NO_x emissions in Singapore may be underestimated. For Jakarta, Figure 7.1c shows that NO_x emissions

from MACCity are around 3 times higher than REAS emission. However, long-term trends of both inventories and NO_2 columns are presented in the similar way with slightly increasing trends of 3.44, 1.59, and 0.93 % per year for REAS NO_x emission, MACCity NO_x emission, and NO_2 columns, respectively. Time series of NO_x emissions and satellite NO_2 retrievals for other cities are presented in Appendix F.1.

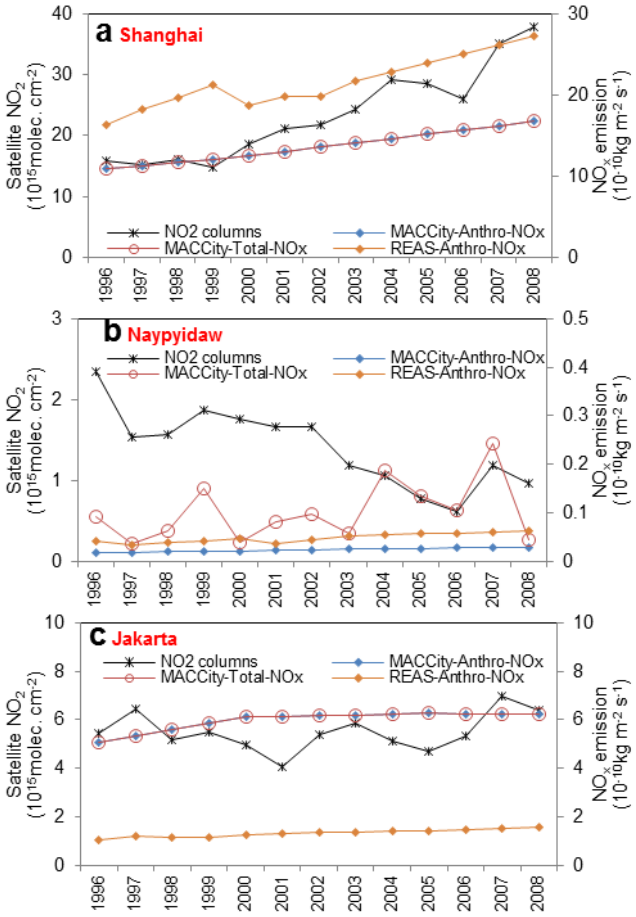

Figure 7.1 Long-term annual analysis of satellite NO_2 columns versus NO_x emissions for Shanghai (a), Naypyidaw (b) and Jakarta (c)

Table 7.1 Summary of percent increasing trends of NO_2 columns and NO_x emissions obtained from REAS and MACCity inventories during 1996-2008

City	NO_2 columns (GOME, SCIAMACHY, GOME-2) (10^{15}molec.cm^{-2})			REAS NO_x emissions Anthropogenic (10^{-10}kg km^{-2} s^{-1})			MACCity NO_x emissions Anthropogenic (10^{-10}kg km^{-2} s^{-1})			MACCity NO_x emissions Anthropogenic + Biomass burning (10^{-10}kg km^{-2} s^{-1})		
	Ref. 1996	%increase 12yr^{-1}	%increase yr^{-1}	Ref. 1996	%increase 12yr^{-1}	%increase yr^{-1}	Ref. 1996	%increase 12yr^{-1}	%increase yr^{-1}	Ref. 1996	%increase 12yr^{-1}	%increase yr^{-1}
Beijing	19.99	113.43	9.45	9.30	44.42	3.70	4.74	79.69	6.64	4.76	79.37	6.61
Shanghai	12.35	179.30	14.94	16.81	56.66	4.72	10.72	55.34	4.61	10.72	55.36	4.61
Tokyo	17.24	-20.52	-1.71	3.79	0.54	0.04	2.32	-46.21	-3.85	2.32	-44.76	-3.73
Hanoi	1.89	83.65	6.97	0.74	70.23	5.85	0.63	131.79	10.98	0.63	131.99	11.00
Naypyidaw	2.03	-61.84	-5.15	0.04	77.05	6.42	0.02	56.94	4.74	0.07	114.65	9.55
Vientiane	2.42	-31.21	-2.60	0.33	-6.00	-0.50	0.10	44.28	3.69	0.14	7.06	0.59
Manila	3.20	2.68	0.22	0.75	23.70	1.98	0.59	22.61	1.88	0.59	22.70	1.89
Bangkok	4.00	37.73	3.14	2.64	33.19	2.77	2.29	35.62	2.97	2.29	35.59	2.97
Phnom Penh	1.03	47.99	4.00	0.20	37.19	3.10	0.03	609.76	50.81	0.04	459.53	38.29
Bandar Seri Begawan	0.86	10.41	0.87	1.25	50.59	4.22	0.79	11.78	0.98	0.83	12.86	1.07
Kuala Lumpur	2.26	28.20	2.35	0.42	64.69	5.39	0.21	40.61	3.38	0.22	44.55	3.71
Singapore	4.94	90.24	7.52	17.81	-9.39	-0.78	10.29	-6.00	-0.50	10.29	-5.99	-0.50
Jakarta	5.20	11.14	0.93	1.11	41.23	3.44	5.46	19.12	1.59	5.46	19.14	1.59
Dili	0.44	-13.37	-1.11	0.02	30.51	2.54	0.11	18.53	1.54	0.11	23.22	1.93

2) satellite CO columns versus CO emissions

For the analysis of long-term annual trends between CO emissions and satellite CO columns, CO emissions were derived from REAS inventory for anthropogenic emission and from MACCity inventory for both anthropogenic and biomass burning emissions. Total CO columns were retrieved from MOPITT satellite. Time series of these datasets are presented during 2000-2008 in Figure 7.2a-c for Shanghai, Naypyidaw, and Jakarta cities, respectively. The results for the other cities are illustrated in Appendix F.2. Table 7.2 summarizes the % increase of CO emissions and CO columns for all the interested cities. In general, most of the cities present relatively constant trends of both CO emissions and CO columns. The trends of MOPITT CO columns for all the cities range from -0.88 to 0.70 % per year. For China, CO emissions from REAS and MACCity present slightly increasing trends of 3.62 and 1.94 % per year, respectively for Shanghai (Figure 7.2a) and of 3.99 % per year for Beijing from both REAS and MACCity. For Naypyidaw (Figure 7.2b) and Bandar Seri Begawan where biomass burning activity is dominant, MACCity CO emissions from biomass burning sources reveal significant increasing trends with the % increase of 10.87 % per year for Naypyidaw and 50.89 % per year for Bandar Seri Begawan. However, the interannual variations of CO emissions from biomass burning for these two cities are quite fluctuated as can be seen in Figure 7.2b for Naypyidaw case. For Jakarta (Figure 7.2c) and other cities, the trends of MACCity CO emissions from both anthropogenic and biomass burning sources range from -3.78 to 2.88 % per year. It should be noted that CO columns do not directly represent CO emission. Since CO gas has relatively long lifetime (about two months) which can transport over a long distance, it is more difficult to trend surface pollutant emissions using CO columns than short-lives gas (e.g., NO_2). Most of the NO_2 gas in vertical column is found near its surface emission source due to its short chemical lifetime and its low background level compared to the level in industrialized areas. On the other side, long-lifetime gas (e.g., CO) can have a high background level (Duncan et al. 2014).

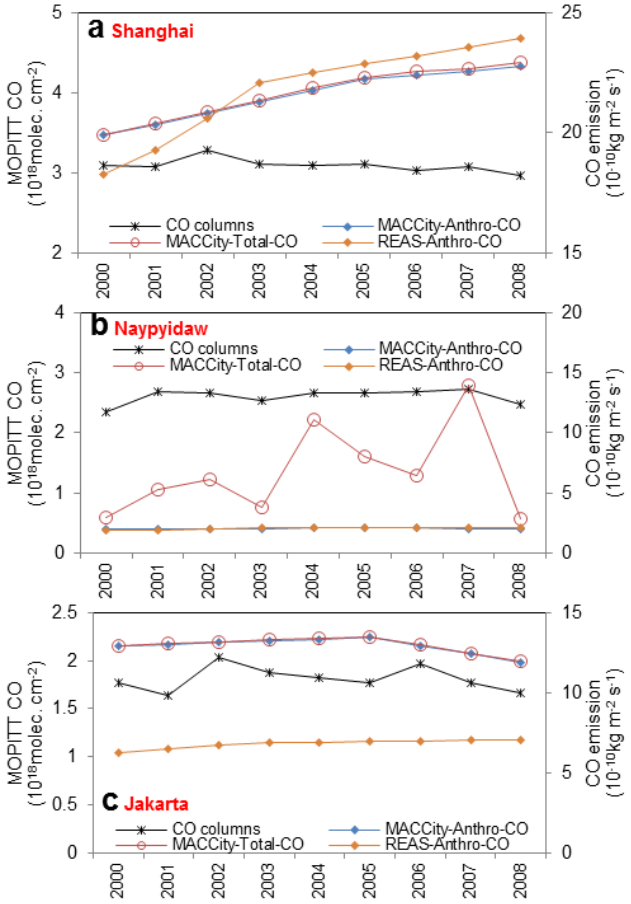

Figure 7.2 Long-term annual analysis of satellite CO columns versus CO emissions for Shanghai (a), Naypyidaw (b) and Jakarta (c)

Table 7.2 Summary of percent increasing trends of CO columns and CO emissions obtained from REAS and MACCity inventories during 2000-2008

City	CO columns (MOPITT) (10^{18}molec.cm^{-2})			REAS CO emissions Anthropogenic (10^{-10}kg km^{-2} s^{-1})			MACCity CO emissions Anthropogenic (10^{-10}kg km^{-2} s^{-1})			MACCity CO emissions Anthropogenic + Biomass burning (10^{-10}kg km^{-2} s^{-1})		
	Ref. 2000	%increase 8yr^{-1}	%increase yr^{-1}	Ref. 2000	%increase 8yr-1	%increase yr^{-1}	Ref. 2000	%increase 8yr^{-1}	%increase yr^{-1}	Ref. 2000	%increase 8yr^{-1}	%increase yr^{-1}
Beijing	3.25	0.20	0.02	27.34	31.89	3.99	15.76	30.76	3.85	15.96	31.93	3.99
Shanghai	3.16	-4.35	-0.54	19.04	29.00	3.62	20.10	14.69	1.84	20.10	15.50	1.94
Tokyo	2.62	-2.86	-0.36	2.73	-25.75	-3.22	4.69	-50.04	-6.25	5.16	-30.27	-3.78
Hanoi	2.95	-7.05	-0.88	9.64	6.71	0.84	10.69	4.92	0.61	10.71	5.33	0.67
Naypyidaw	2.54	4.55	0.57	1.98	8.95	1.12	2.05	1.77	0.22	4.69	86.98	10.87
Vientiane	2.75	5.62	0.70	4.93	15.09	1.89	3.62	3.49	0.44	4.26	-5.38	-0.67
Manila	1.92	-2.89	-0.36	5.95	20.23	2.53	5.04	-3.40	-0.42	5.18	-2.49	-0.31
Bangkok	2.27	-2.99	-0.37	8.15	18.65	2.33	7.93	0.04	0.01	7.97	-0.07	-0.01
Phnom Penh	2.17	-3.19	-0.40	3.99	6.23	0.78	3.09	12.84	1.60	3.39	23.07	2.88
Bandar Seri Begawan	1.81	-1.30	-0.16	1.00	17.53	2.19	0.74	-4.51	-0.56	1.80	407.09	50.89
Kuala Lumpur	2.13	2.65	0.33	3.04	15.40	1.93	4.30	-5.41	-0.68	7.23	-16.83	-2.10
Singapore	2.09	-1.18	-0.15	5.41	5.43	0.68	2.82	-7.39	-0.92	2.92	-8.44	-1.06
Jakarta	1.83	-2.19	-0.27	6.44	11.32	1.41	13.33	-5.95	-0.74	13.35	-5.75	-0.72
Dili	1.61	-2.26	-0.28	1.56	9.63	1.20	0.48	-5.51	-0.69	0.66	5.82	0.73

7.2.2 Monthly analysis

MACCity emission inventory of NO_x and CO was derived in term of monthly average from year 1996-2008 to study the evolution and seasonal pattern of the pollutant emissions over the study area, and to investigate the consistency between satellite retrievals and emission data. Both anthropogenic emissions and biomass burning emissions of NO_x and CO were used to compare with satellite retrievals of NO_2 columns and CO columns, respectively. Below, three cities (Shanghai, Naypyidaw, and Jakarta) with notable seasonal variability in the emissions are described.

1) satellite NO_2 columns versus NO_x emissions

Figure 7.3a-c show the results of long-term analysis of NO_x emissions for Shanghai, Naypyidaw, and Jakarta cities, respectively. Since OMI satellite has the local equator crossing time in the afternoon (~13:45LT) while GOME, SCIAMACHY and GOME-2 satellites are in the morning (~9:30-10:30LT), full black circle symbol in Figure 7.3 represents retrieved OMI data and open black circle symbol represents averaged data of GOME, SCIAMACHY and GOME-2 retrievals. Figure 7.3 demonstrates that satellite observations are generally able to capture the interannual and seasonal variability of total NO_x emissions (sum of anthropogenic and biomass burning emissions). In case of Shanghai, Figure 7.3a shows that both satellite data and total NO_x emissions have significantly increasing trends during 1996-2008. Figure 7.4a-c shows the averaged seasonal cycle of observed NO_2 columns and NO_x emissions data, it presents that the maximum levels of NO_2 columns and NO_x emissions in Shanghai (Figure 7.4a) are revealed in the winter and the minimum in the summer as also mentioned in previous chapter (Chapter 4 and 5). Figure 7.5a-c presents the comparison of NO_x emissions from anthropogenic versus biomass burning activities. In case of Shanghai (Figure 7.5a), NO_x from biomass burning emissions has a peak during May-July while NO_x from anthropogenic emissions has a peak during November-February. However, satellite observations only catch the seasonal trend of NO_x emissions from anthropogenic activities which are dominant in this area. For Naypyidaw, the city is surrounded by the agricultural land causing biomass burning activities predominant in this area. Figure 7.5b shows that

NO_x emitted from anthropogenic activities are relatively constant throughout the year, but biomass burning emissions have the peak in March. From the graph of long-term time series in Figure 7.3b, satellite NO_2 columns have similar seasonal trend with total NO_x emissions and are able to capture the high NO_x episodes from biomass burning activities as also shown in Figure 7.4b. However, in term of quantitative level, there are still discrepancies of interannual variability between satellite observations and surface emissions which is the reason for the opposite long-term trends between these two datasets as presented earlier in Section 7.2.1 for yearly analysis. For Jakarta, Figure 7.5c shows that the major emissions in this area are from anthropogenic activities. The city is located close to Equator zone with the effects of heavy rainfall and tropical monsoons, yet satellite instruments are capable to capture the seasonal cycle of NO_x emissions which the maximum takes place in dry season (June-September) and the minimum in wet season (November-February) as illustrated in Figure 7.3c and Figure 7.4c. The results for others cities are presents in Appendix G.1.

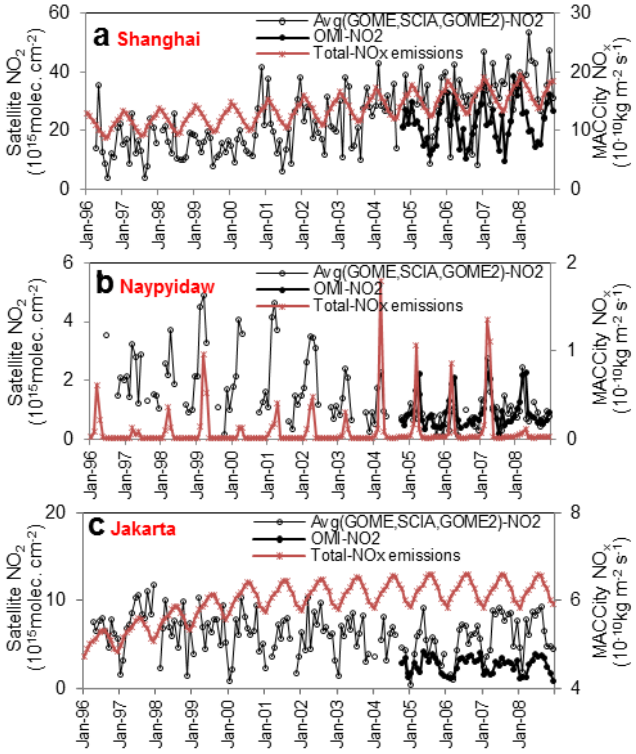

Figure 7.3 Long-term monthly analysis of satellite NO_2 columns versus MACCity total NO_x emissions over Shanghai (a), Naypyidaw (b) and Jakarta (c)

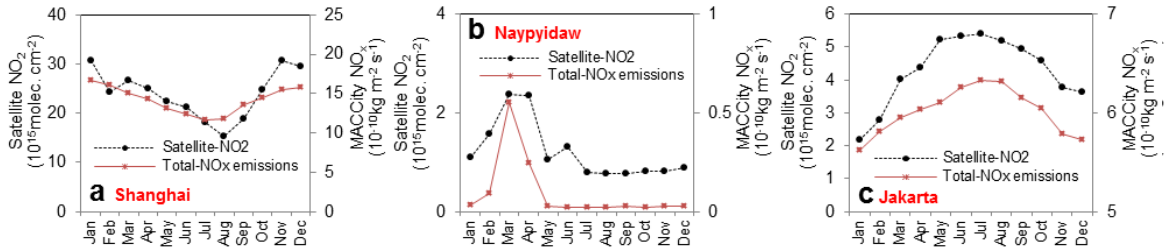

Figure 7.4 Seasonal cycle of satellite NO_2 columns versus MACCity total NO_x emissions over Shanghai (a), Naypyidaw (b) and Jakarta (c)

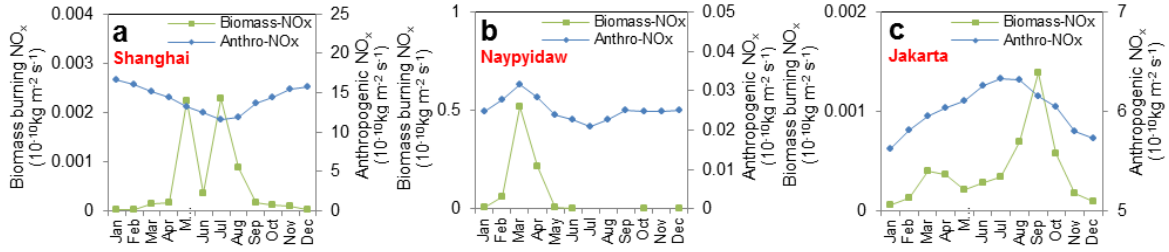

Figure 7.5 Seasonal cycle of MACCity NO_x emissions from biomass burning versus anthropogenic activities over Shanghai (a), Naypyidaw (b) and Jakarta (c)

Table 7.3 summarizes the correlation coefficients between total NO_x emissions and retrieved NO_2 columns for all the considered cities. Most of the cities that have good correlations between NO_x emissions and satellite observations are located in mainland with the less effect of meteorological variations. For the cities located near coastal area or Equator zone, mostly the correlations of MACCity NO_x emissions and tropospheric NO_2 columns are generally low and presented no clear seasonal pattern of both tropospheric NO_2 columns and NO_x emissions as presented in Appendix G.1 for Manila, Bandar Seri Begawan, Kuala Lumpur, Singapore, and Dili cases. The possible bias can be caused by the uncertainty in satellite retrievals, the influence of elevated pollutant from other sources, the meteorological effects, or the inaccuracy of emission estimation. Moreover, the mismatch of time and space averaging between surface emissions and satellite observations can introduce another uncertainty factor.

Table 7.3 Summary of correlation coefficients (r) between satellite columns and MACCity emissions

Country	City	$r_{NO2\text{-}NOx}$	$r_{CO\text{-}CO}$
China	Beijing	0.67	0.14
China	Shanghai	0.72	0.52
Japan	Tokyo	0.50	0.27
Vietnam	Hanoi	0.66	0.70
Burma	Naypyidaw	0.46	0.60
Laos	Vientiane	0.69	0.69
Philippines	Manila	0.30	0.71
Thailand	Bangkok	0.73	0.87
Cambodia	Phnom Penh	0.47	0.74
Brunei	Bandar Seri Begawan	0.34	-0.07
Malaysia	Kuala Lumpur	0.14	0.27
Singapore	Singapore	0.19	0.27
Indonesia	Jakarta	0.67	0.16
East Timor	Dili	-0.38	0.64

In order to examine the effect of the meteorological condition on the relationship of NO_x emissions and satellite NO_2 retrievals, the amount of precipitation was derived from The National Oceanic and Atmospheric Administration (NOAA) website for the available meteorological stations. Figure 7.6 demonstrates an effect of the precipitation parameter on the relationship of tropospheric NO_2 columns and MACCity NO_x emissions by depicting the scattering plot of the precipitation versus the ratio of tropospheric NO_2 columns to NO_x emission, *"L_{NOx}"* (which have the same unit as NO_x lifetime), in term of monthly data (January-December) averaged from year 1996 to 2008. From Figure 7.6a-c, examples are provided for Tokyo, Phnom Penh and Kuala Lumpur cities as a representative for the cities that located in mid-latitude, upper part of low-latitude, and Equator belt, respectively. The analysis for other cities is given in Appendix H.1. The results show that when the precipitation is high, the tropospheric NO_2 columns would be low due to the interaction with water causing the small value of L_{NOx}. The summary of the correlation coefficient between the precipitation and L_{NOx} for all selected cities is presented in Table 7.4. For most of the cities, the relations of the precipitation and L_{NOx} (hour) have the correlation coefficients in range of -0.35 to -0.85 (except for Manila city),

which support the hypothesis that meteorological parameters play a role in NO_x lifetime and the relationship between tropospheric NO_2 columns and NO_x emissions. Figure 7.7a-c provides the seasonal variations of monthly averages precipitation and L_{NOx}. The results shows that during the rainy season the lifetime of NO_x is shorter than other months which is also correlated with the seasonal cycle of NO_2 columns and NO_x emissions presented in Figure 7.4 for the cities that located in the same latitude zones. The results for other cities are provided in Appendix H.2.

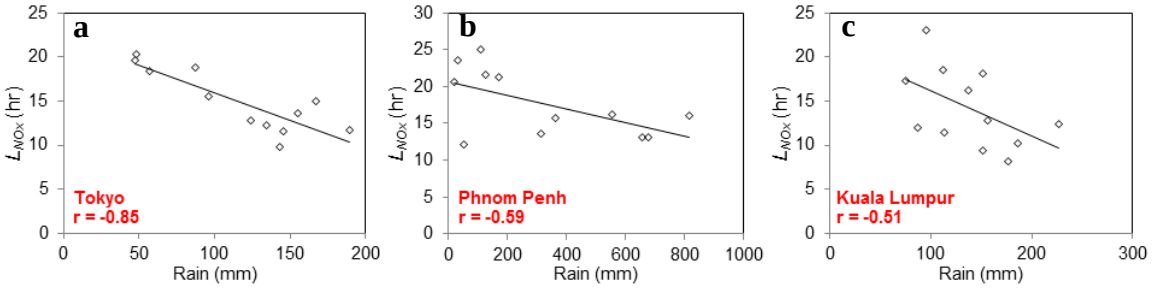

Figure 7.6 Scatter plot of monthly averages of the precipitation and L_{NOx} (hour) in Tokyo (a), Phnom Penh (b), and Kuala Lumpur (c)

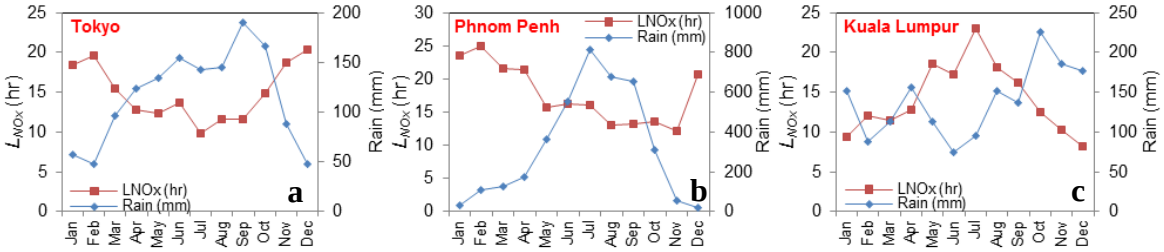

Figure 7.7 Seasonal variability of monthly averages of the precipitation and L_{NOx} (hour) in Tokyo (a), Phnom Penh (b), and Kuala Lumpur (c)

Table 7.4 Summary of correlation coefficients (r) between the precipitation and L_{NOx} (hour)

Country	City	r
China	Beijing	-0.63
China	Shanghai	-0.35
Japan	Tokyo	-0.85
Vietnam	Hanoi	-
Burma	Naypyidaw	-0.55
Laos	Vientiane	-0.46
Philippines	Manila	0.42
Thailand	Bangkok	-0.65
Cambodia	Phnom Penh	-0.59
Brunei	Bandar Seri Begawan	-0.49
Malaysia	Kuala Lumpur	-0.51
Singapore	Singapore	-
Indonesia	Jakarta	-
East Timor	Dili	-

2) satellite CO columns versus CO emissions

Regarding CO emissions, Figure 7.8a-c and Figure 7.9a-c present the comparative analysis of long-term trend and seasonal variability of MOPITT CO columns versus CO emissions for Shanghai, Naypyidaw and Jakarta, respectively. Overall, Figure 7.8 and 7.9 shows that satellite observations of CO columns are able to capture the high episodes and follow the seasonal cycle of total CO emissions (sum of anthropogenic and biomass burning emissions) for all the cities. Figure 7.10a-c presents the comparison of CO emissions from anthropogenic versus biomass burning activities. Figure 7.10a shows that the seasonal cycle of CO emitted from biomass burning and anthropogenic activities in Shanghai city is similar with NO_x emissions with the maximum values of anthropogenic emissions in the winter. In addition, the long-term trends of CO columns and CO emissions are both relatively constant. In case of Naypyidaw city, as mentioned previously that biomass burning emissions are predominant in this area, the maximum peak of CO emissions from biomass burning sources presents in March (Figure 7.10b). Figure 7.8b and Figure 7.9b also show that satellite CO columns can observe the peak of the

emissions. However, satellite also catches another small peak of CO column during October-November. With regard to Streets et al. (2003), they show that in Southeast Asian region there are two periods of biomass burning that emitted high CO. The first peak occurs in February-April and the second occurs in August-October. The latter takes less burned area. This could be the reason of the second small peak shown up in Figure 7.8b, implying that there might be an underestimation of NO_x emissions during these months. For Jakarta, there are two small peaks of CO emissions during April-June and August-October dominated by anthropogenic activities (Figure 7.10c). However, Figure 7.8c reveals that in some years satellite can only observe the latter one. The possible causes of the inconsistency could be due to the uncertainties in satellite retrievals and also the seasonal difference of the chemical reaction between CO and OH since Jakarta's wet season starts from November to June. The long-term time series for other cities are provided in Appendix G.2. Table 7.3 summarizes the correlation coefficients between CO emissions and retrieved CO columns for all the considered cities. Most of the cities provide moderate agreements between CO emissions and satellite observations except for the cities located near Equator zone, and in China and Japan. As mentioned earlier that the discrepancy between satellite observations and surface emissions can be influenced by meteorological effects, especially for the the cities that are located near coastal lines or Equator zone due to their strong weather variance (e.g., strong wind, heavy rain). Moreover, Emmons et al. (2009) and Worden et al. (2010) demonstrate that the possible satellite retrieval bias of MOPITT satellite can occur in polluted condition. Aerosol contamination could be the reason for this bias in Beijing, Shanghai, and Tokyo during the dust storm period in March-May that hit China and then pass through Korea and Japan.

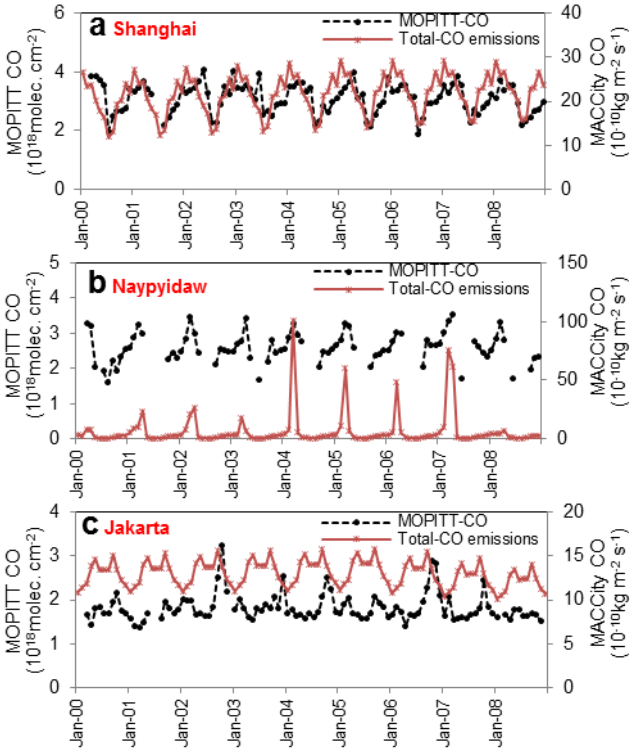

Figure 7.8 Long-term monthly analysis of satellite CO columns versus MACCity total CO emissions over Shanghai (a), Naypyidaw (b) and Jakarta (c)

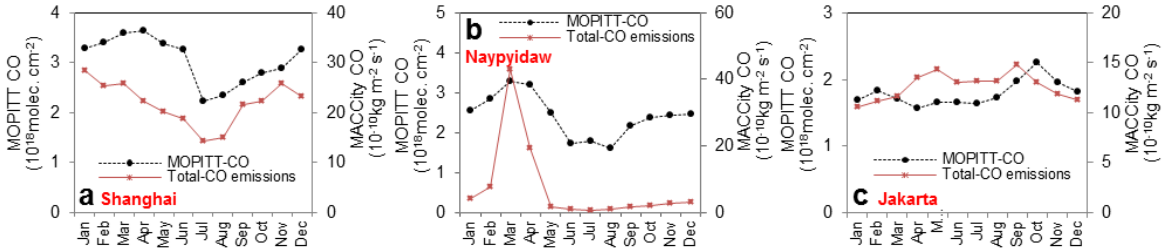

Figure 7.9 Seasonal cycle of satellite CO columns versus MACCity total CO emissions over Shanghai (a), Naypyidaw (b) and Jakarta (c)

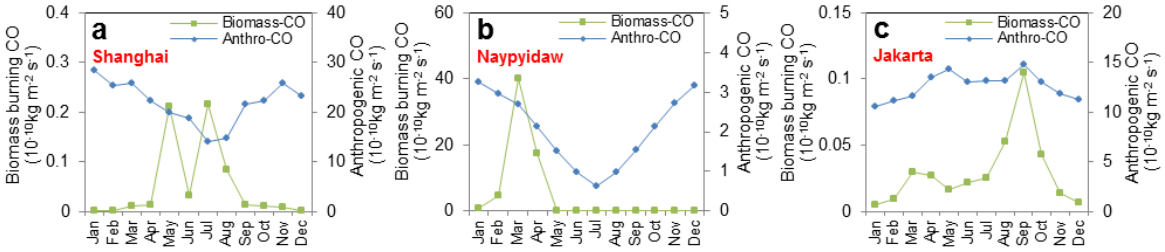

Figure 7.10 Seasonal cycle of MACCity CO emissions from biomass burning versus anthropogenic activities over Shanghai (a), Naypyidaw (b) and Jakarta (c)

Chapter 8 Comparison of Model Outputs and Satellite Observations

8.1 Model and input data description

The objective of this chapter is to comparably analyze the consistency between observed satellite data and simulated model results. Simulations for air quality in this study were conducted by using GEOS-Chem and CMAQ models.

1) GEOS-Chem model

GEOS–Chem is a global 3-D chemical transport model (CTM) for atmospheric composition driven by meteorological input from the Goddard Earth Observing System (GEOS) of the NASA Global Modeling and Assimilation Office. It has been extensively evaluated and applied by many research groups around the world to study a wide range of atmospheric composition problems. More information of the GEOS-Chem model is available through GEOS-Chem website (http://acmg.seas.harvard.edu/geos/).

In this study, the GEOS-Chem model was simulated covering the globe with a spatial resolution of 2° × 2.5° grid size. The meteorological fields were derived from GEOS-5. The emissions were taken from EMAP, BRAVO, EDGAR, STREETS, CAC, NEI2005, RETRO, MEGAN and GFED3 emission inventories. The output from the model was extracted for tropospheric NO_2 columns from surface up to tropopause layer during the time period from 01 January 2005 to 31 December 2005, at the time window 10:00LT – 12:00LT and 12:00LT – 14:00LT corresponding to the satellite overpass time of SCIAMACHY (10:00LT) and OMI (13:45LT), respectively. The averaged 2-hour tropospheric NO_2 columns simulated from GEOS-Chem were compared with those from satellite retrievals in term of monthly averages over the capital cities of interested countries. The comparisons were performed by averaging all satellite pixels falling within 2° × 2.5° grid boxes centering at considered cities in order to fit with model grid-cells.

2) CMAQ model

The Community Multi-scale Air Quality (CMAQ) modeling system is a third-generation air quality model published by US EPA in 1998 (Byun and Ching 1999). The Model-3/CMAQ model is developed for applications ranging from regulatory and policy analysis to understanding the complex interactions of atmospheric chemistry and physics. It has been designed as community-based "one-atmosphere approach" modeling system which includes state-of-the-science capabilities for modeling multiple air quality issues taking all air pollutions and their interaction into account. More information of the CMAQ model is provided in Community Modeling and Analysis System (CMAS) website (http://cmascenter.org/cmaq/).

In this study, the CMAQ model version 4.7 was simulated covering Asian region with a spatial resolution of 80 × 80 km^2. The meteorological fields were derived from WRF model version 3.4. The meteorological input data for the WRF model were derived from the National Centers for Environmental Prediction Climate Forecast System Reanalysis (Saha et al. 2010). The emission data applied in the CMAQ model were Kyoto University emission inventory for the year 2005. The emissions were generated by collecting the data from Zhang et al. (2009) for anthropogenic emissions and from GEIA (Global Emissions InitiAtive) for biomass burning, natural and biogenic emissions. The datasets were then calibrated the sectoral activities for each country based on Fujimori and Matsuoka (2011). The emissions were processed using the Sparse Matrix Operator Kernel Emissions (SMOKE) modeling system version 2.1 and then fed to the CMAQ model for the simulations. The output from the model was extracted for tropospheric NO_2 columns and total CO columns for the entire year 2005 with the monthly averaged values. For tropospheric NO_2 columns, the column extraction was performed in the same method as GEOS-Chem model at 10:00LT and 13:00LT following the satellite overpass time of SCIAMACHY (10:00LT) and OMI (13:45LT), respectively. For total CO columns, the extraction time was at 10:00LT following the satellite overpass time of MOPITT (10:30LT). For the comparison, monthly simulated tropospheric NO_2 columns and total CO columns were compared with those from satellite retrievals in term of spatial distribution for the whole Asian region with the coordinate of 20°S-60°N, 50°E-170°E

(latitude, longitude). Moreover, the comparison was also separated into two regions by covering China and Japan for region1 and covering SEA for region2 as shown in Figure 8.1.

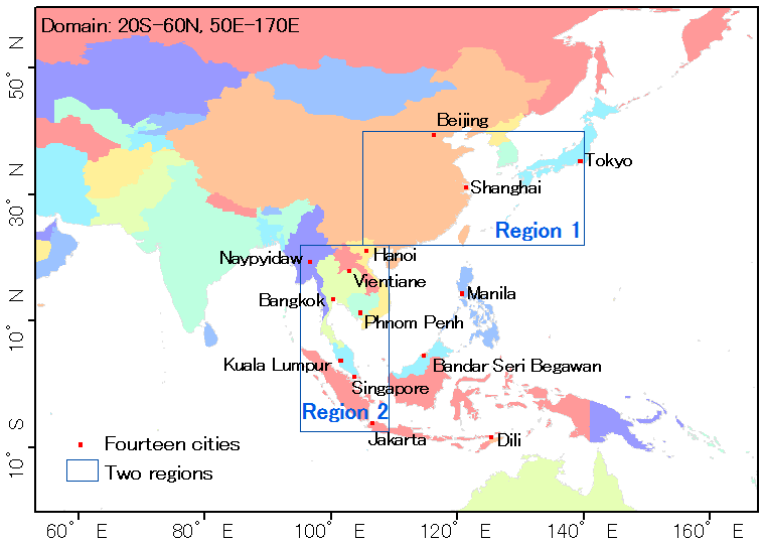

Figure 8.1 Modeling domain and location of two regions

8.2 Comparison of satellite observations and GEOS-Chem results

In this section, the consistency of the seasonal variability of tropospheric NO_2 columns measured by satellite instruments and simulated by GEOS-Chem was investigated over the 14 selected cities for year 2005. Tropospheric NO_2 columns from SCIAMACHY and OMI satellites were used to compare with the results from the model. SCIAMACHY and OMI have a local equator crossing time around 10:00LT and 13:45LT, respectively, correspondingly the model output for each city is extracted at 10:00LT – 12:00LT and 12:00LT – 14:00LT, respectively for the comparison. Figure 8.2a-c show examples of the comparison of the seasonal variation between the observed tropospheric NO_2 columns by SCIAMACHY and OMI versus the estimated results by GEOS-Chem over Shanghai, Bangkok and Bandar Seri Begawan, respectively in order to verify the accuracy of the emissions used in the model simulations. For the other cities, the comparisons are provided in Appendix I.1. The results of comparative analysis for all the cities are presented in Table 8.1 for the comparison with SCIAMACHY and in Table 8.2 with OMI. Most of the results from OMI provide better correlations than from SCIAMACHY. This is

due to the finer horizontal resolution of OMI instrument. In addition, the results of model simulations and satellite observations presented in Figure 8.2, Table 8.1, and 8.2 show that in year 2005 China has the highest level of the mean values of tropospheric NO_2 abundances with the column concentrations over Beijing of 7.23 and 27.19 molecules/cm^2, and over Shanghai of 2.56 and 12.60 molecules/cm^2 for GEOS-Chem outputs and SCIAMACHY observations, respectively.

In term of seasonal analysis, the results in Figure 8.2 show that for most of the cities located in mid-latitude zones, simulated tropospheric NO_2 columns illustrate the maximum values during the winter months (November–January) and minimum values during summer months (June–August) which is consistent with the satellite observations as can be seen in Figure 8.2a for Shanghai with the correlation coefficients (r) of 0.88 and 0.91 for SCIAMACHY and OMI cases, respectively. For the cities in upper part of low-latitude zone, most of the cities present the maximum levels of observed and simulated NO_2 columns during dry season between winter to summer months of December to April and the minimum during rainy season of June–August as presented in Figure 8.2b for Bangkok case. For the cities that located near Equator zone, simulated and observed tropospheric NO_2 columns demonstrate the different seasonal pattern compared with the citied in the upper latitude zones. As shown in Figure 8.2c for Bandar Seri Begawan case, the maximum values for both simulated and observed tropospheric NO_2 columns are presented during dry season (February–April, July–September) with the driest month in August, while the minimum values are presented during rainy season (October–January, May–June) with the highest amount of precipitation in November–December. However, for SCIAMACHY observations, the seasonal variation is not as clear as OMI.

The results of tropospheric NO_2 columns from the model provide moderate to good agreements ($r \geq 0.5$) with those retrieved from the satellites in case of Beijing, Shanghai (Figure 8.2a), Tokyo, Hanoi and Bangkok (Figure 8.2b), especially for the comparison with OMI satellite with the correlation coefficients (r) of 0.91, 0.91, 0.56, 0.89, and 0.84, respectively. However, the results from the model seem to under-estimate tropospheric NO_2 columns from both SCIAMACHY and OMI satellites as shown in Table 8.1 and 8.2 for the ratio of satellite NO_2 columns to GEOS-Chem NO_2 columns. Overall, the model

underestimated the retrieved tropospheric NO_2 columns by the factor around 3–4. Similar results were also found in He et al. (2007) and Uno et al. (2007). They showed that the modeled NO_2 columns underestimate the satellite retrievals of GOME and SCIAMACHY by the factor more than 2 over CEC and around 1-3 over Japan. The bias could be due to the uncertainties in satellite retrievals, the mismatch between the satellite and model horizontal resolution and extracting time, the inaccuracy of the emission inventories applied in the GEOS-Chem model that underestimate NO_x emissions during the study period, and also the coarse horizontal resolution of the GEOS-Chem model that smooth out the characteristic of pollution hotspots in urban areas. Furthermore, the results in Table 8.1 and 8.2 show that all the cities located near Equator belt reveal weak correlation coefficients ($r \leq 0.5$). This could be caused by the relatively large uncertainties in satellite retrievals for the cities that are located near coastal areas or tropical zone, since the interpretation of data in coastal locations is difficult due to complex natural variability (e.g., stronger wind and cloud effects). Therefore, more effort is needed to better quantify the uncertainties in satellite retrievals for air quality applications.

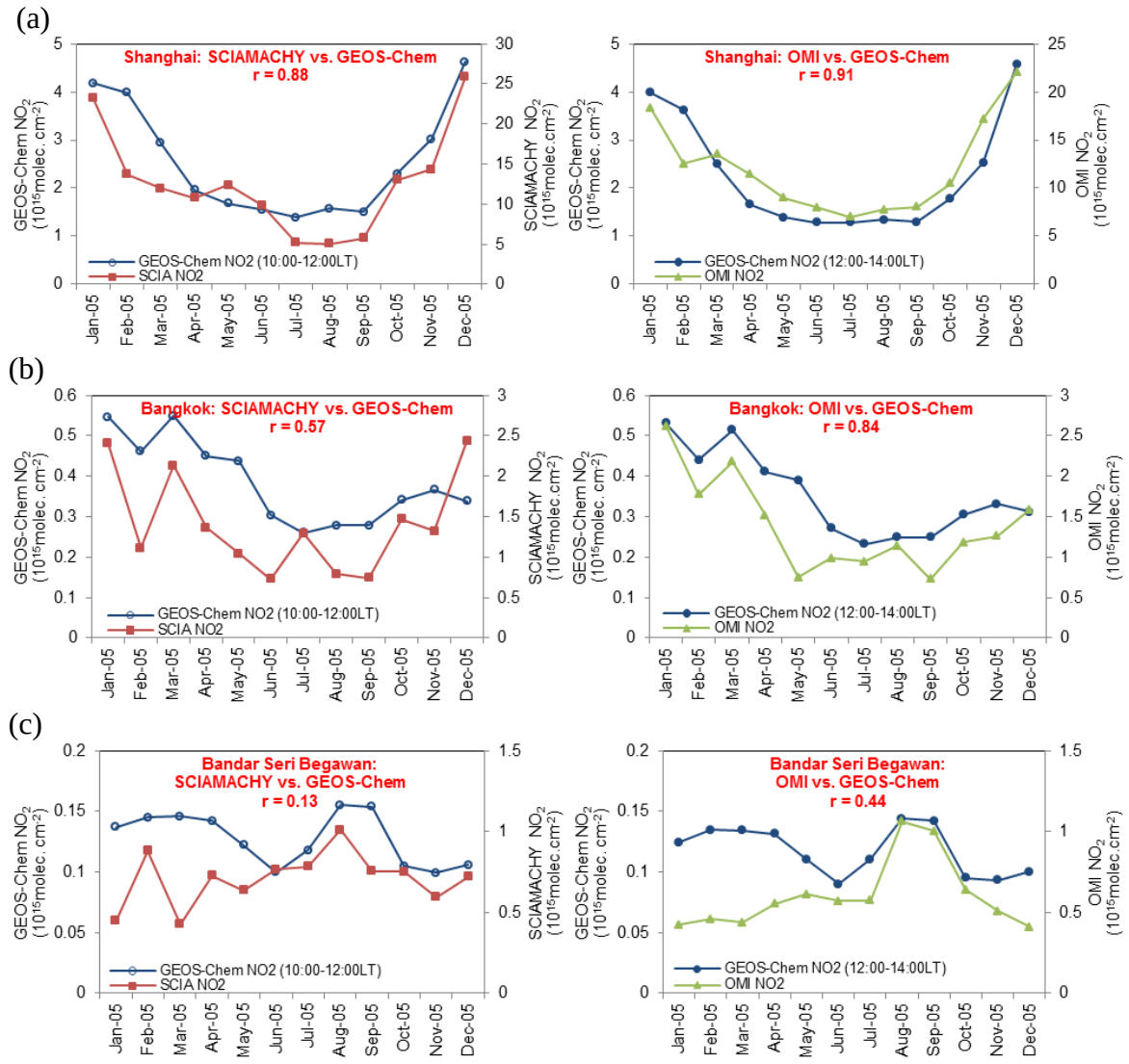

Figure 8.2 Seasonal variation of tropospheric NO_2 columns simulated from model and retrieved from satellites over Shanghai (a), Bangkok (b), and Bandar Seri Begawan (c)

Table 8.1 Summary of the results of the comparison between tropospheric NO_2 columns retrieved from SCIAMACHY and modeled from GEOS-Chem

City	Mean NO_2 columns (2005)			$r_{SCIA-GEOS}$
	SCIAMACHY (10^{15}molecules/cm^2)	GEOS-Chem (10-12:00LT) (10^{15}molecules/cm^2)	Ratio (SCIAMACHY/GEOS-Chem)	
Beijing	27.19	7.23	3.76	0.78
Shanghai	12.60	2.56	4.92	0.88
Tokyo	3.22	0.73	4.39	0.63
Hanoi	1.65	0.71	2.33	0.53
Naypyidaw	0.67	0.35	1.94	0.58
Vientiane	1.66	0.95	1.74	0.24
Manila	1.39	0.24	5.77	0.34
Bangkok	1.40	0.38	3.65	0.57
Phnom Penh	0.70	0.37	1.90	-0.52
Bandar Seri Begawan	0.71	0.13	5.56	0.13
Kuala Lumpur	2.16	1.10	1.97	0.22
Singapore	1.96	0.54	3.67	0.81
Jakarta	1.60	0.22	7.40	0.26
Dili	0.27	0.29	0.92	0.34

Table 8.2 Summary of the results of the comparison between tropospheric NO_2 columns retrieved from OMI and modeled from GEOS-Chem

City	Mean NO_2 columns (2005)			$r_{OMI-GEOS}$
	OMI (10^{15}molecules/cm^2)	GEOS-Chem (12-14:00LT) (10^{15}molecules/cm^2)	Ratio (OMI/GEOS-Chem)	
Beijing	11.22	6.98	1.61	0.91
Shanghai	12.11	2.27	5.34	0.91
Tokyo	3.15	0.66	4.81	0.56
Hanoi	1.42	0.62	2.27	0.89
Naypyidaw	0.65	0.33	1.97	0.40
Vientiane	1.45	0.89	1.63	0.38
Manila	1.08	0.22	4.95	0.66
Bangkok	1.39	0.35	3.93	0.84
Phnom Penh	0.70	0.32	2.17	-0.21
Bandar Seri Begawan	0.60	0.12	5.14	0.44
Kuala Lumpur	1.69	1.00	1.68	0.34
Singapore	1.86	0.51	3.67	0.36
Jakarta	1.56	0.20	7.69	0.39
Dili	0.49	0.28	1.71	0.43

8.3 Comparison of satellite observations and CMAQ results

In this section, the CMAQ model simulations were performed for calculating tropospheric NO_2 vertical columns and total CO vertical columns over Asia for year 2005 to investigate the consistency with the satellite observations.

1) Tropospheric NO_2 columns

In order to obtain the vertical column densities, the simulated concentrations of NO_2 were integrated from the surface layer to the tropopause layer. The data of NO_2 columns from SCIAMACHY and OMI satellites were adopted to compare with the model results. Since SCIAMACHY and OMI satellites have the local equator crossing time around 10:00LT and 13:45LT, the model outputs at 10:00LT and 13:00LT was extracted for comparably analysis with the satellite data of SCIAMACHY and OMI NO_2 columns, respectively. Figure 8.3a, b and 8.4a, b present the spatial distribution of 3-month averaged NO_2 columns over Asia in 2005 for SCIAMACHY, CMAQ results at 10:00LT, OMI, and CMAQ results at 13:00LT, respectively. December-January-February (DJF), March-April-May (MAM), June-July-August (JJA) and September-October-November (SON) were grouped to be the representatives of winter, spring, summer and autumn, respectively. The results of NO_2 columns in Figure 8.3a, b and 8.4a, b show that the CMAQ simulations generally agree well with SCIAMACHY and OMI observations in term of spatial distributions and seasonal variations. Both observed and simulated results show that CEC has the highest level of NO_2 columns. The maximum magnitude of NO_2 columns from both satellites and CMAQ are revealed in winter (DJF) and the minimum in summer (JJA) as can be obviously seen in East Asian region, especially in CEC. The results in this section confirm that China is the main contributor of NO_2 over this area. Furthermore, a grid-to-grid comparison was conducted between two datasets of NO_2 columns from satellite measurements and those from simulations for each month and each region; region1 and region2 (Figure 8.1). The summarized results of correlation coefficient between satellite and simulated data are shown in Table 8.3. Region1 represents the area including CEC, Korea and Japan. Region2 represents part of SEA region. Table 8.3 shows that correlation coefficient over Asia for the comparison between SCIAMACHY and

simulated data is approximately 0.73 with the correlation coefficients of 0.79 and 0.63 over region1 and 2, respectively. For the comparison between OMI and simulated data, correlation coefficients over Asia, region1 and 2 are approximately 0.83, 0.86 and 0.56, respectively. Most of the results from OMI observations provide better correlations than from SCIAMACHY owing to the finer resolution of the OMI instrument. Moreover, the results in Figure 8.3a, b and 8.4a, b also illustrate that both observed and simulated NO_2 columns in the afternoon is smaller than in the morning. This supports the idea that during rush hour in the morning, tropospheric NO_2 is significantly produced by the transportation especially in the urban area, and then subsequently causes high level of SCIAMACHY measurement during this period. On the other hand, in the afternoon the photolysis rate is higher than in the morning causing the loss of NO_2 and resulting in the low measurements of tropospheric NO_2 during the overpass time of OMI satellite.

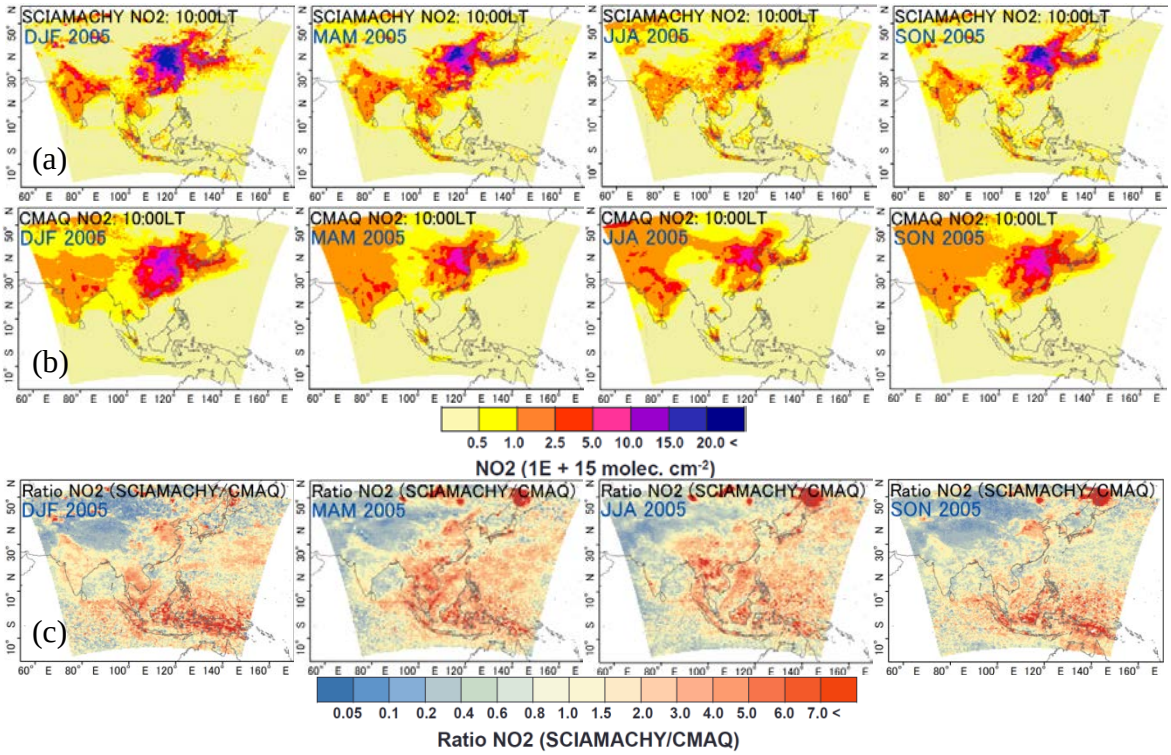

Figure 8.3 Spatial distributions of NO_2 columns retrieved from SCIAMACHY (a), simulated from CMAQ (b), and ratio of NO_2 columns (SCIAMACHY/CMAQ) (c)

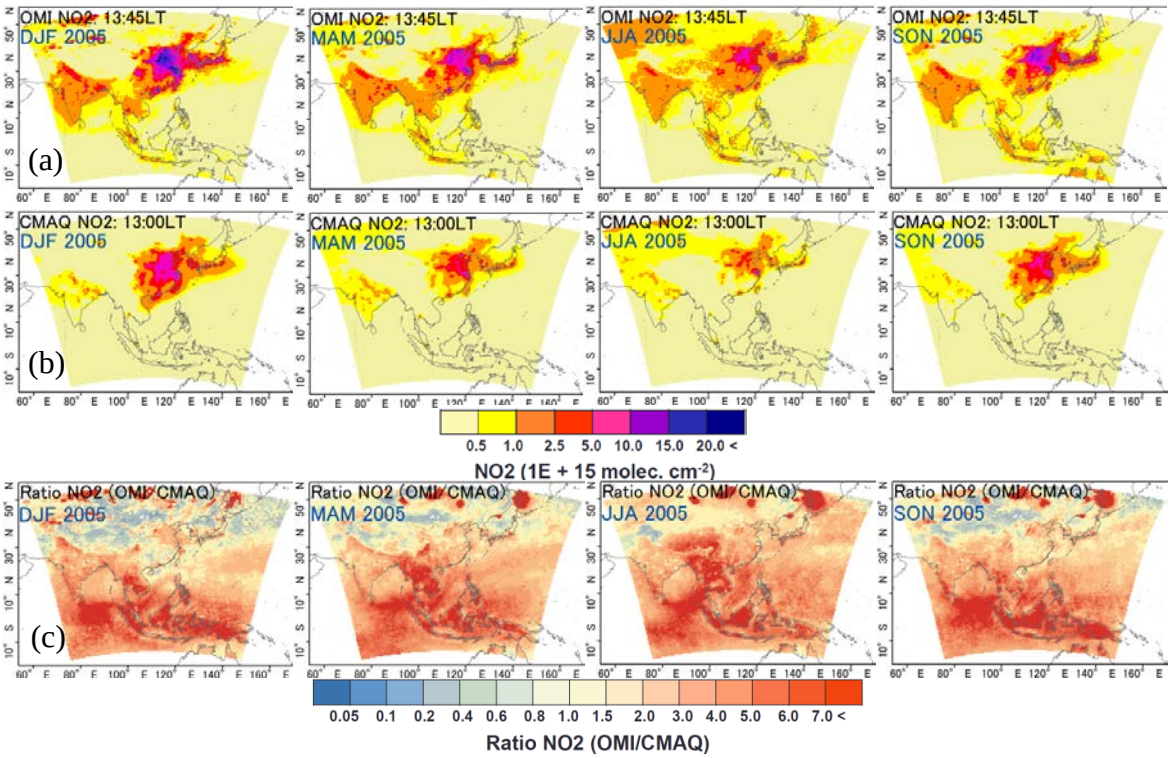

Figure 8.4 Spatial distributions of NO_2 columns retrieved from OMI (a), simulated from CMAQ (b), and ratio of NO_2 columns (OMI/CMAQ) (c)

As presented in Table 8.3, it is interesting to note that the results in region1 give better agreement than region2. Figure 8.3c and 8.4c, present the ratio of SCIAMACHY NO_2 columns to CMAQ NO_2 columns and the ratio of OMI NO_2 columns to CMAQ NO_2 columns, respectively. The overall results show that modeled NO_2 columns seem to underestimate observed columns by the factor around 1.98 and 4.83 over Asia for SCIAMACHY and OMI measurements, respectively. Table 8.3 also presents the ratio of satellite observations to model simulations for each month and each region. In case of SCIAMACHY, the model underestimates observed NO_2 columns by the factor of 1.76 and 2.39 over region1 and 2, respectively. For OMI, the results of model underestimate observed NO_2 columns by the factor of 2.09 over region1 and 5.57 over region2. These results are similar with the results of the comparison between satellite and GEOS-Chem data in the previous section. The higher ratio of region2 compared to region1 caused by the inaccuracy of the surface emission estimation is possibly the reason of lower correlations of region2 than of region1. Secondly, as mentioned in the previous section of the comparison between GEOS-Chem outputs and satellite observations, more

uncertainties in satellite retrievals can be found in coastal regions and tropical areas due to the complex meteorological variability. Irie et al. (2013) demonstrated that an improvement of CMAQ horizontal resolutions (from 80 to 10 km) can increase the level of simulated NO_2 columns as large as that caused by increasing emissions by 20%. Since the horizontal resolution in this study was set at 80×80 km^2, this could be also the cause of the underestimation. Itahashi et al. (2013) showed that the CMAQ modeling results using the updated REAS inventory (version 2.1) remarkably captured the absolute values of OMI NO_2 columns over East Asia throughout the year 2000-2008. This suggests that more efforts are needed to improve the emission inventory used in this study. Another noteworthy result in Table 8.3 is that during summer the ratios over Asia are higher than other months (June: 2.85 for SCIAMACHY and 8.38 for OMI, July: 2.64 for SCIAMACHY and 6.66 for OMI). van der A et al. (2006) reports that in the western part of China which is a remote area with a low population density, the seasonal cycle of tropospheric NO_2 shows the maximum in summer, and this cycle is attributed to natural emissions, especially soil emissions and lightning. In the work by Christian et al. (2003), it is also presented that lightning above China has the flash rate in summer about 5-6 times higher than in winter. Since lightning emissions are not included in this study, this is possibly the reason of higher ratios in summer over Asia domain. Another possible reason is that there is an underestimation of soil NO_x emissions as suggested in Yienger and Levy (1995) that in remote and agricultural regions, the percent contribution of soil emissions to the total NO_x budget can be increased during summer. Overall, the probable reasons for the discrepancy between observed and simulated datasets in this study are the underestimation of NO_x emissions, the horizontal resolution set in the model, the differences in model and satellite horizontal resolutions and extracting times, and also the uncertainty in satellite retrievals (Boersma et al. 2011; Bucsela et al. 2013; Celarier et al. 2008).

Table 8.3 Summary of correlation coefficients (r) of NO_2 columns from SCIAMACHY and OMI satellites versus CMAQ results, and ratio of NO_2 columns from SCIAMACHY and OMI to CMAQ results

Month (2005)	$r_{SCIAMACHY-CMAQ}$			Ratio (SCIAMACHY/CMAQ)			$r_{OMI-CMAQ}$			Ratio (OMI/CMAQ)		
	Asia	Region 1	Region 2	Asia	Region 1	Region 2	Asia	Region 1	Region 2	Asia	Region 1	Region 2
Jan	0.83	0.82	0.70	1.63	1.51	2.42	0.88	0.88	0.55	2.98	1.78	5.59
Feb	0.70	0.69	0.62	1.90	2.66	3.32	0.83	0.84	0.57	3.26	1.62	6.12
Mar	0.77	0.83	0.66	1.52	1.64	3.10	0.84	0.90	0.62	2.83	1.79	6.98
Apr	0.72	0.80	0.69	1.60	1.60	2.88	0.83	0.88	0.69	2.96	1.83	5.26
May	0.71	0.85	0.61	2.38	3.67	3.11	0.79	0.85	0.65	4.68	2.83	5.70
Jun	0.71	0.79	0.64	2.85	2.22	2.41	0.81	0.88	0.57	8.38	2.42	5.63
Jul	0.67	0.77	0.62	2.64	1.88	2.06	0.80	0.95	0.53	6.66	2.66	5.37
Aug	0.66	0.80	0.66	2.22	2.11	2.22	0.79	0.89	0.61	5.84	2.74	6.65
Sep	0.64	0.75	0.64	1.94	1.18	2.17	0.80	0.96	0.47	5.95	2.24	7.08
Oct	0.77	0.82	0.65	2.42	1.05	1.91	0.85	0.84	0.53	5.58	1.81	5.49
Nov	0.80	0.79	0.54	1.41	0.85	1.65	0.84	0.76	0.43	4.51	1.53	3.91
Dec	0.82	0.83	0.49	1.29	0.76	1.39	0.82	0.75	0.50	2.84	1.59	3.54
Mean	0.73	0.79	0.63	1.98	1.76	2.39	0.83	0.86	0.56	4.83	2.09	5.57

2) Total CO columns

In case of total column CO, Figure 8.5a, b present the spatial distributions of MOPITT retrieved and CMAQ simulated 3-month mean total CO columns during winter (DJF), spring (MAM), summer (JJA), and autumn (SON) of the year 2005, respectively. Figure 8.5 a, b shows that the results from the model failed to catch the hotspots of CO columns compared to the satellite observed one, especially in CEC and in the upper part of SEA. However, the seasonal variability of simulated total CO columns is able to follow the trend of MOPITT CO retrievals which has the maximum levels during winter (DFJ) and spring (MAM) and minimum during summer (JJA) for both East and Southeast Asian countries. The difference between simulated and satellite retrieved data is shown in Figure 8.5c using ratio of total CO columns observed from MOPITT to those calculated from model. Overall, the modeled results underestimate MOPITT values for all the Asian regions, particularly over hotspot areas, except over the western part of China. Table 8.4 summarizes the correlation coefficients (r) and also the ratios of total CO columns compared between satellite retrievals and model results for each month and each region (region1 and region2). The correlation between observed and simulated CO columns is relatively low with the correlation coefficient around 0.33 over Asia, 0.42 over region1, and 0.28 over region2. It is noteworthy that in Table 8.4 the correlation coefficients are higher during May-August (r = 0.61-0.79) for region1, and during January-May (r = 0.54-0.74) and October-December (r = 0.41-0.75) for region2 compared to other months. The periods that have better correlation are match with the periods of high biomass burning activities over these areas. This means that the main influence for the underestimation of the levels of total CO columns is from the miscalculation of anthropogenic emission both in term of absolute quantity and spatial distribution. Moreover, from Table 8.4 it shows that the ratios of satellite data to modeled results also have the higher values during the biomass burning season both under region1 (May-August) and 2 (January-May, October-December). This implies that it is not only the anthropogenic but also the biomass burning emission that is underestimated over these areas. However, in region1 the ratios during biomass burning period are not much higher than other periods compared to region2. This is because the dominant emission in region1 is from anthropogenic activities. The study of Kumar et al. (2012) demonstrates that the simulated total CO columns generally agree

well with MOPITT retrievals in term of seasonal variability over Burma during 2008. However, mean negative bias is highest during spring (MAM) which matches with high fire activity season in this area. In addition, the lowest correlation coefficient reveal during summer (JJA). Their results are similar with this study as can be seen in Table 8.4. Nevertheless, their overall correlation coefficients are better than this study. This probably due to the higher horizontal resolution of their study (45 × 45 km^2) compared to this study (80 × 80 km^2). They also suggest that including of plumerise parameterization in simulation can increase tropospheric CO columns by 10–50% over biomass burning regions.

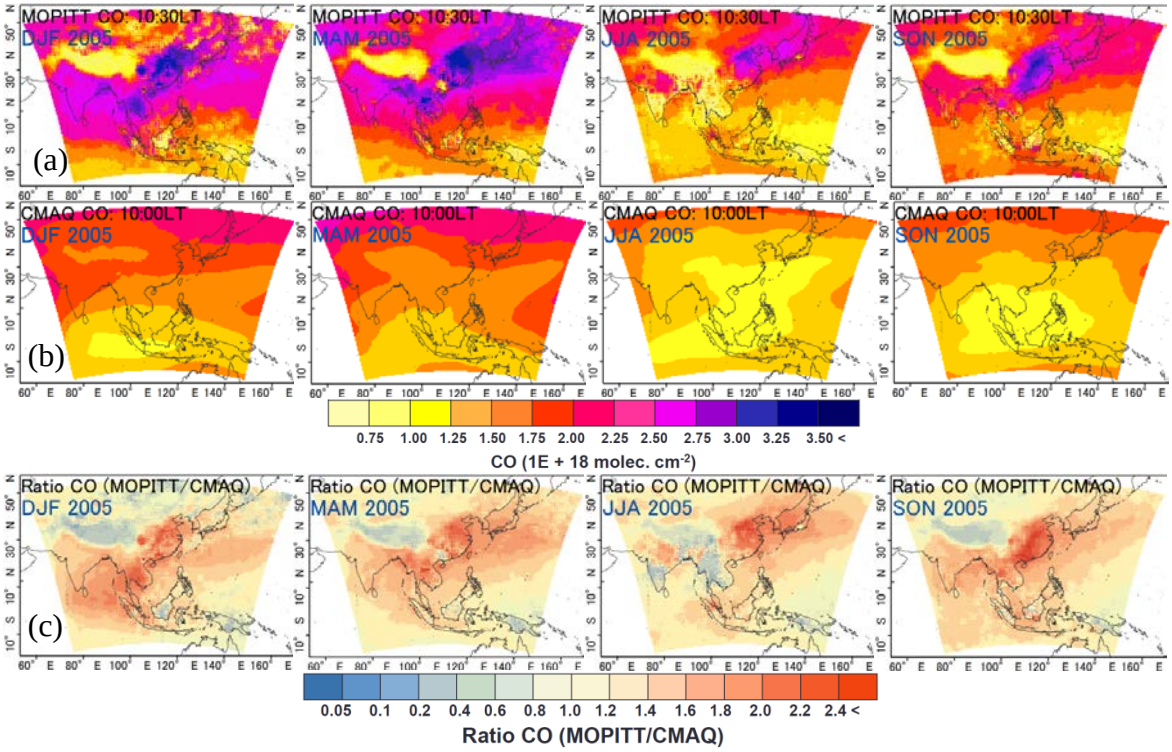

Figure 8.5 Spatial distributions of CO columns retrieved from MOPITT (a), simulated from CMAQ (b), and ratio of CO columns (MOPITT/CMAQ) (c)

Table 8.4 Summary of correlation coefficients (r) of CO columns from MOPITT satellite versus CMAQ results, and ratio of CO columns from MOPITT satellite to CMAQ results

Month (2005)	$r_{MOPITT-CMAQ}$			Ratio (MOPITT/CMAQ)		
	Asia	Region 1	Region 2	Asia	Region 1	Region 2
Jan	0.20	0.10	0.60	1.23	1.56	1.74
Feb	0.13	0.19	0.64	1.18	1.41	1.68
Mar	0.37	0.37	0.67	1.27	1.62	1.72
Apr	0.48	0.48	0.74	1.23	1.71	1.41
May	0.55	0.79	0.54	1.23	1.74	1.18
Jun	0.38	0.62	-0.45	1.20	1.76	1.08
Jul	0.39	0.61	-0.51	1.19	1.65	1.14
Aug	0.45	0.77	-0.27	1.24	1.66	1.30
Sep	0.24	0.32	-0.08	1.27	1.75	1.38
Oct	0.27	0.30	0.41	1.24	1.62	1.49
Nov	0.25	0.39	0.59	1.22	1.61	1.46
Dec	0.23	0.11	0.75	1.20	1.61	1.52
Mean	0.33	0.42	0.28	1.22	1.63	1.42

Chapter 9 Conclusions and Recommendation

9.1 Concluding remarks

There are two main objectives of this study which are (1) to investigate the capability of the satellite instruments to observe spatial and temporal variability of atmospheric pollutants (NO_2, CO and aerosols) over Southeast Asian region and some parts of China and Japan during the period of 1996-2012 and (2) to develop methodology using atmospheric pollution information retrieved from satellite observations and those simulated from models in order to validate and improve emission inventories. This chapter concludes the overall results discussed in the previous chapters that fulfill these two objectives. The analysis presented in Chapter 3-6 was set up in order to complete the first objective. For the second objective, the analysis was performed and presented in Chapter 7-8.

Chapter 3, the main purpose of this chapter is to investigate the consistency between the satellite products. This research adopted several satellite products in order to obtain long-term data of air pollution during 1996-2012. Tropospheric NO_2 columns were retrieved from GOME, SCIAMACHY, OMI, and GOME-2 satellites, CO columns were retrieved from MOPITT and SCIAMACHY satellites, and AODs were retrieved from MODIS-Terra and MODIS Aqua satellites. The satellite inter-comparisons of tropospheric NO_2 columns show good agreements, especially in term of seasonal variation with the correlation coefficients larger than 0.85. However, SCIAMACHY data present higher absolute values compared to others mainly due to the differences in satellite overpass times and horizontal resolutions. For CO columns, the correlation coefficient between MOPITT and SCIAMACHY is around 0.58. The discrepancy is mainly caused by the differences of wavelength bands used to measure the pollutants and horizontal resolutions. For MODIS-Terra and MODIS-Aqua AODs, the correlation coefficient is approximately 0.92. The reasons for the disagreement between each satellite product are also from the differences in retrieval algorithms and the effects of instrument noise errors. Therefore, in

order to study long-term trend of the pollutants, it is necessary for the user to understand the strengths and limitations of a particular product.

Chapter 4, the main purpose of this chapter is to study the characteristics of spatial distribution, long-term trend, and seasonal variability of satellite observations. The results show that China, especially in CEC, has the highest level of NO_2 columns, CO columns, and AODs compared with other cities in East Asia and SEA. Moreover, CEC also shows the significant increasing trend of NO_2 columns with 174.5% and 117.3% over 16 years (ref. year 1996) over Shanghai and Beijing, respectively. For the seasonal analysis, satellites are able to observe the high episode of the pollutants and also the long-range transport of the pollutant plumes. In case of NO_2 columns, the maximum levels are revealed in wintertime for the cities located in mid-latitude and upper part of low-latitude zones. For the cities located near Equator zone, the maximum abundances show in dry season and during biomass burning period. Similarly to NO_2 columns, CO columns in mid-latitude zone start being high in wintertime, but stay last until springtime during biomass burning season. For the cities in low-latitude zone, high CO columns can be observed during biomass burning period. For AODs, all the cities reveal the maximum peaks during biomass burning season and also during Asian dust-storm period in springtime for the cities in mid-latitude zone.

Chapter 5, the main purpose of this chapter is to investigate the consistency between the ground-based and satellite-based measurements. The results show that there are some discrepancies between satellite and ground data since ground data are collected from point source, but satellite data are spatial average of integrated columnar loads from the ground to the top of the atmosphere. However, satellite observations are able to capture the seasonal trend of NO_2 concentrations, especially by OMI satellite which provides the highest correlation with ground data ($0.61 \leq r \leq 0.89$) when compared to other satellites due to its finest resolution. In Bangkok and Rayong where anthropogenic emissions are dominant, both satellite and surface data of NO_2 give the maximum levels during winter, while in Chiangmai the maximum presents during biomass burning period. The seasonal variations of ground CO and PM_{10} concentrations are similar to NO_2 concentrations. Nevertheless, the peak levels of CO columns and AODs in Bangkok and Rayong show

during biomass burning period. The reason is due to the influence of the elevated pollutants from biomass burning activities around the suburban site that transport into the pollutant columns over the considered ground monitoring stations. In case of Chiangmai, both satellite and ground data of CO and aerosol present the maximum during biomass burning period. Therefore, in order to incorporate the use of satellite data with ground data, it is necessary to properly validate the satellite information.

Chapter 6, the main purpose of this chapter is to improve the relationship between satellite AODs and surface PM_{10} concentrations by considering the effects of meteorological parameter on their correlations. The analysis focused on three provinces of Thailand including Bangkok, Rayong, and Chiangmai. The regression was performed without and with cloud screening procedure. The latter gave stronger correlation coefficients for lower cloud fractions ($CF \leq 1/10$, $r = 0.40\text{-}0.85$). The multiple linear regression models were then developed using 5-year (2008-2012) data of AODs at $CF \leq 1/10$ with the incorporation of surface meteorological parameters including RH, WS, and T. The results show that the correlation coefficients of AODs-PM_{10} relationship increased when incorporated meteorological parameters into the models, especially in case of Bangkok and Rayong. Such models were applied to estimate surface PM_{10} mass concentrations and evaluated with those measured from ground monitors for year 2007 and 2013. The estimated results in Chiangmai are reasonably correlated with the actual ones in term of both quantitative levels and diurnal variations. However, in Bangkok and Rayong the correlations are weaker. The developed models for Chiangmai city were then used to estimate surface PM_{10} mass concentrations for other seven cities in northern Thailand. Most of the results show that the models can well capture the surface PM_{10} mass concentrations, especially during biomass burning period. The models with the inclusion of meteorological parameters slightly improve the estimation of PM_{10} mass for all cities. This analysis implies that satellite AODs are possible to be used as a surrogate for surface PM_{10} mass concentrations, particularly during high episode of PM_{10} mass concentration.

Chapter 7, the main purpose of this chapter is to investigate the consistency between source emissions and satellite observations. Time series of NO_x and CO emissions from REAS and MACCity emission inventories were applied and plotted together with satellite

NO_2 and CO columns. The long-term monthly comparison shows that in general satellite observations can catch the seasonal cycle and the high episode of the pollutants both from anthropogenic and biomass burning emissions. Better relationships mostly reveal in the cities that located in mainland while the cities that located near coastal line or Equator zone present weaker correlations. It should be noted that the vertical columns of satellite observations do not directly represent surface emissions. Therefore, the reasons for the discrepancy can be from the effect of meteorological conditions (e.g., precipitation, wind) or the uncertainties in satellite retrievals. In addition, the inaccuracy of the surface emission estimation, especially from biomass burning activities can also be another factor for the discrepancy.

Chapter 8, the main purpose of this chapter is to investigate the consistency between the results from model simulations and satellite observations in order to validate the emissions applied in the models. NO_2 and CO columns retrieved from satellite were compared with those from GEOS-Chem and CMAQ model simulations over Asia for year 2005. The seasonal variations of simulated GEOS-Chem NO_2 columns are reasonably correlated with satellite NO_2 columns mostly for the cities that are located in mid- and upper part of low-latitude zones. However, weak correlations are found over the cities near Equator zone due to relative large uncertainties in satellite retrievals caused by complex meteorological variability. Moreover, the model underestimated satellite data by the factor of 3–4. For CMAQ, the simulated vertical columns of NO_2 generally agree with observed ones in term of spatial distribution and seasonal variability with the correlation coefficient around 0.73 and 0.83 for SCIAMACHY and OMI over Asia, respectively. However, the model underestimated the retrieved satellite data by the factor of 1.98 and 4.83 for SCIAMACHY and OMI, respectively. The reasons for the discrepancy could be due to the underestimation of NO_x emissions, the model performance, and also the uncertainty in satellite retrievals. In term of CO columns, the modeling results failed to catch the hotspots of satellite CO columns and presented low correlations between them, suggesting that there should be more efforts to improve the emission estimates of CO sources.

9.2 Recommendation for applications of research results

The results in this study suggest that satellite observations are beneficial to AQM in term of air quality monitoring, emission inventories, and air pollution modeling, which are parts of the main technical components of AQM. While ground monitoring data provide the most accurate measurements of air quality at specific location where ground monitors are available, the strength of satellite data over ground monitoring network is spatial coverage. The results in this study highlight that satellite data are able to provide complementary to ground measurement by gaining the missing ground monitoring data. These indicate that satellite retrievals are able to provide valuable inputs to AQM in order to determine population exposure, health impact assessment, and compliance with national and international standards, which is essential for policy making and management. Moreover, satellite data are possible to be used as a tool to study long-term trend and seasonal variation of the atmospheric pollutants (NO_2, CO, and aerosol). However, there are still the limitations of the satellite information due to the uncertainties in satellite retrievals, the lack of vertical structure of pollutants in the atmosphere (which cannot directly provide ground-level information) and the gaps in spatial coverage caused by the cloud. For these reasons, it is necessary that the user should understand the strengths and limitations of a particular satellite product and perform proper validation of the satellite products before apply for air quality study. In addition satellite observations can provide qualitative information on the high pollution episodes in regional scale including a large scale plumes to study the regional transport phenomena. Furthermore, by incorporating satellite information with air quality models, satellite observations provide valuable datasets to assess the accuracy of current emission inventories especially in the limited in situ availability, and can be perhaps used to enhance such emission estimates by using inverse modeling technique.

9.3 Recommendation for future work

In spite of every effort to pursue the objectives of this study, there are some limitations of the research. This study focused mostly on the capital cities and the cities in urban areas, further analysis should extend to broader areas including suburban and rural locations. The

comparative analysis between ground-based and satellite-based datasets was performed intensively over Thailand. More analysis in other countries would help validate the capability of the satellite to be used as a surrogate for surface air pollutant monitoring.

For the development of regression models to estimate PM mass concentrations, since human activities and local meteorological conditions vary seasonally and likely to play an important role in AOD-PM correlations, further multivariate analysis in different season for the effects of other meteorological parameters such as wind direction, atmospheric pressure, boundary layer height, and haze layer height would help determining the strengths of such correlations. In addition, ground-level PM monitoring are restricted to the surface layer, applied aerosol vertical profile to split the total AOD columns could increase AOD-PM correlations. Since geographical conditions vary regionally, the difference in the surface reflectance in different regions and seasons can effect on the accuracy of AOD retrievals. Thus, further study on the geographical factors by comparing many stations at different locations in Asia would provide a better understanding of the AOD-PM relationships. AOD retrievals also depend on PM compositions and particle size due to their effect on light scattering/absorption. Further investigations on PM compositions and particle size would also help in a better understanding of the correlation between satellite AODs and surface PM concentrations. Since the chemical reactions in the atmosphere related to temperature are non-linear, the next study should consider more on the non-linear regression models.

For model simulations, increasing model horizontal resolution would increase the accuracy of the simulated results which in turn improve the correlation with the satellite observations that is used to validate the emission inventories. Moreover, applying different emission inventories in the model and comparing with ground-based and satellite-based measurements would also help evaluating the current emission inventories. Finally, this study has considered only three atmospheric species (NO_2, CO, and aerosol) due to the intensive validation from the previous studies. However, there are also other species that have been already provided by satellite observations such as SO_2, O_3, VOCs, etc., hence the next study should consider these pollutants to investigate the correlation between them.

Bibliography

Akimoto H (2003) Global air quality and pollution. Science 302:1716–1719. doi: 10.1126/science.1092666

Andreae MO, Merlet P (2001) Emission of trace gases and aerosols from biomass burning. Global Biogeochem Cycles 15:955–966. doi: 10.1029/2000GB001382

APMA (Air Pollution of Mega Cities in Asia) (2002) Benchmarking Urban Air Quality Management and Practice in Major and Mega Cities of Asia Stage 1. Haq G, Han WJ, and Kim C (ed), Korea Environment Institute, Seoul

Barladeanu R, Stefan S, Radulescu R (2012) Correlation between the particulate matter (PM10) mass concentrations and aerosol optical depth in Bucharest, Romania. Rom Reports Phys 64:1085–1096.

Bates TS, Kelly KC, Johnson JE, Gammon RH (1995) Regional and seasonal variations in the flux of oceanic carbon monoxide to the atmosphere. J Geophys Res 100:23093–23101. doi: 10.1029/95JD02737

Beverland I., Crowther J., Srinivas MS., Heal M. (1998) The influence of meteorology and atmospheric transport patterns on the chemical composition of rainfall in south-east England. Atmos Environ 32:1039–1048. doi: 10.1016/S1352-2310(97)00365-8

Blond N, Boersma KF, Eskes HJ, et al. (2007) Intercomparison of SCIAMACHY nitrogen dioxide observations, in situ measurements and air quality modeling results over Western Europe. J Geophys Res 112:D10311. doi: 10.1029/2006JD007277

Boersma KF, Eskes HJ, Brinksma EJ (2004) Error analysis for tropospheric NO2 retrieval from space. J Geophys Res 109:D04311. doi: 10.1029/2003JD003962

Boersma KF, Eskes HJ, Dirksen RJ, et al. (2011) An improved tropospheric NO_2 column retrieval algorithm for the Ozone Monitoring Instrument. Atmos Meas Tech 4:1905–1928. doi: 10.5194/amt-4-1905-2011

Boersma KF, Eskes HJ, Veefkind JP, et al. (2007) Near-real time retrieval of tropospheric NO2 from OMI. Atmos Chem Phys 7:2103–2118. doi: 10.5194/acp-7-2103-2007

Bonnet S, Suwanprik N, Garivait S (2006) Potential Impact of Biomass Burning on Urban Air Quality : Case-study of Chiang Mai. 2nd Jt. Int. Conf. “Sustainable Energy Environ. (SEE 2006).”Bangkok, Thailand, p D–025 (O)

Bovensmann H, Burrows JP, Buchwitz M, et al. (1999) SCIAMACHY: Mission Objectives and Measurement Modes. J Atmos Sci 56:127–150. doi: 10.1175/1520-0469(1999)056<0127:SMOAMM>2.0.CO;2

Buchwitz M, Khlystova I, Bovensmann H, Burrows JP (2007) Three years of global carbon monoxide from SCIAMACHY: comparison with MOPITT and first results related to the

detection of enhanced CO over cities. Atmos Chem Phys Discuss 7:405–428. doi: 10.5194/acpd-7-405-2007

Bucsela EJ, Krotkov NA, Celarier EA, et al. (2013) A new stratospheric and tropospheric NO2 retrieval algorithm for nadir-viewing satellite instruments: applications to OMI. Atmos Meas Tech Discuss 6:1361–1407. doi: 10.5194/amtd-6-1361-2013

Burrows JP, Weber M, Buchwitz M, et al. (1999) The Global Ozone Monitoring Experiment (GOME): Mission Concept and First Scientific Results. J Atmos Sci 56:151–175. doi: 10.1175/1520-0469(1999)056<0151:TGOMEG>2.0.CO;2

Byun DW, Ching JKS (1999) Science Algorithms of the EPA Models-3 Community Multiscale Air Quality (CMAQ) modeling system. United States Environ. Prot. Agency

Callies J, Corpaccioli E, Eisinger M, et al. (2000) GOME-2-Metop's second-generation sensor for operational ozone monitoring. ESA Bull. 102

Cao J, Chow JC, Lee FSC, Watson JG (2013) Evolution of PM2.5 Measurements and Standards in the U.S. and Future Perspectives for China. Aerosol Air Qual Res 1197–1211. doi: 10.4209/aaqr.2012.11.0302

CCSP (U.S. Climate Change Science Program and the Subcommittee on Global Change Research) (2009) Atmospheric Aerosol Properties and Climate Impacts. Washington, DC, pp 11

Celarier EA, Brinksma EJ, Gleason JF, et al. (2008) Validation of Ozone Monitoring Instrument nitrogen dioxide columns. J Geophys Res 113:D15S15. doi: 10.1029/2007JD008908

Christian HJ, Blakeslee RJ, Boccippio DJ, et al. (2003) Global frequency and distribution of lightning as observed from space by the Optical Transient Detector. J Geophys Res 108:4005. doi: 10.1029/2002JD002347

Chu DA, Kaufman YJ, Ichoku C, et al. (2002) Validation of MODIS aerosol optical depth retrieval over land. 29:4–7.

Chu DA, Kaufman YJ, Zibordi G, et al. (2003) Global monitoring of air pollution over land from the Earth Observing System-Terra Moderate Resolution Imaging Spectroradiometer (MODIS). J Geophys Res 108:4661. doi: 10.1029/2002JD003179

Clerbaux C, George M, Turquety S, et al. (2008) and Physics CO measurements from the ACE-FTS satellite instrument : data analysis and validation using ground-based , airborne and spaceborne observations. 2569–2594.

Crutzen PJ, Zimmermann PH (1991) The changing photochemistry of the troposphere. Tellus B 43:136–151. doi: 10.1034/j.1600-0889.1991.t01-1-00012.x

Dawson JP, Adams PJ, Pandis SN (2007) and Physics Sensitivity of PM 2 . 5 to climate in the Eastern US : a modeling case study. 4295–4309.

Day DE, Malm WC (2001) Aerosol light scattering measurements as a function of relative humidity: a comparison between measurements made at three different sites. Atmos Environ 35:5169–5176. doi: 10.1016/S1352-2310(01)00320-X

Deeter MN, Edwards DP, Gille JC, et al. (2010) The MOPITT version 4 CO product: Algorithm enhancements, validation, and long-term stability. J Geophys Res 115:D07306. doi: 10.1029/2009JD013005

Deeter MN, Edwards DP, Gille JC, Drummond JR (2007) Sensitivity of MOPITT observations to carbon monoxide in the lower troposphere. J Geophys Res 112:D24306. doi: 10.1029/2007JD008929

Deeter MN, Emmons LK, Francis GL, et al. (2004) Evaluation of operational radiances for the Measurements of Pollution in the Troposphere (MOPITT) instrument CO thermal band channels. J Geophys Res 109:D03308. doi: 10.1029/2003JD003970

Deeter MN, Martínez-Alonso S, Edwards DP, et al. (2013) Validation of MOPITT Version 5 thermal-infrared, near-infrared, and multispectral carbon monoxide profile retrievals for 2000-2011. J Geophys Res Atmos 118:6710–6725. doi: 10.1002/jgrd.50272

Diehl T, Heil a., Chin M, et al. (2012) Anthropogenic, biomass burning, and volcanic emissions of black carbon, organic carbon, and SO_2 from 1980 to 2010 for hindcast model experiments. Atmos Chem Phys Discuss 12:24895–24954. doi: 10.5194/acpd-12-24895-2012

Dinoi A, Perrone MR, Burlizzi P (2010) Application of MODIS Products for Air Quality Studies Over Southeastern Italy. Remote Sens 2:1767–1796. doi: 10.3390/rs2071767

De Laat ATJ, Gloudemans AMS, Aben I, Schrijver H (2010a) Global evaluation of SCIAMACHY and MOPITT carbon monoxide column differences for 2004–2005. J Geophys Res 115:D06307. doi: 10.1029/2009JD012698

De Laat ATJ, Gloudemans AMS, Schrijver H, et al. (2010b) Validation of five years (2003–2007) of SCIAMACHY CO total column measurements using ground-based spectrometer observations. Atmos Meas Tech 3:1457–1471. doi: 10.5194/amt-3-1457-2010

De Laat ATJ, Gloudemans AMS, Schrijver H, et al. (2006) Quantitative analysis of SCIAMACHY carbon monoxide total column measurements. Geophys Res Lett 33:L07807. doi: 10.1029/2005GL025530

Duncan BN, Prados AI, Lamsal L, et al. (2014) Satellite Data of Atmospheric Pollution for U.S. Air Quality Applications: Examples of Applications, Summary of Data End-User Resources, Answers to FAQs, and Common Mistakes to Avoid. Atmos Environ. doi: 10.1016/j.atmosenv.2014.05.061

Edwards DP, Emmons LK, Gille JC, et al. (2006) Satellite-observed pollution from Southern Hemisphere biomass burning. J Geophys Res 111:D14312. doi: 10.1029/2005JD006655

Edwards DP, Emmons LK, Hauglustaine DA, et al. (2004) Observations of carbon monoxide and aerosols from the Terra satellite: Northern Hemisphere variability. J Geophys Res 109:D24202. doi: 10.1029/2004JD004727

EIA (U.S. Energy Information Administration). International Energy Statistic. http://www.eia.gov/cfapps/ipdbproject/IEDIndex3.cfm. Accessed 14 February 2013

Emmons LK, Deeter MN, Gille JC, et al. (2004) Validation of Measurements of Pollution in the Troposphere (MOPITT) CO retrievals with aircraft in situ profiles. J Geophys Res 109:D03309. doi: 10.1029/2003JD004101

Emmons LK, Edwards DP, Deeter MN, et al. (2009) Measurements of Pollution In The Troposphere (MOPITT) validation through 2006. Atmos Chem Phys 9:1795–1803. doi: 10.5194/acp-9-1795-2009

Emmons LK, Pfister GG, Edwards DP, et al. (2007) Measurements of Pollution in the Troposphere (MOPITT) validation exercises during summer 2004 field campaigns over North America. J Geophys Res 112:D12S02. doi: 10.1029/2006JD007833

Engel-Cox JA, Hoff RM, Rogers R, et al. (2006) Integrating lidar and satellite optical depth with ambient monitoring for 3-dimensional particulate characterization. Atmos Environ 40:8056–8067. doi: 10.1016/j.atmosenv.2006.02.039

Engel-Cox JA, Holloman CH, Coutant BW, Hoff RM (2004) Qualitative and quantitative evaluation of MODIS satellite sensor data for regional and urban scale air quality. Atmos Environ 38:2495–2509. doi: 10.1016/j.atmosenv.2004.01.039

Fujimori S, Matsuoka Y (2011) Development of method for estimation of world industrial energy consumption and its application. Energy Econ 33:461–473. doi: 10.1016/j.eneco.2011.01.010

Galanter M, Levy H, Carmichael GR (2000) Impacts of biomass burning on tropospheric CO, NOx , and O3. J Geophys Res 105:6633–6653. doi: 10.1029/1999JD901113

Ghude SD, Van der A RJ, Beig G, et al. (2009) Satellite derived trends in NO2 over the major global hotspot regions during the past decade and their inter-comparison. Environ Pollut 157:1873–1878. doi: 10.1016/j.envpol.2009.01.013

Ghude SD, Fadnavis S, Beig G, et al. (2008) Detection of surface emission hot spots, trends, and seasonal cycle from satellite-retrieved NO 2 over India. J Geophys Res 113:D20305. doi: 10.1029/2007JD009615

Gloudemans AMS, de Laat ATJ, Schrijver H, et al. (2009) SCIAMACHY CO over land and oceans: 2003–2007 interannual variability. Atmos Chem Phys 9:3799–3813. doi: 10.5194/acp-9-3799-2009

Gloudemans AMS, Schrijver H, Hasekamp OP, Aben I (2008) Error analysis for CO and CH4 total column retrievals from SCIAMACHY 2.3 μm spectra. Atmos Chem Phys 8:3999–4017. doi: 10.5194/acp-8-3999-2008

Granier C, Bessagnet B, Bond T, et al. (2011) Evolution of anthropogenic and biomass burning emissions of air pollutants at global and regional scales during the 1980–2010 period. Clim Change 109:163–190. doi: 10.1007/s10584-011-0154-1

Granier C, Pétron G, Müller J-F, Brasseur G (2000) The impact of natural and anthropogenic hydrocarbons on the tropospheric budget of carbon monoxide. Atmos Environ 34:5255–5270. doi: 10.1016/S1352-2310(00)00299-5

Guo J-P, Zhang X-Y, Che H-Z, et al. (2009) Correlation between PM concentrations and aerosol optical depth in eastern China. Atmos Environ 43:5876–5886. doi: 10.1016/j.atmosenv.2009.08.026

Guo J-P, Zhang X-Y, Wu Y-R, et al. (2011) Spatio-temporal variation trends of satellite-based aerosol optical depth in China during 1980–2008. Atmos Environ 45:6802–6811. doi: 10.1016/j.atmosenv.2011.03.068

Gupta P, Christopher S a. (2008a) Seven year particulate matter air quality assessment from surface and satellite measurements. Atmos Chem Phys Discuss 8:327–365. doi: 10.5194/acpd-8-327-2008

Gupta P, Christopher S a. (2008b) An evaluation of Terra-MODIS sampling for monthly and annual particulate matter air quality assessment over the Southeastern United States. Atmos Environ 42:6465–6471. doi: 10.1016/j.atmosenv.2008.04.044

Gupta P, Christopher SA, Box MA, Box GP (2007) Multi year satellite remote sensing of particulate matter air quality over Sydney, Australia. Int J Remote Sens 28:4483–4498. doi: 10.1080/01431160701241738

Gupta P, Christopher SA, Wang J, et al. (2006) Satellite remote sensing of particulate matter and air quality assessment over global cities. Atmos Environ 40:5880–5892. doi: 10.1016/j.atmosenv.2006.03.016

Hadjimitsis DG (2009) Aerosol optical thickness (AOT) retrieval over land using satellite image-based algorithm. Air Qual Atmos Heal 2:89–97. doi: 10.1007/s11869-009-0036-0

Han KM, Lee CK, Lee J, et al. (2011) A comparison study between model-predicted and OMI-retrieved tropospheric NO2 columns over the Korean peninsula. Atmos Environ 45:2962–2971. doi: 10.1016/j.atmosenv.2010.10.016

Han KM, Song CH, Ahn HJ, et al. (2009) Investigation of NO x emissions and NO x -related chemistry in East Asia using CMAQ-predicted and GOME-derived NO 2 columns. Atmos Chem Phys 9:1017–1036.

Hao J, He K, Duan L, et al. (2007) Air pollution and its control in China. Front Environ Sci Eng China 1:129–142. doi: 10.1007/s11783-007-0024-2

He Q, Li C, Geng F, et al. (2012) Study on Long-term Aerosol Distribution over the Land of East China Using MODIS Data. Aerosol Air Qual Res 12:304–319. doi: 10.4209/aaqr.2011.11.0200

He Y, Uno I, Wang Z, et al. (2007) Variations of the increasing trend of tropospheric NO2 over central east China during the past decade. Atmos Environ 41:4865–4876. doi: 10.1016/j.atmosenv.2007.02.009

HEI (Health Effects Institute) (2010) Outdoor Air Pollution and Health in the Developing Countries of Asia: A Comprehensive Review, Special Report 18. HEI International Oversight Committee, Boston, MA

Heland J, Schlager H, Richter A, Burrows JP (2002) First comparison of tropospheric NO2 column densities retrieved from GOME measurements and in situ aircraft profile measurements. Geophys Res Lett 29:1983. doi: 10.1029/2002GL015528

Holben BN, Eck TF, Slutsker I, et al. (1998) AERONET — A Federated Instrument Network and Data Archive for Aerosol Characterization. Remote Sens Environ 66:1–16. doi: http://dx.doi.org/10.1016/S0034-4257(98)00031-5

Irie H, Yamaji K, Ikeda K, et al. (2013) An evaluation of the CMAQ reproducibility of satellite tropospheric NO_2 column observations at different local times over East Asia. Atmos Chem Phys Discuss 13:14037–14067. doi: 10.5194/acpd-13-14037-2013

Itahashi S, Uno I, Irie H, et al. (2013) Trend analysis of tropospheric NO_2 column density over East Asia during 2000–2010: multi-satellite observations and model simulations with the updated REAS emission inventory. Atmos Chem Phys Discuss 13:11247–11268. doi: 10.5194/acpd-13-11247-2013

Jiang X, Liu Y, Yu B, Jiang M (2007) Comparison of MISR aerosol optical thickness with AERONET measurements in Beijing metropolitan area. Remote Sens Environ 107:45–53. doi: 10.1016/j.rse.2006.06.022

Khalil MA, Rasmussen RA (1984) Carbon Monoxide in the Earth's Atmosphere: Increasing Trend. Science 224:54–6. doi: 10.1126/science.224.4644.54

Kim Oanh NT (2012) Integrated air quality management: Asian case studies. CRC Press, Florida

Kim Oanh NT, Leelasakultum K (2011) Analysis of meteorology and emission in haze episode prevalence over mountain-bounded region for early warning. Sci Total Environ 409:2261–71. doi: 10.1016/j.scitotenv.2011.02.022

Kim S-W, Yoon S-C, Kim J, Kim S-Y (2007) Seasonal and monthly variations of columnar aerosol optical properties over east Asia determined from multi-year MODIS, LIDAR, and AERONET Sun/sky radiometer measurements. Atmos Environ 41:1634–1651. doi: 10.1016/j.atmosenv.2006.10.044

Koelemeijer RBA, Homan CD, Matthijsen J (2006) Comparison of spatial and temporal variations of aerosol optical thickness and particulate matter over Europe. Atmos Environ 40:5304–5315. doi: 10.1016/j.atmosenv.2006.04.044

Kopacz M, Jacob DJ, Fisher J a., et al. (2010) Global estimates of CO sources with high resolution by adjoint inversion of multiple satellite datasets (MOPITT, AIRS, SCIAMACHY, TES). Atmos Chem Phys 10:855–876. doi: 10.5194/acp-10-855-2010

Kopacz M, Jacob DJ, Henze DK, et al. (2009) Comparison of adjoint and analytical Bayesian inversion methods for constraining Asian sources of carbon monoxide using satellite (MOPITT) measurements of CO columns. J Geophys Res 114:D04305. doi: 10.1029/2007JD009264

Kumar N, Chu A, Foster A (2007) An empirical relationship between PM(2.5) and aerosol optical depth in Delhi Metropolitan. Atmos Environ (1994) 41:4492–4503. doi: 10.1016/j.atmosenv.2007.01.046

Kumar R, Naja M, Pfister GG, et al. (2012) Simulations over South Asia using the Weather Research and Forecasting model with Chemistry (WRF-Chem): chemistry evaluation and initial results. Geosci Model Dev 5:619–648. doi: 10.5194/gmd-5-619-2012

LAADS (Level 1 and Atmosphere Archive and Distribution System). Goddard Space Flight Center. http://ladsweb.nascom.nasa.gov/. Accessed 3 May 2014

Lamarque J-F, Bond TC, Eyring V, et al. (2010) Historical (1850–2000) gridded anthropogenic and biomass burning emissions of reactive gases and aerosols: methodology and application. Atmos Chem Phys 10:7017–7039. doi: 10.5194/acp-10-7017-2010

Levelt P, van den Oord GHJ, Dobber MR, et al. (2006) The ozone monitoring instrument. IEEE Trans Geosci Remote Sens 44:1093–1101. doi: 10.1109/TGRS.2006.872333

Levy RC, Remer L a., Mattoo S, et al. (2007a) Second-generation operational algorithm: Retrieval of aerosol properties over land from inversion of Moderate Resolution Imaging Spectroradiometer spectral reflectance. J Geophys Res 112:D13211. doi: 10.1029/2006JD007811

Levy RC, Remer LA, Dubovik O (2007b) Global aerosol optical properties and application to Moderate Resolution Imaging Spectroradiometer aerosol retrieval over land. J Geophys Res 112:D13210. doi: 10.1029/2006JD007815

Lin J-T, McElroy MB, Boersma KF (2010) Constraint of anthropogenic NOx emissions in China from different sectors: a new methodology using multiple satellite retrievals. Atmos Chem Phys 10:63–78. doi: 10.5194/acp-10-63-2010

Liu Y, Franklin M, Kahn R, Koutrakis P (2007) Using aerosol optical thickness to predict ground-level PM2.5 concentrations in the St. Louis area: A comparison between MISR and MODIS. Remote Sens Environ 107:33–44. doi: 10.1016/j.rse.2006.05.022

Liu Y, Paciorek CJ, Koutrakis P (2009) Estimating regional spatial and temporal variability of PM(2.5) concentrations using satellite data, meteorology, and land use information. Environ Health Perspect 117:886–92. doi: 10.1289/ehp.0800123

Luo M, Rinsland CP, Rodgers CD, et al. (2007) Comparison of carbon monoxide measurements by TES and MOPITT: Influence of a priori data and instrument characteristics on nadir atmospheric species retrievals. J Geophys Res 112:D09303. doi: 10.1029/2006JD007663

Ma J, Richter A, Burrows JP, et al. (2006) Comparison of model-simulated tropospheric NO2 over China with GOME-satellite data. Atmos Environ 40:593–604. doi: 10.1016/j.atmosenv.2005.09.029

Martin R V. (2008) Satellite remote sensing of surface air quality. Atmos Environ 42:7823–7843. doi: 10.1016/j.atmosenv.2008.07.018

Martin R V., Parrish DD, Ryerson TB, et al. (2004) Evaluation of GOME satellite measurements of tropospheric NO2 and HCHO using regional data from aircraft campaigns in the southeastern United States. J Geophys Res 109:D24307. doi: 10.1029/2004JD004869

Matsui H, Koike M, Kondo Y, et al. (2009) Spatial and temporal variations of aerosols around Beijing in summer 2006: Model evaluation and source apportionment. J Geophys Res 114:D00G13. doi: 10.1029/2008JD010906

Mishchenko MI, Liu L, Geogdzhayev I V., et al. (2010) Toward unified satellite climatology of aerosol properties. J Quant Spectrosc Radiat Transf 111:540–552. doi: 10.1016/j.jqsrt.2009.11.003

NCAR (The National Center for Atmospheric Research). Measurements Of Pollution In The Troposphere (MOPITT). http://www.acd.ucar.edu/mopitt/visualize.shtml. Accessed 3 May 2014

Ohara T, Akimoto H, Kurokawa J, et al. (2007) An Asian emission inventory of anthropogenic emission sources for the period 1980–2020. Atmos Chem Phys Discuss 7:6843–6902. doi: 10.5194/acpd-7-6843-2007

Panicker a. S, Pandithurai G, Dipu S (2010) Aerosol indirect effect during successive contrasting monsoon seasons over Indian subcontinent using MODIS data. Atmos Environ 44:1937–1943. doi: 10.1016/j.atmosenv.2010.02.015

Paramee S, Chidthaisong A, Towprayoon S, et al. (2005) Three-year monitoring results of nitrate and ammonium wet deposition in Thailand. Environ Monit Assess 102:27–40. doi: 10.1007/s10661-005-1593-9

Pelletier B, Santer R, Vidot J (2007) Retrieving of particulate matter from optical measurements: A semiparametric approach. J Geophys Res 112:D06208. doi: 10.1029/2005JD006737

Permadi DA, Kim Oanh NT (2008) Episodic ozone air quality in Jakarta in relation to meteorological conditions. Atmos Environ 42:6806–6815. doi: 10.1016/j.atmosenv.2008.05.014

Retalis A, Hadjimitsis DG, Michaelides S, et al. (2010) Comparison of aerosol optical thickness with in situ visibility data over Cyprus. Nat Hazards Earth Syst Sci 10:421–428. doi: 10.5194/nhess-10-421-2010

Richter A, Burrows JP, Nüss H, et al. (2005) Increase in tropospheric nitrogen dioxide over China observed from space. Nature 437:129–32. doi: 10.1038/nature04092

Saha S, Moorthi S, Pan H-L, et al. (2010) The NCEP Climate Forecast System Reanalysis. Bull Am Meteorol Soc 91:1015–1057. doi: 10.1175/2010BAMS3001.1

Schaap M, Apituley A, Timmermans RMA, et al. (2009) Exploring the relation between aerosol optical depth and PM2.5 at Cabauw, the Netherlands. Atmos Chem Phys 9:909–925. doi: 10.5194/acp-9-909-2009

Schaap M, Timmermans RM a., Koelemeijer RB a., et al. (2008) Evaluation of MODIS aerosol optical thickness over Europe using sun photometer observations. Atmos Environ 42:2187–2197. doi: 10.1016/j.atmosenv.2007.11.044

Shi C, Fernando HJS, Wang Z, et al. (2008) Tropospheric NO2 columns over East Central China: Comparisons between SCIAMACHY measurements and nested CMAQ simulations. Atmos Environ 42:7165–7173. doi: 10.1016/j.atmosenv.2008.05.046

Shindell DT, Faluvegi G, Stevenson DS, et al. (2006) Multimodel simulations of carbon monoxide: Comparison with observations and projected near-future changes. J Geophys Res 111:D19306. doi: 10.1029/2006JD007100

Solomon S, Portmann RW, Sanders RW, et al. (1999) On the role of nitrogen dioxide in the absorption of solar radiation. J Geophys Res 104:12,047–12,058. doi: 10.1029/1999JD900035

Streets DG, Yarber KF, Woo J-H, Carmichael GR (2003) Biomass burning in Asia: Annual and seasonal estimates and atmospheric emissions. Global Biogeochem Cycles 17:n/a–n/a. doi: 10.1029/2003GB002040

Sukitpaneenit M, Kim Oanh NT (2014) Satellite monitoring for carbon monoxide and particulate matter during forest fire episodes in Northern Thailand. Environ Monit Assess 186:2495–504. doi: 10.1007/s10661-013-3556-x

Sun YL, Wang ZF, Fu PQ, et al. (2013) Aerosol composition, sources and processes during wintertime in Beijing, China. Atmos Chem Phys 13:4577–4592. doi: 10.5194/acp-13-4577-2013

TEMIS (Tropospheric Emission Monitoring Internet Service). Tropospheric NO_2 from satellites. http://www.temis.nl/airpollution/no2.html. Accessed 3 May 2014

Tian J, Chen D (2010) A semi-empirical model for predicting hourly ground-level fine particulate matter (PM2.5) concentration in southern Ontario from satellite remote sensing and ground-based meteorological measurements. Remote Sens Environ 114:221–229. doi: 10.1016/j.rse.2009.09.011

Tipayarom D, Kim Oanh NT (2007) Effects from Open Rice Straw Burning Emission on Air Quality in the Bangkok Metropolitan Region. ScienceAsia 33:339–345. doi: 10.2306/scienceasia1513-1874.2007.33.339

Tsai T-C, Jeng Y-J, Chu DA, et al. (2011) Analysis of the relationship between MODIS aerosol optical depth and particulate matter from 2006 to 2008. Atmos Environ 45:4777–4788. doi: 10.1016/j.atmosenv.2009.10.006

UNEP (United Nations Environment Program) (2012) Global Environment Outlook 5. Progress Press, Malta

Uno I, He Y, Ohara T, et al. (2007) Systematic analysis of interannual and seasonal variations of model-simulated tropospheric NO2 in Asia and comparison with GOME-satellite data. Atmos Chem Phys 7:1671–1681. doi: 10.5194/acp-7-1671-2007

van der A RJ, Eskes HJ, Boersma KF, et al. (2008) Trends, seasonal variability and dominant NO x source derived from a ten year record of NO 2 measured from space. J Geophys Res 113:D04302. doi: 10.1029/2007JD009021

van der A RJ, Peters DHMU, Eskes H, et al. (2006) Detection of the trend and seasonal variation in tropospheric NO 2 over China. J Geophys Res 111:D12317. doi: 10.1029/2005JD006594

van Donkelaar A, Martin R V., Park RJ (2006) Estimating ground-level PM 2.5 using aerosol optical depth determined from satellite remote sensing. J Geophys Res 111:D21201. doi: 10.1029/2005JD006996

van der Werf GR, Randerson JT, Giglio L, et al. (2006) Interannual variability in global biomass burning emissions from 1997 to 2004. Atmos Chem Phys 6:3423–3441. doi: 10.5194/acp-6-3423-2006

Velders GJM, Granier C, Potmann RW, et al. (2001) Global tropospheric NO2 columns distributions comparing 3-dimensional model calculations with GOME measurements. J Geophys Res 106:12643–12660. doi: 10.1029/2000JD900762

Venkataraman C, Habib G, Kadamba D, et al. (2006) Emissions from open biomass burning in India: Integrating the inventory approach with high-resolution Moderate Resolution Imaging Spectroradiometer (MODIS) active-fire and land cover data. Global Biogeochem Cycles 20:n/a–n/a. doi: 10.1029/2005GB002547

Wang J, Christopher SA (2003) Intercomparison between satellite-derived aerosol optical thickness and PM 2.5 mass: Implications for air quality studies. Geophys Res Lett 30:2095. doi: 10.1029/2003GL018174

Wang J, Martin ST (2007) Satellite characterization of urban aerosols: Importance of including hygroscopicity and mixing state in the retrieval algorithms. J Geophys Res 112:D17203. doi: 10.1029/2006JD008078

Wang L, Wang Y, Xin J, et al. (2010) Assessment and comparison of three years of Terra and Aqua MODIS Aerosol Optical Depth Retrieval (C005) in Chinese terrestrial regions. Atmos Res 97:229–240. doi: 10.1016/j.atmosres.2010.04.004

Warner J, Comer MM, Barnet CD, et al. (2007) A comparison of satellite tropospheric carbon monoxide measurements from AIRS and MOPITT during INTEX-A. J Geophys Res 112:D12S17. doi: 10.1029/2006JD007925

WHO (World Health Organization) (2006) Air quality guideline: global update 2005, particulate matter, ozone, nitrogen dioxide, sulfur dioxide. WHO Regional Office for Europe, Copenhagen

Worden HM, Deeter MN, Edwards DP, et al. (2010) Observations of near-surface carbon monoxide from space using MOPITT multispectral retrievals. J Geophys Res 115:D18314. doi: 10.1029/2010JD014242

Worden HM, Deeter MN, Frankenberg C, et al. (2013) Decadal record of satellite carbon monoxide observations. Atmos Chem Phys 13:837–850. doi: 10.5194/acp-13-837-2013

Xin J, Wang L, Wang Y, et al. (2011) Trends in aerosol optical properties over the Bohai Rim in Northeast China from 2004 to 2010. Atmos Environ 45:6317–6325. doi: 10.1016/j.atmosenv.2011.08.052

Xing J, Wang SX, Chatani S, et al. (2011) Projections of air pollutant emissions and its impacts on regional air quality in China in 2020. Atmos Chem Phys 11:3119–3136. doi: 10.5194/acp-11-3119-2011

Yamaji K, Ohara T, Akimoto H (2003) A country-specific, high-resolution emission inventory for methane from livestock in Asia in 2000. Atmos Environ 37:4393–4406. doi: 10.1016/S1352-2310(03)00586-7

Yan X, Cai Z, Ohara T, Akimoto H (2003a) Methane emission from rice fields in mainland China: Amount and seasonal and spatial distribution. J Geophys Res 108:4505. doi: 10.1029/2002JD003182

Yan X, Ohara T, Akimoto H (2003b) Development of region-specific emission factors and estimation of methane emission from rice fields in the East, Southeast and South Asian countries. Glob Chang Biol 9:237–254. doi: 10.1046/j.1365-2486.2003.00564.x

Yienger JJ, Levy H (1995) Empirical model of global soil-biogenic NO χ emissions. J Geophys Res 100:11447. doi: 10.1029/95JD00370

Yurganov L, McMillan W, Grechko E, Dzhola A (2010) Analysis of global and regional CO burdens measured from space between 2000 and 2009 and validated by ground-based solar tracking spectrometers. Atmos Chem Phys 10:3479–3494. doi: 10.5194/acp-10-3479-2010

Yurganov LN, Duchatelet P, Dzhola A V., et al. (2005) Increased Northern Hemispheric carbon monoxide burden in the troposphere in 2002 and 2003 detected from the ground and from space. Atmos Chem Phys 5:563–573. doi: 10.5194/acp-5-563-2005

Yurganov LN, McMillan WW, Dzhola A V., et al. (2008) Global AIRS and MOPITT CO measurements: Validation, comparison, and links to biomass burning variations and carbon cycle. J Geophys Res 113:D09301. doi: 10.1029/2007JD009229

Zhang G, Li J, Li X-D, et al. (2010) Impact of anthropogenic emissions and open biomass burning on regional carbonaceous aerosols in South China. Environ Pollut 158:3392–400. doi: 10.1016/j.envpol.2010.07.036

Zhang H, Hoff RM, Engel-cox JA (2009a) The Relation between Moderate Resolution Imaging Spectroradiometer (MODIS) Aerosol Optical Depth and PM 2 . 5 over the United States : A Geographical Comparison by U . S . Environmental Protection Agency Regions. 59:2–5. doi: 10.3155/1047-3289.59.10.1

Zhang Q, Streets DG, Carmichael GR, et al. (2009b) Asian emissions in 2006 for the NASA INTEX-B mission. Atmos Chem Phys 9:5131–5153. doi: 10.5194/acp-9-5131-2009

Zhang X, Zwiers FW, Stoot PA (2005) Multimodel Multisignal Climate Change Detection at Regional Scale. J Clim 19:4294–4307. doi: http://dx.doi.org/10.1175/JCLI3851.1

Zyrichidou I, Koukouli ME, Balis DS, et al. (2009a) Satellite NO_2 observations and model simulations of tropospheric columns over South-eastern Europe. Atmos Chem Phys Discuss 9:12171–12205. doi: 10.5194/acpd-9-12171-2009

Zyrichidou I, Koukouli ME, Balis DS, et al. (2009b) Satellite observations and model simulations of tropospheric NO2 columns over south-eastern Europe. Atmos Chem Phys 9:6119–6134. doi: 10.5194/acp-9-6119-2009

Appendices

Appendix A: Retrievals of satellite remote sensing

Remote sensing for Earth observation refers to the technique that uses electromagnetic radiation to acquire information without being in direct contact with the object or phenomenon under investigation, which in this case is the atmosphere. Earth-observing satellites include several components. The satellite platform is the infrastructure of the satellite sensor, which typically includes solar panels for power and hardware for instruments. Each platform generally consists of one to four sensors (Kim Oanh 2012). Detection of atmospheric pollutants bases on the principle that each pollutant absorbs or/and reflects specific wavelengths throughout the electromagnetic spectrum. This spectral signature is unique to that pollutants (Duncan et al. 2014). Satellite instruments can employ either passive or active technique. In general, the Sun is the source of radiation that is absorbed and reemitted, reflected, and backscattered by the atmosphere and Earth's surface and then detected by passive sensors. In contrast, active sensors transmit internal energy downward and measure the radiation that is returned. The infrared (IR), visibal, and ultraviolet (UV) regions of the eletramegnetic spectrum contain the most useful wavelengths for observaing pollutants relevant for air quality study. The atmospheric constituents cause specific spectral wavelength dependent absorption and scattering of radiation, known as attenuation or extinction. Trace gas and aerosol remote sensing take advantage of attenuation in the intensity of radiation traversing the atmosphere combining with variety of algorithms to retrieve a value that represents the constituents being measured. There are two defining features of satellite data which are spatial resolution and temporal resolution. Spatial resolution refers to the smallest area of Earth's surface that can be observed by a satellite sensor. Temporal resolution refers to the period that a satellite sensor requires to observe the same location of Earth's surface which depends on the orbit of the satellite. Many satellite instruments for Earth observation have been lunched since the mid-1990s. Table A.1 provides information on satellite remote sensing for air quality study considered in this research.

Table A.1 Characteristics of satellite remote sensing of air quality used in this study

Sensor	GOME	SCIAMACHY	OMI	GOME-2	MOPITT	MODIS
Platform	ERS-2	ENVISAT	Aura	MetOp	Terra	Terra/Aqua
Spectral range (μm)	0.23-0.79	0.23-2.38	0.27-0.50	0.24-0.79	2.20, 2.30, 4.70	36[a] λ/0.41-14.2
Ground pixel res. (km)	320 × 40	60 × 30	24 × 13	80 × 40	22 × 22	10 × 10
Global coverage (day)	3	6	1	1	3.5	2
Overpass local time	10:30	10:00	13:45	09:30	10:30	10:30/13:30
Operating time	1995-2003	2002-2012	2004-	2006-	2000-	2000-/2002-
Data products	NO_2, HCHO, SO_2, O_3	NO_2, HCHO, SO_2, O_3, CO	NO_2, HCHO, SO_2, O_3, aerosol	NO_2, HCHO, SO_2, O_3	CO	aerosol
Reference	Burrows et al. 1999	Bovensmann et al. 1999; Gloudemans et al. 2008	Boersma et al. 2007; Levelt et al. 2006	Boersma et al. 2004; Callies et al. 2000	Deeter et al. 2004	Levy et al. 2007a; Levy et al. 2007b

[a] Number of discrete wavelengths

Appendix B: Time series of satellite observations over the cities in Asia

Appendix B.1: Time series of tropospheric NO_2 columns retrieved from GOME, SCIAMACHY, OMI, and GOME-2 during 1996-2012

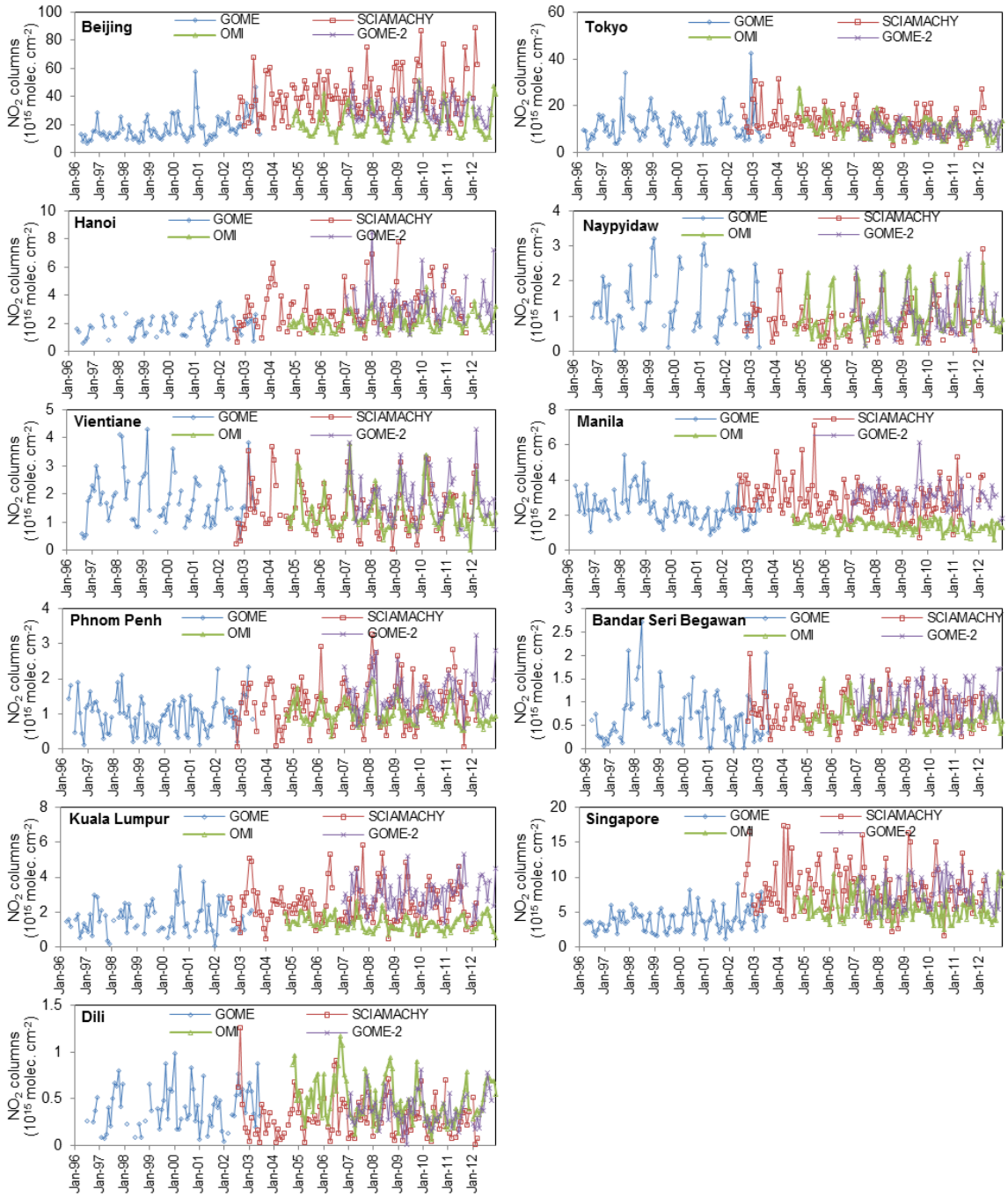

Appendix B.2: Time series of total CO columns retrieved from MOPITT and SCIAMACHY during 2000-2012

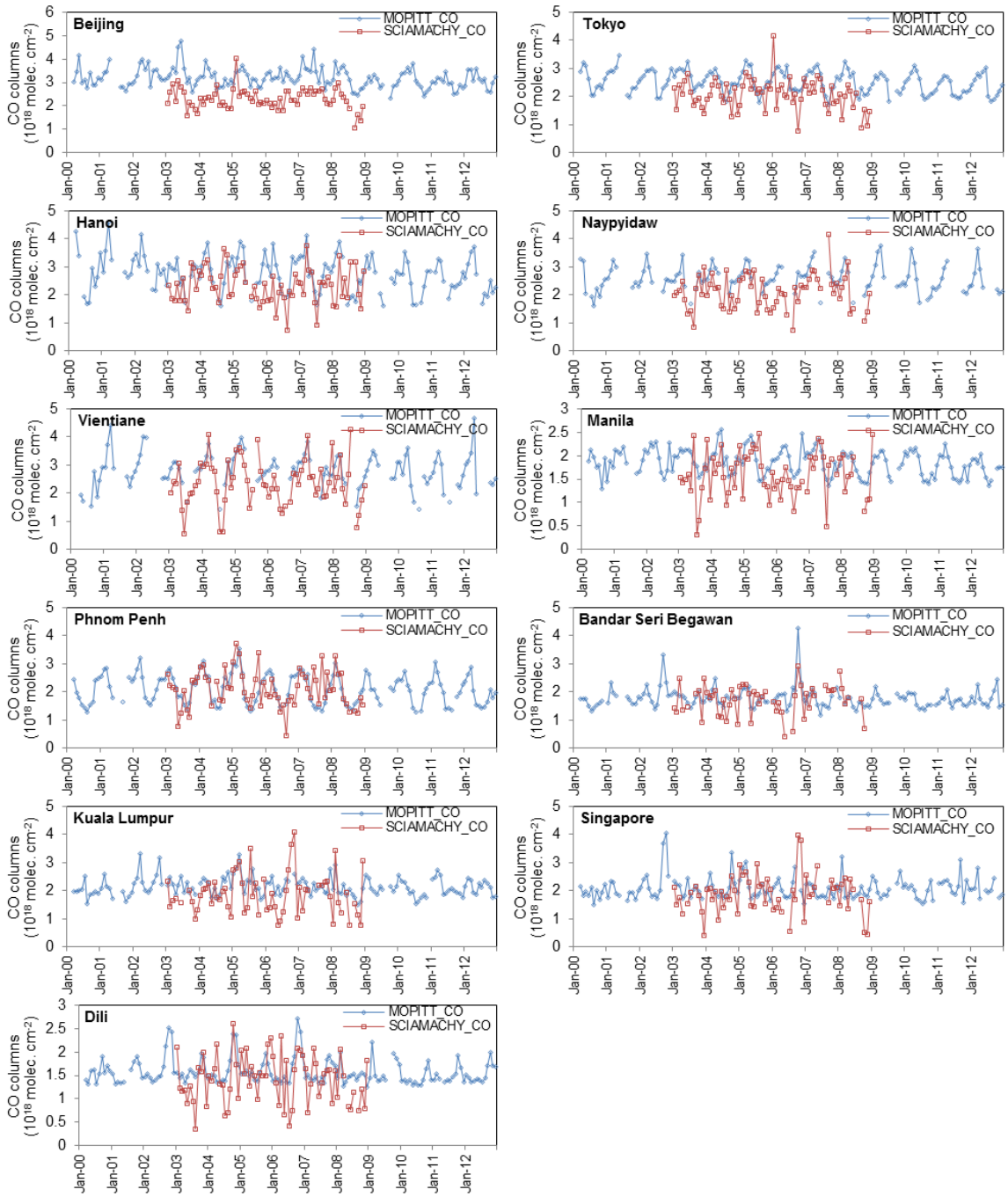

Appendix B.3: Time series of AOD retrieved from MODIS-Terra and MODIS-Aqua during 2000-2012

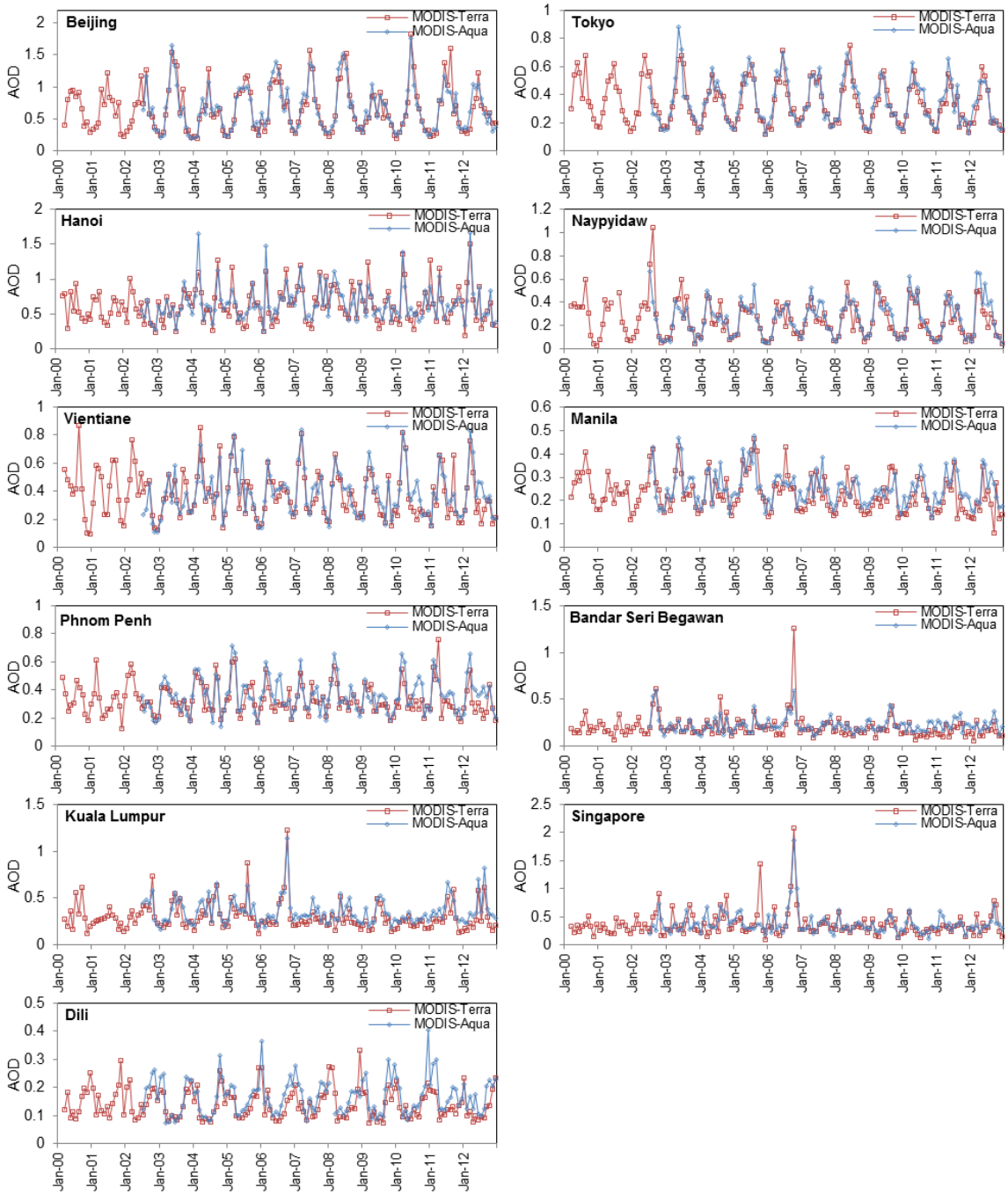

Appendix C: Significance (*p* value) of the variables considered in the models for PM_{10} concentration estimations

City	AOD-PM_{10}	Regression Model at CF ≤ 1/10	*P* value				
			Intercept	AOD	RH	WS	T
Chiangmai	AOD(Terra)-PM_{10}(9-12:00LT)	Model 1: PM_{10} = 24.30 + 171.42 (AOD)	4.5E-07	3.1E-32	-	-	-
		Model 2: PM_{10} = 232.66 + 153.80 (AOD) - 1.71 (RH) - 14.93 (WS) - 2.77 (T)	1.8E-06	4.2E-28	5.4E-06	6.1E-05	0.0211
	AOD(Aqua)-PM_{10}(12-15:00LT)	Model 1: PM_{10} = 20.71 + 124.22 (AOD)	2.2E-07	2.7E-29	-	-	-
		Model 2: PM_{10} = 109.32 + 128.01 (AOD) - 0.68 (RH) + 1.08 (WS) - 2.28 (T)	0.0346	1.8E-25	0.1497	0.7783	0.0934
	AOD(Terra-Aqua)-PM_{10}(24hrs)	Model 1: PM_{10} = 36.49 + 121.94 (AOD)	1.3E-72	1.2E-104	-	-	-
		Model 2: PM_{10} = 100.24 + 110.43 (AOD) - 0.77 (RH) - 5.07 (WS) - 0.22 (T)	1.8E-08	3.4E-82	1.6E-09	0.0297	0.6454
Bangkok	AOD(Terra)-PM_{10}(9-12:00LT)	Model 1: PM_{10} = 37.35 + 38.64 (AOD)	2.0E-09	0.0003	-	-	-
		Model 2: PM_{10} = 146.92 + 43.20 (AOD) - 0.39 (RH) - 27.80 (WS) - 1.94 (T)	2.7E-09	6.6E-06	0.0917	1.0E-06	0.0053
	AOD(Aqua)-PM_{10}(12-15:00LT)	Model 1: PM_{10} = 16.14 + 56.42 (AOD)	0.0018	2.3E-08	-	-	-
		Model 2: PM_{10} = 36.05 + 51.35 (AOD) - 0.51 (RH) + 1.31 (WS) - 0.12 (T)	0.1104	1.6E-07	0.0122	0.7792	0.8477
	AOD(Terra-Aqua)-PM_{10}(24hrs)	Model 1: PM_{10} = 36.94 + 48.49 (AOD)	7.5E-14	1.0E-08	-	-	-
		Model 2: PM_{10} = 154.65 + 50.53 (AOD) - 0.87 (RH) - 40.94 (WS) - 0.8 (T)	8.4E-17	5.2E-14	2.1E-08	5.6E-07	0.1253
Rayong	AOD(Terra)-PM_{10}(9-12:00LT)	Model 1: PM_{10} = 29.46 + 110.14 (AOD)	4.8E-08	3.7E-08	-	-	-
		Model 2: PM_{10} = 129.57 + 113.99 (AOD) - 0.93 (RH) - 4.55 (WS) - 1.27 (T)	0.0141	4.1E-08	0.0052	0.1507	0.3698
	AOD(Aqua)-PM_{10}(12-15:00LT)	Model 1: PM_{10} = 28.65 + 62.89 (AOD)	7.7E-11	5.8E-07	-	-	-
		Model 2: PM_{10} = 37.12 + 67.68 (AOD) - 0.21 (RH) + 1.03 (WS) - 0.02 (T)	0.3076	4.5E-07	0.2519	0.7826	0.9901
	AOD(Terra-Aqua)-PM_{10}(24hrs)	Model 1: PM_{10} = 44.17 + 96.22 (AOD)	2.6E-18	4.6E-09	-	-	-
		Model 2: PM_{10} = 155.72 + 90.96 (AOD) - 1.11 (RH) - 11.98 (WS) - 0.70 (T)	0.0003	3.2E-09	0.0016	0.0005	0.6319

Appendix D: Scatter plots of estimated vs. measured surface PM_{10} mass for year 2013

Appendix D.1: Scatter plots over Chiangmai during dry season (January-April) for 9-12:00LT (a), 12-15:00LT (b), and 24-hr (c) time windows

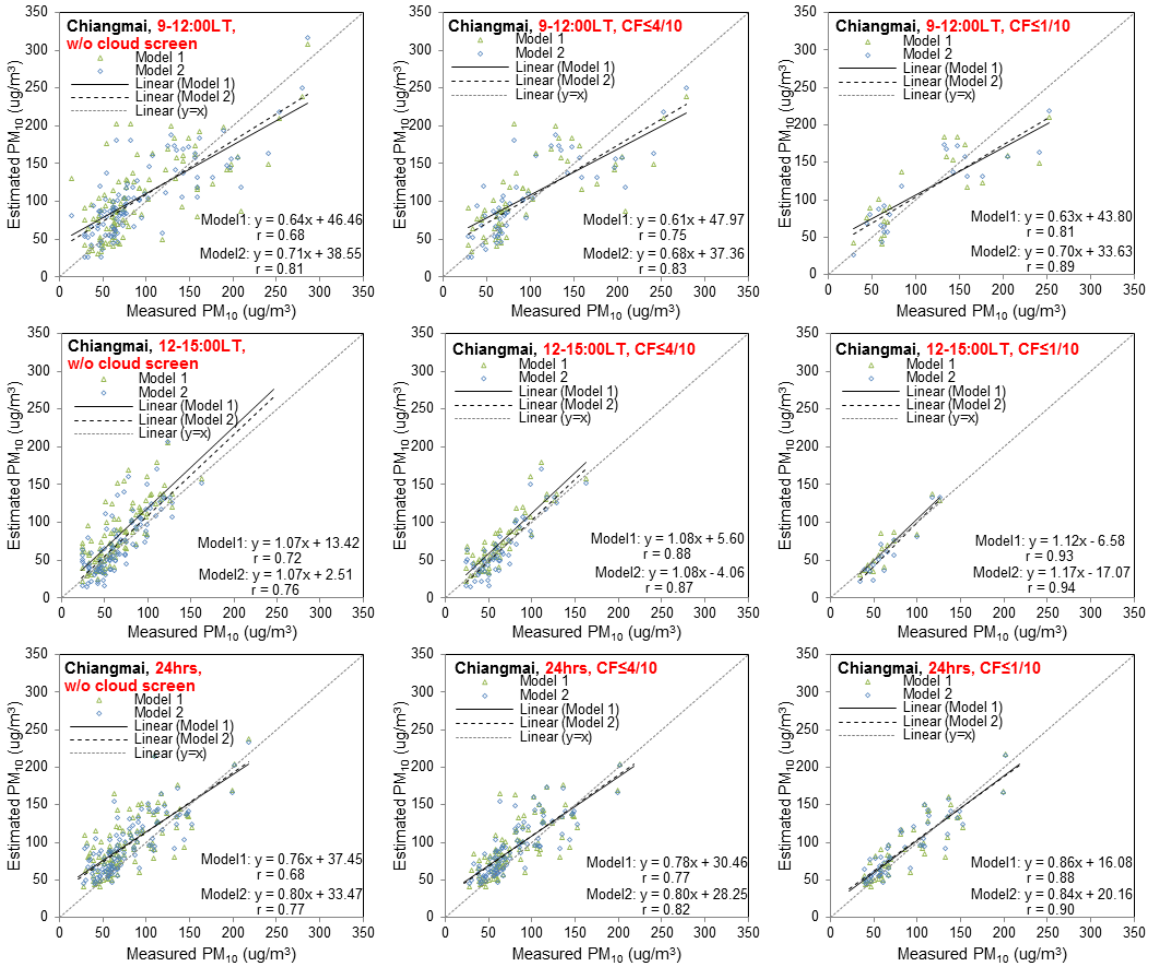

Appendix D.2: Scatter plots over Bangkok during dry season (January-April) for 9-12:00LT (a), 12-15:00LT (b), and 24-hr (c) time windows

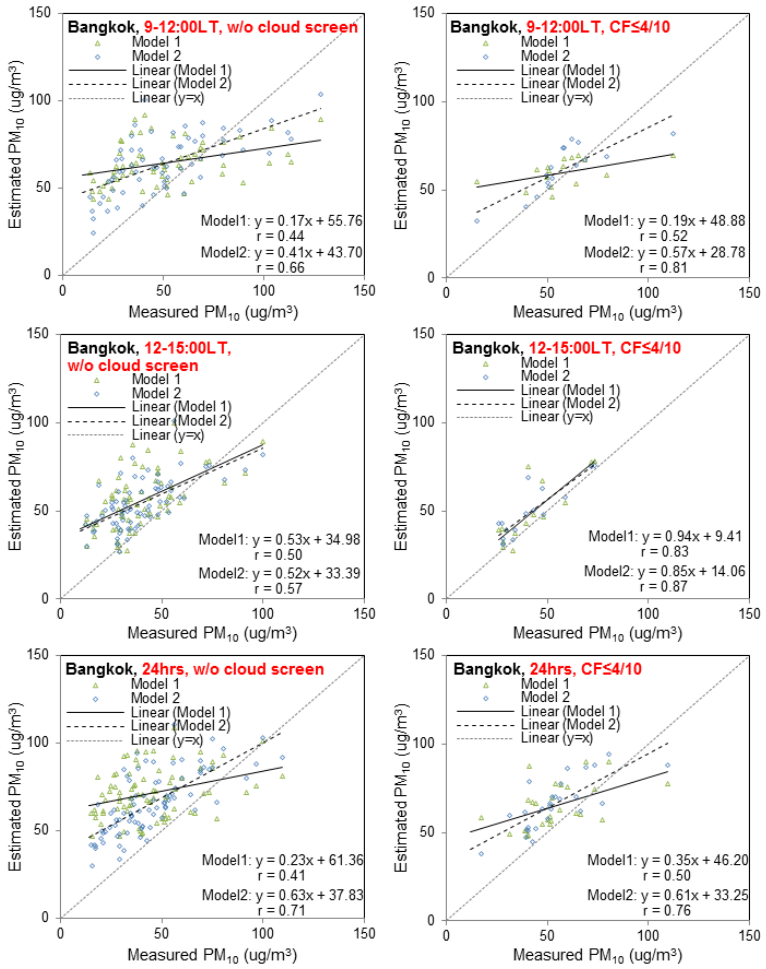

Appendix D.3: Scatter plots over Rayong during dry season (January-April) for 9-12:00LT (a), 12-15:00LT (b), and 24-hr (c) time windows

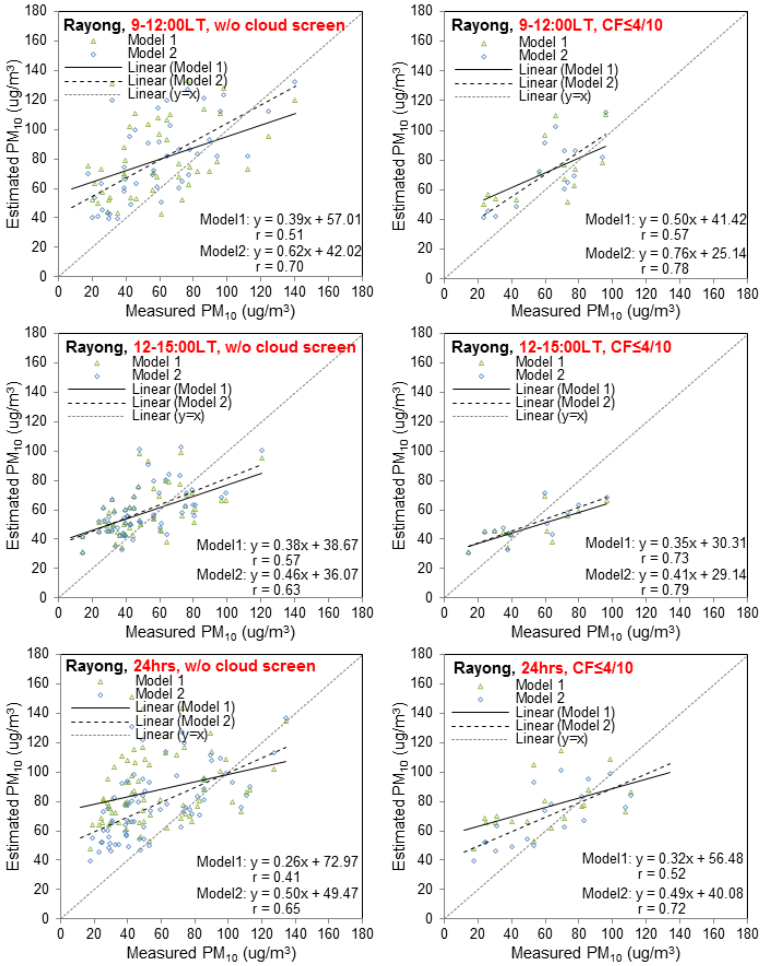

Appendix D.4: Scatter plots over northern Thailand during dry season (January-March) for 9-12:00LT (a), 12-15:00LT (b), and 24-hr (c) time windows

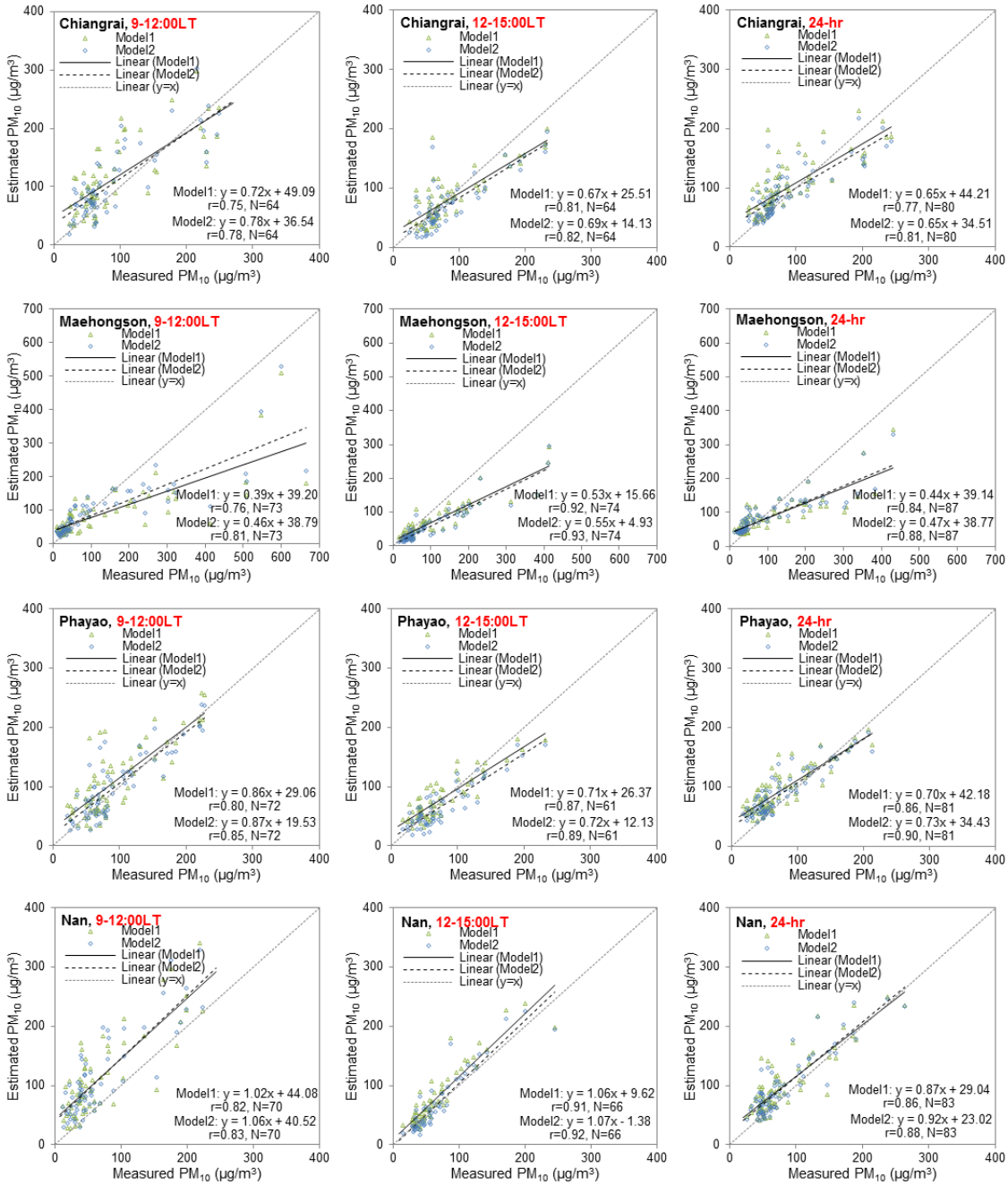

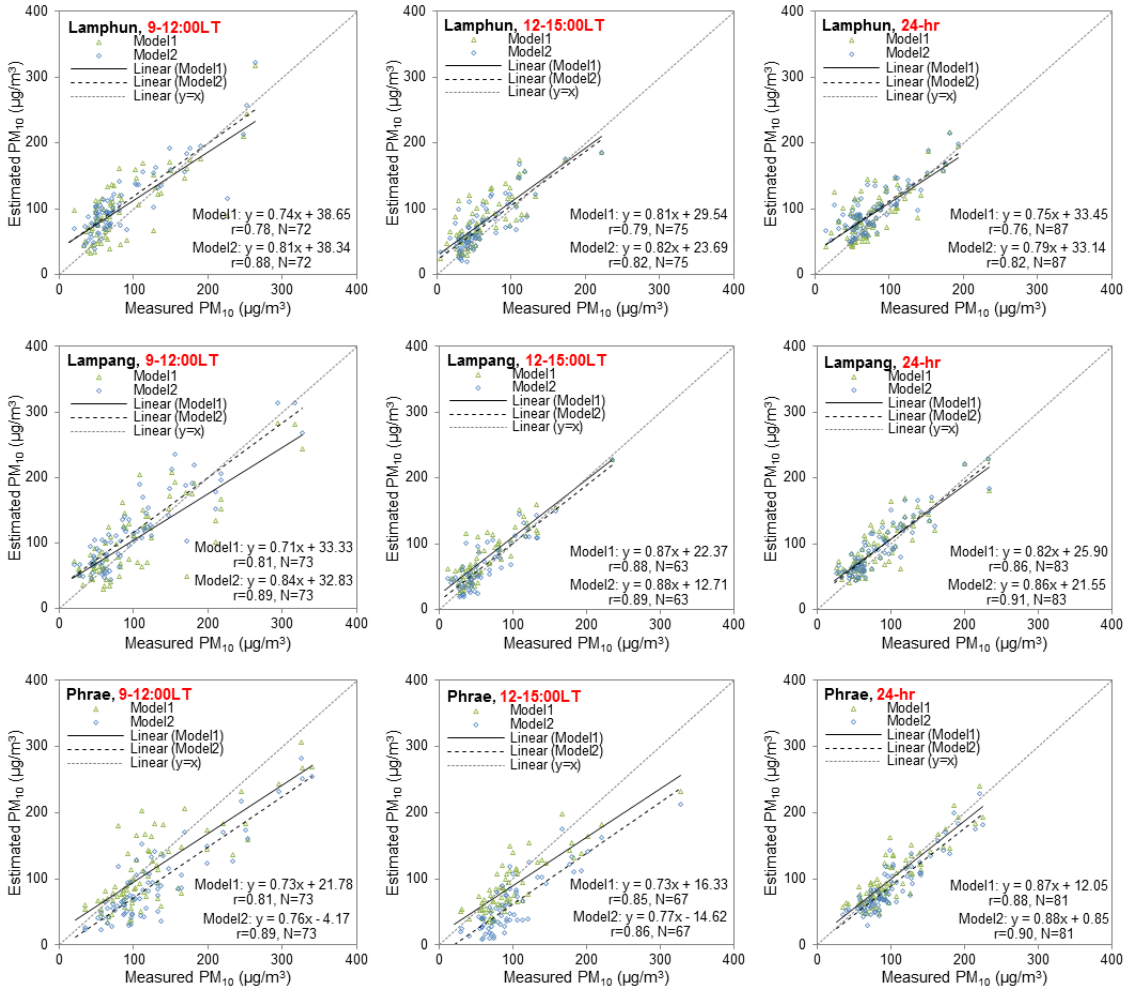
Lamphun, 9-12:00LT
Model1
Model2
Linear (Model1)
Linear (Model2)
Linear (y=x)
Model1: y = 0.74x + 38.65
r=0.78, N=72
Model2: y = 0.81x + 38.34
r=0.88, N=72
Lamphun, 12-15:00LT
Model1: y = 0.81x + 29.54
r=0.79, N=75
Model2: y = 0.82x + 23.69
r=0.82, N=75
Lamphun, 24-hr
Model1: y = 0.75x + 33.45
r=0.76, N=87
Model2: y = 0.79x + 33.14
r=0.82, N=87
Lampang, 9-12:00LT
Model1: y = 0.71x + 33.33
r=0.81, N=73
Model2: y = 0.84x + 32.83
r=0.89, N=73
Lampang, 12-15:00LT
Model1: y = 0.87x + 22.37
r=0.88, N=63
Model2: y = 0.88x + 12.71
r=0.89, N=63
Lampang, 24-hr
Model1: y = 0.82x + 25.90
r=0.86, N=83
Model2: y = 0.86x + 21.55
r=0.91, N=83
Phrae, 9-12:00LT
Model1: y = 0.73x + 21.78
r=0.81, N=73
Model2: y = 0.76x - 4.17
r=0.89, N=73
Phrae, 12-15:00LT
Model1: y = 0.73x + 16.33
r=0.85, N=67
Model2: y = 0.77x - 14.62
r=0.86, N=67
Phrae, 24-hr
Model1: y = 0.87x + 12.05
r=0.88, N=81
Model2: y = 0.88x + 0.85
r=0.90, N=81
Estimated PM10 (µg/m³)
Measured PM10 (µg/m³)
0
100
200
300
400

Appendix E Daily plots of estimated vs. measured surface PM_{10} mass over northern Thailand

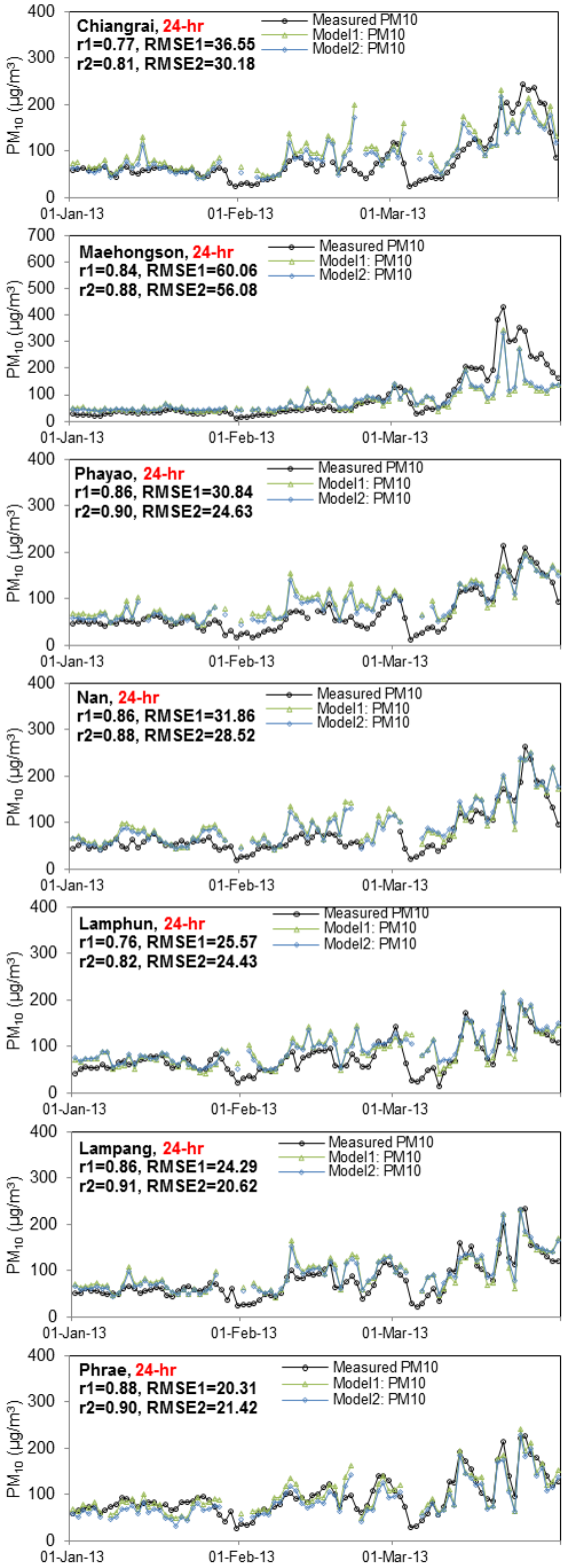

Appendix F: Long-term annual analysis of satellite observations versus surface emissions

Appendix F.1: Long-term annual analysis of satellite NO_2 columns versus NO_x emissions

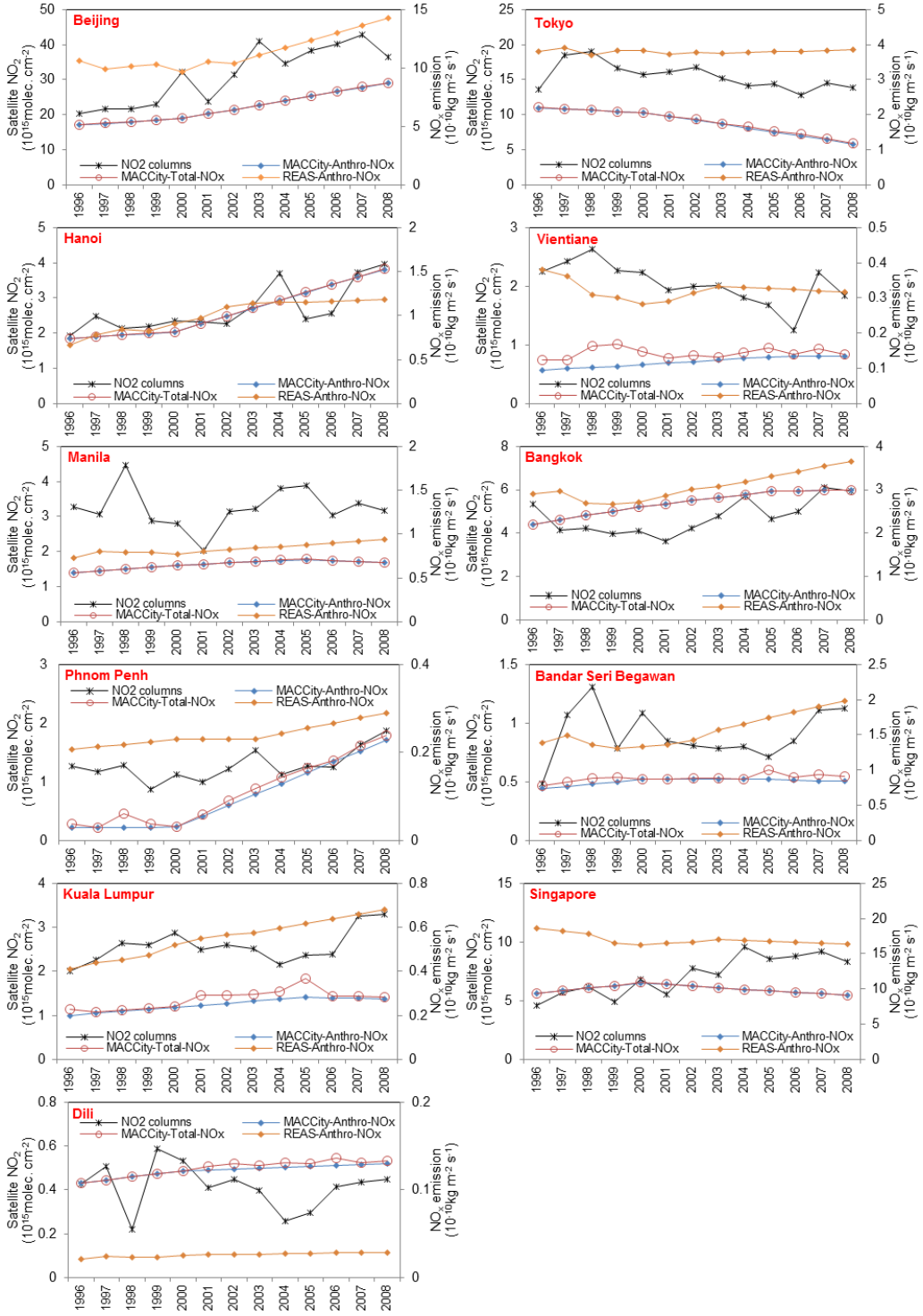

Appendix F.2: Long-term annual analysis of satellite CO columns versus CO emissions

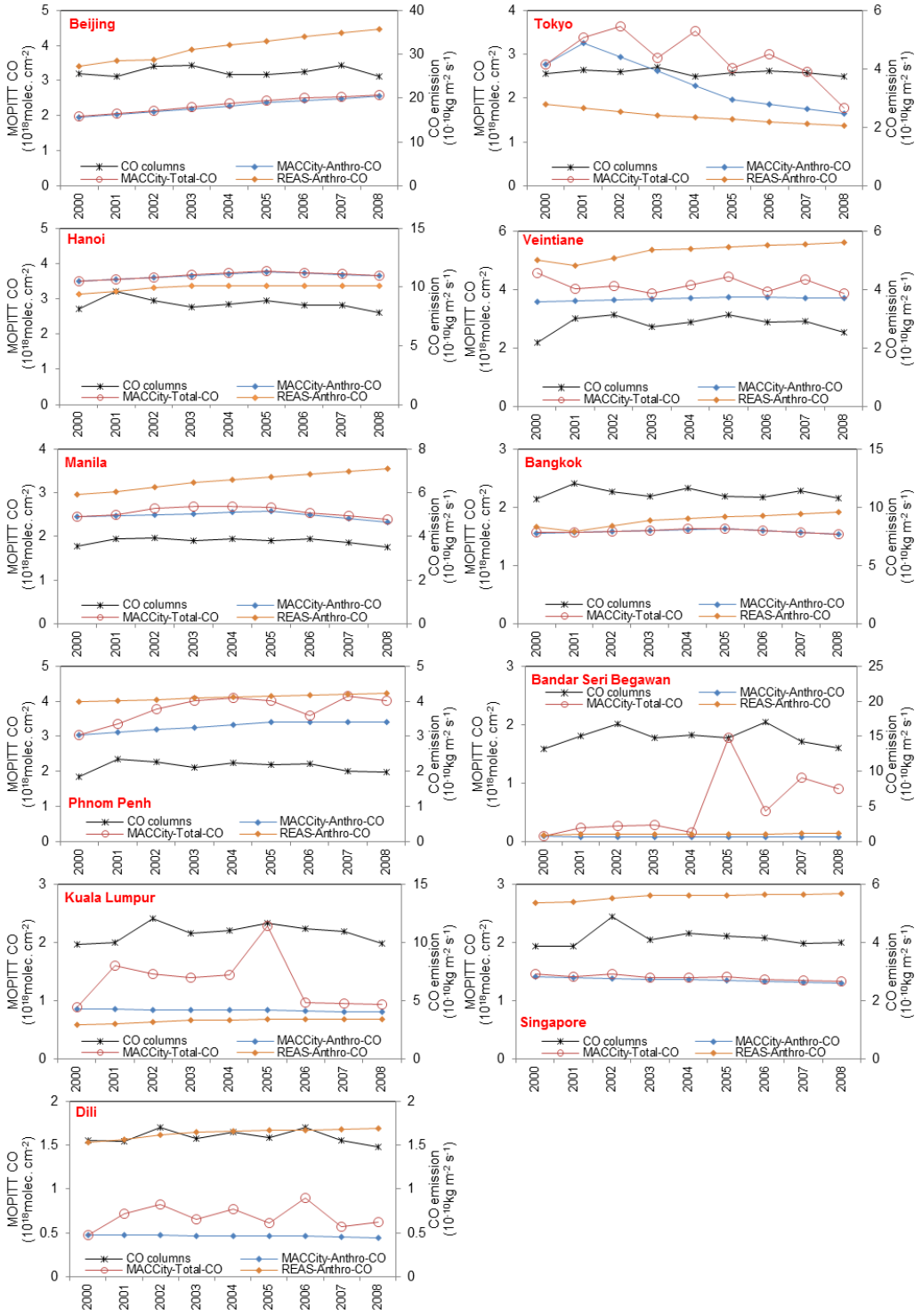

Appendix G: Long-term monthly analysis of satellite observations versus surface emissions

Appendix G.1: Long-term monthly analysis of satellite NO_2 columns versus NO_x emissions

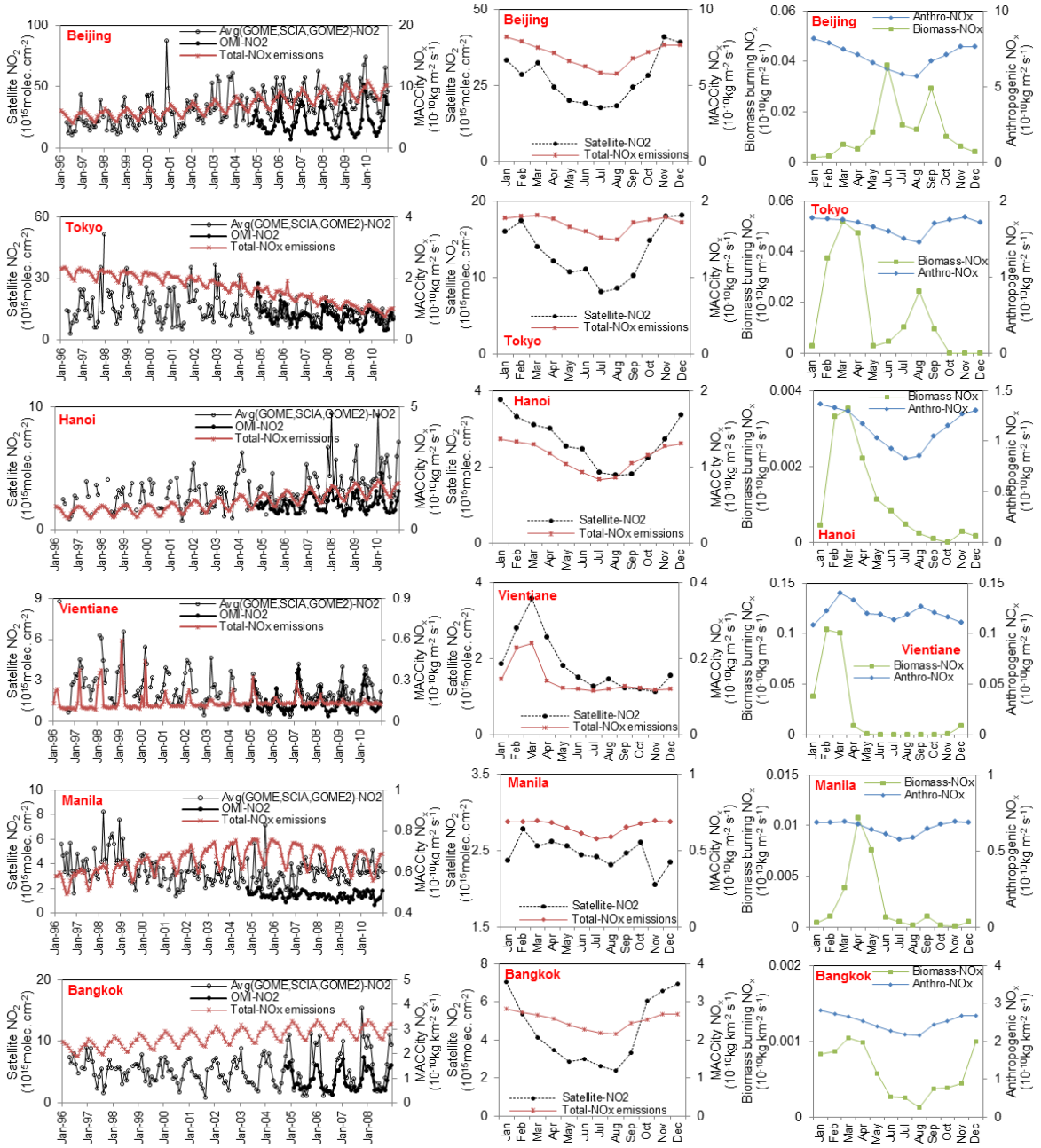

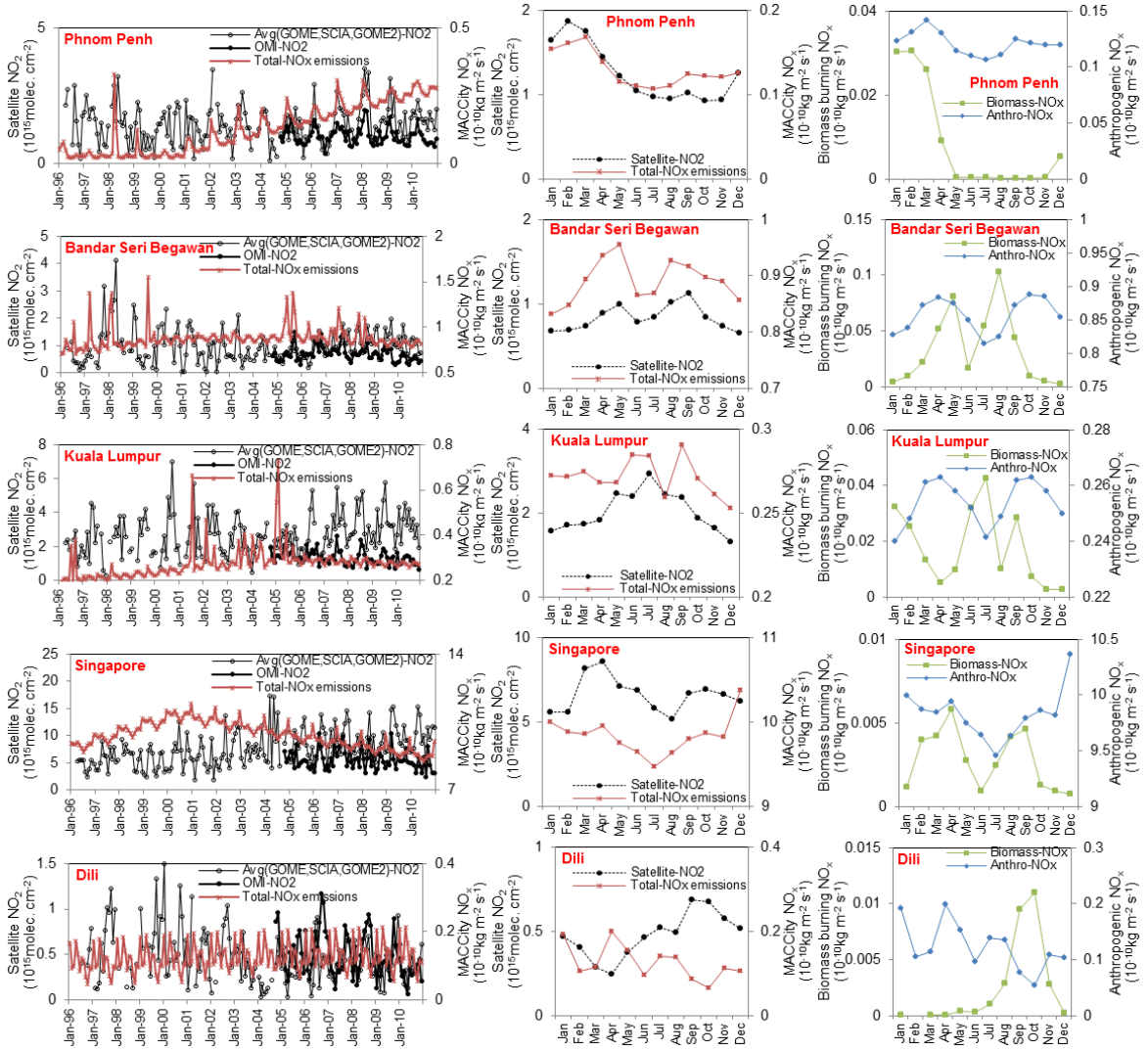
Phnom Penh
Avg(GOME,SCIA,GOME2)-NO2
OMI-NO2
Total-NOx emissions
Satellite-NO2
Total-NOx emissions
Biomass-NOx
Anthro-NOx
Bandar Seri Begawan
Kuala Lumpur
Singapore
Dili
Satellite NO2 (10^15molec. cm^-2)
MACCity NOx (10^-10kg m^-2 s^-1)
Biomass burning NOx (10^-10kg m^-2 s^-1)
Anthropogenic NOx (10^-10kg m^-2 s^-1)

Appendix G.2: Long-term monthly analysis of satellite CO columns versus CO emissions

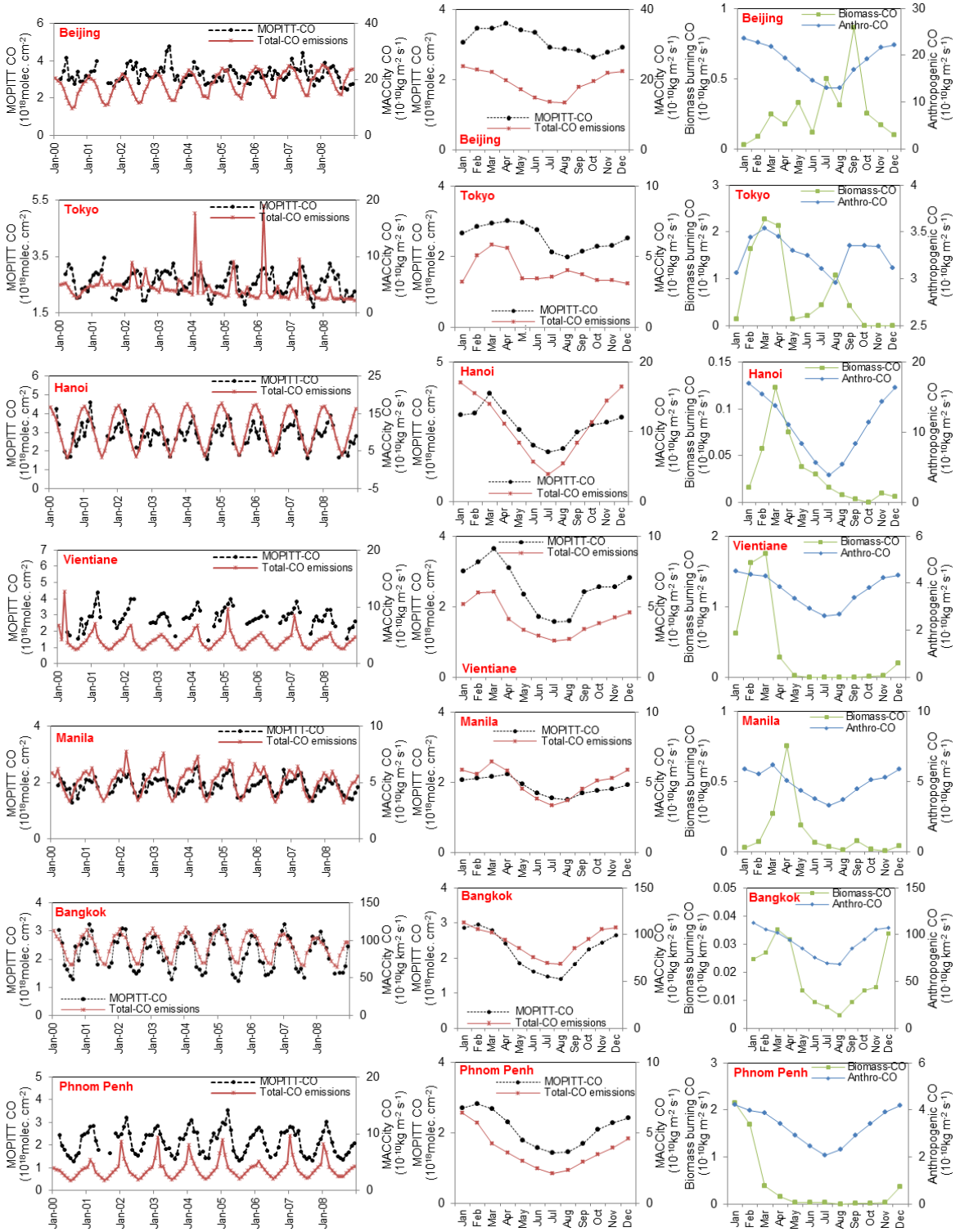

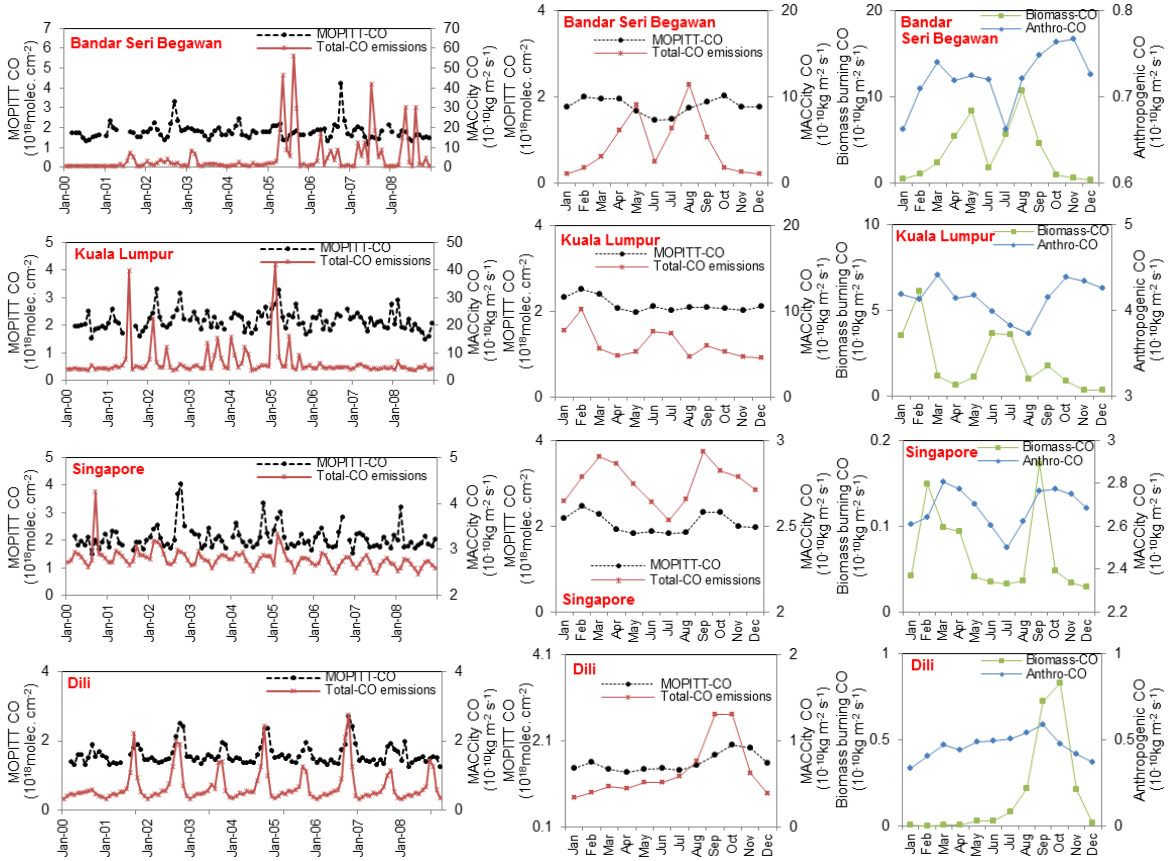
Bandar Seri Begawan
MOPITT-CO
Total-CO emissions
MOPITT CO (10^18 molec. cm^-2)
MACCity CO (10^-10 kg m^-2 s^-1)
Bandar Seri Begawan
MOPITT-CO
Total-CO emissions
MOPITT CO (10^18 molec. cm^-2)
MACCity CO (10^-10 kg m^-2 s^-1)
Bandar Seri Begawan
Biomass-CO
Anthro-CO
Biomass burning CO (10^-10 kg m^-2 s^-1)
Anthropogenic CO (10^-10 kg m^-2 s^-1)
Kuala Lumpur
MOPITT-CO
Total-CO emissions
MOPITT CO (10^18 molec. cm^-2)
MACCity CO (10^-10 kg m^-2 s^-1)
Kuala Lumpur
MOPITT-CO
Total-CO emissions
MOPITT CO (10^18 molec. cm^-2)
MACCity CO (10^-10 kg m^-2 s^-1)
Kuala Lumpur
Biomass-CO
Anthro-CO
Biomass burning CO (10^-10 kg m^-2 s^-1)
Anthropogenic CO (10^-10 kg m^-2 s^-1)
Singapore
MOPITT-CO
Total-CO emissions
MOPITT CO (10^18 molec. cm^-2)
MACCity CO (10^-10 kg m^-2 s^-1)
Singapore
MOPITT-CO
Total-CO emissions
MOPITT CO (10^18 molec. cm^-2)
MACCity CO (10^-10 kg m^-2 s^-1)
Singapore
Biomass-CO
Anthro-CO
Biomass burning CO (10^-10 kg m^-2 s^-1)
MACCity CO (10^-10 kg m^-2 s^-1)
Dili
MOPITT-CO
Total-CO emissions
MOPITT CO (10^18 molec. cm^-2)
MACCity CO (10^-10 kg m^-2 s^-1)
Dili
MOPITT-CO
Total-CO emissions
MOPITT CO (10^18 molec. cm^-2)
MACCity CO (10^-10 kg m^-2 s^-1)
Dili
Biomass-CO
Anthro-CO
Biomass burning CO (10^-10 kg m^-2 s^-1)
Anthropogenic CO (10^-10 kg m^-2 s^-1)
Jan-00
Jan-01
Jan-02
Jan-03
Jan-04
Jan-05
Jan-06
Jan-07
Jan-08
Jan
Feb
Mar
Apr
May
Jun
Jul
Aug
Sep
Oct
Nov
Dec

Appendix H: The comparison of the precipitation and L_{NOx} (hour)

Appendix H.1: Scattering plot of monthly averages of the precipitation and L_{NOx} (hour)

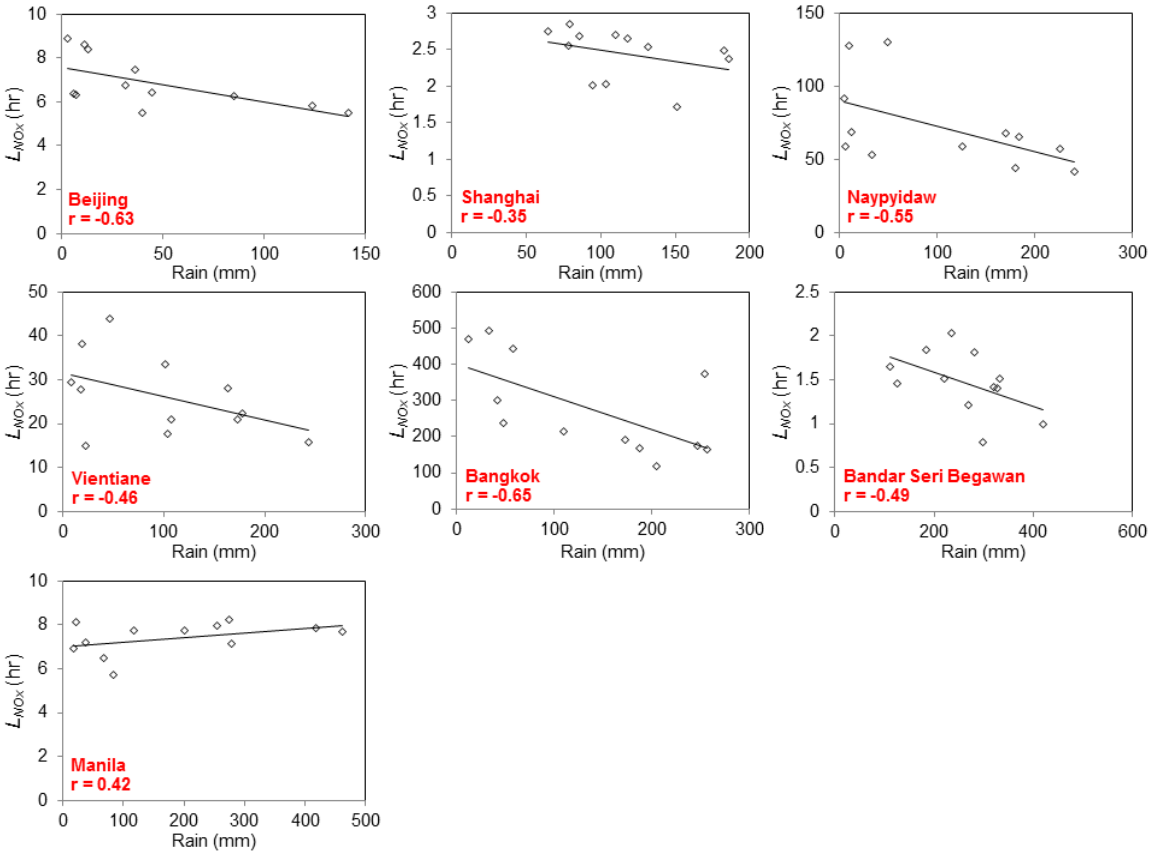

Appendix H.2: Seasonal variability of monthly averages of the precipitation and L_{NOx} (hour)

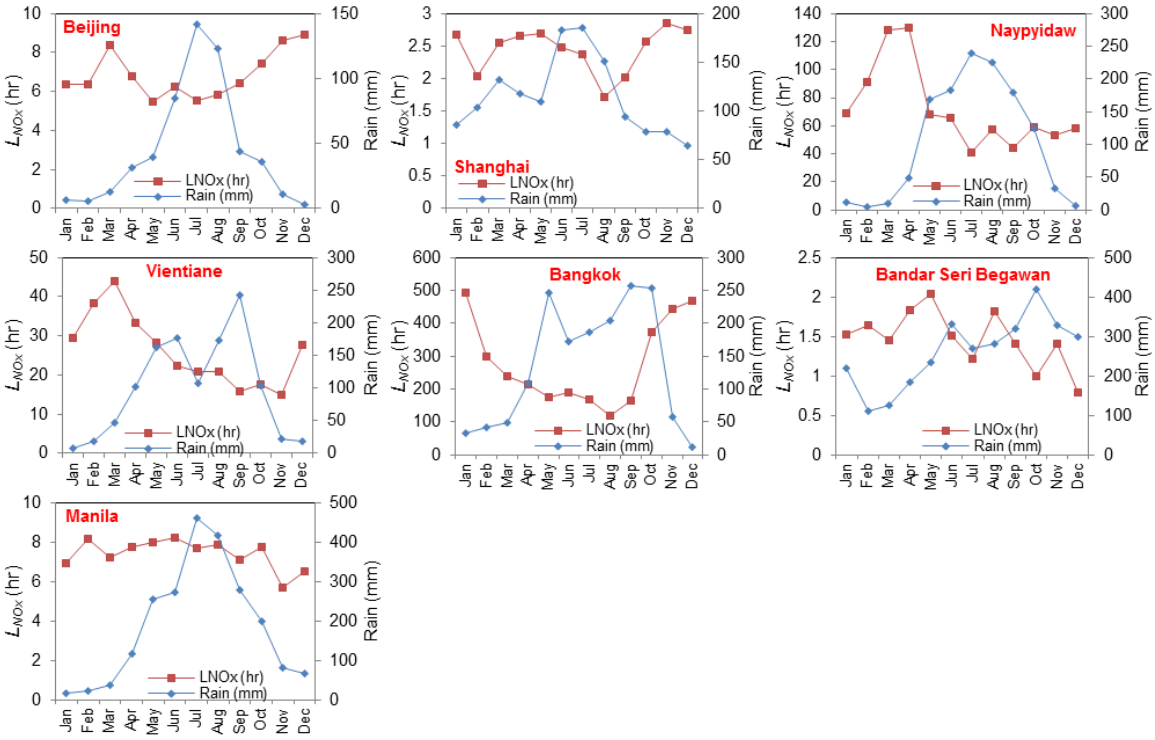

Appendix I: The comparative analysis of NO_2 columns simulated from GEOS-Chem and retrieved from satellites

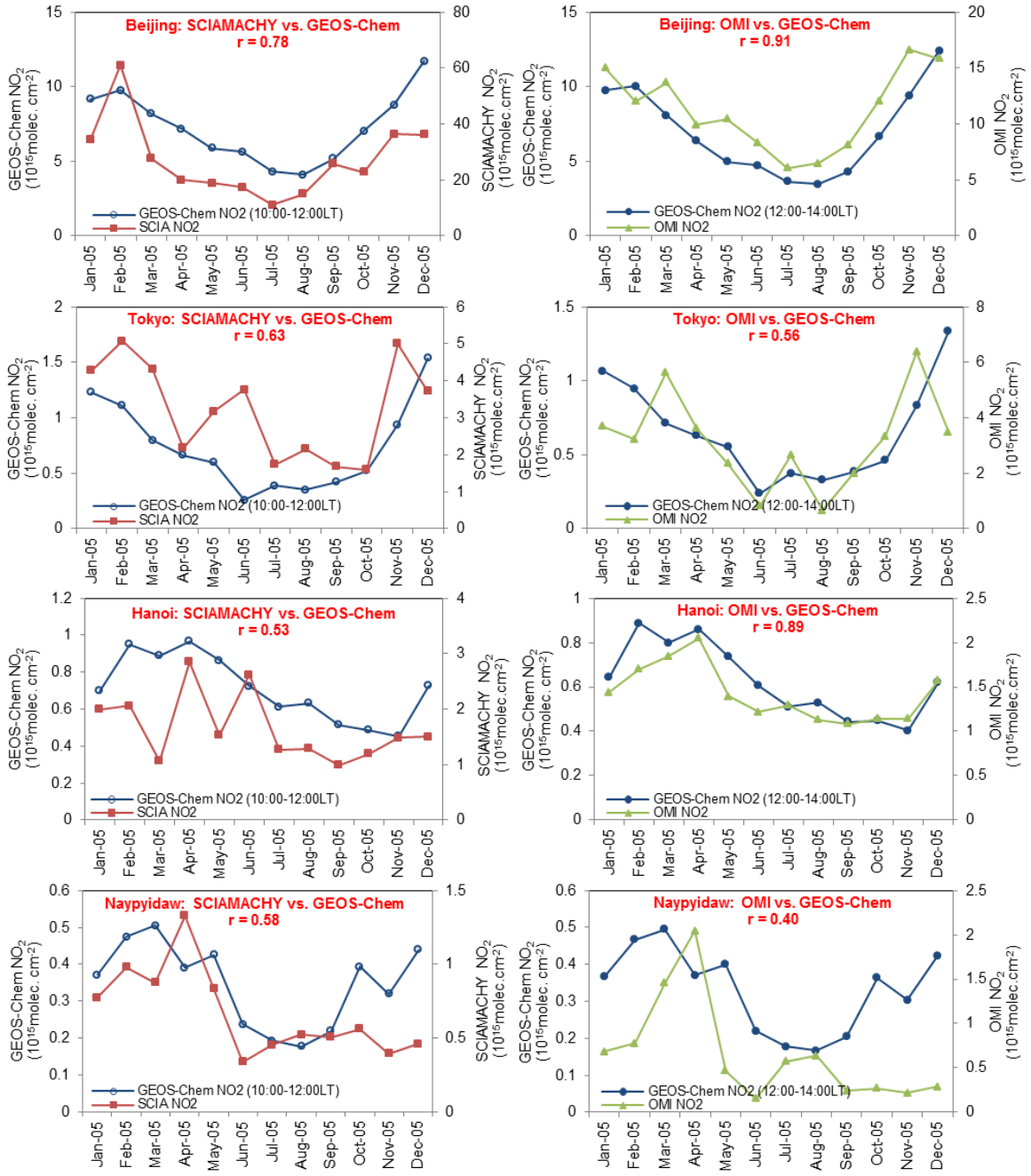

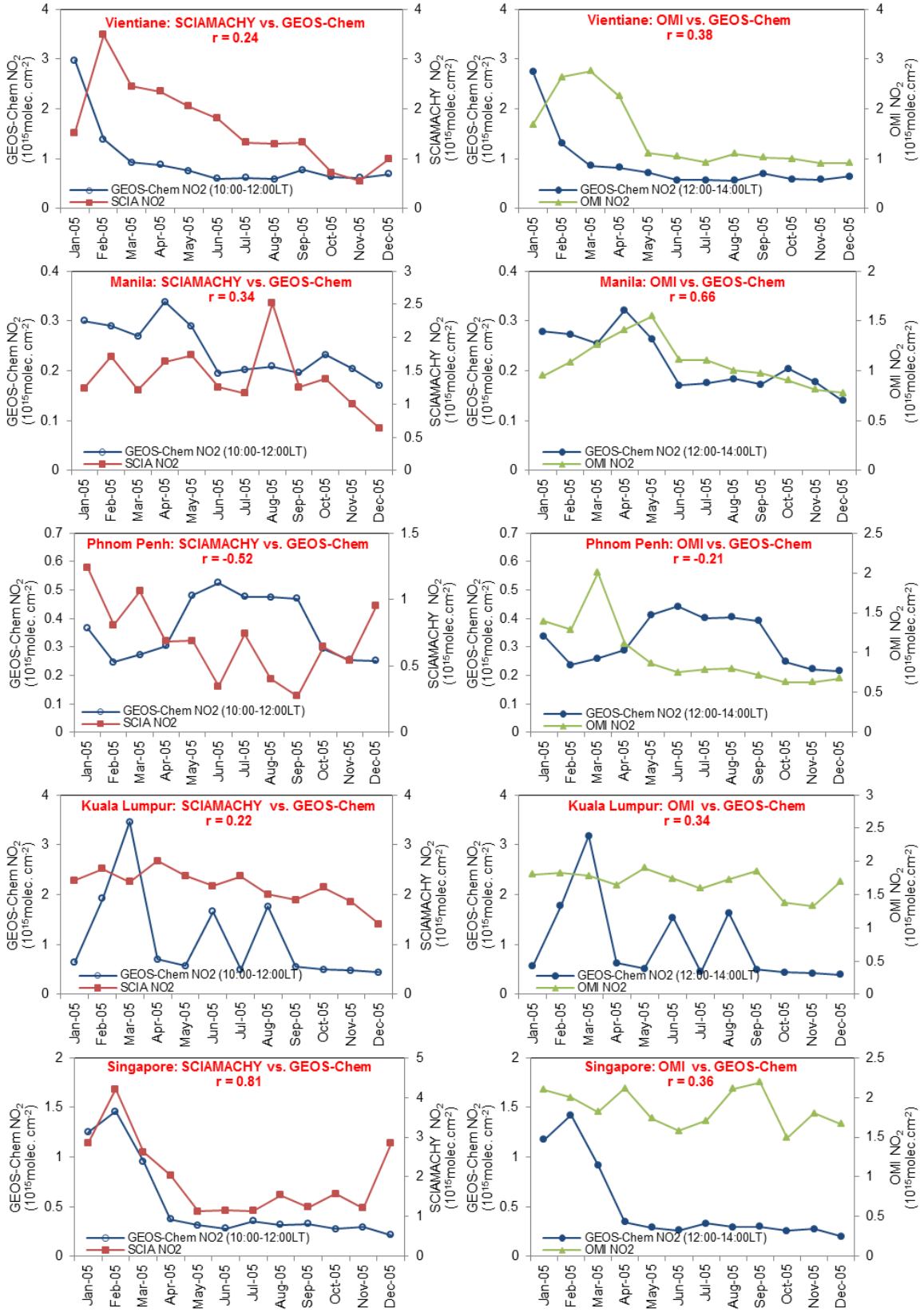
Vientiane: SCIAMACHY vs. GEOS-Chem
r = 0.24
GEOS-Chem NO2 (10:00-12:00LT)
SCIA NO2
Vientiane: OMI vs. GEOS-Chem
r = 0.38
GEOS-Chem NO2 (12:00-14:00LT)
OMI NO2
Manila: SCIAMACHY vs. GEOS-Chem
r = 0.34
Manila: OMI vs. GEOS-Chem
r = 0.66
Phnom Penh: SCIAMACHY vs. GEOS-Chem
r = -0.52
Phnom Penh: OMI vs. GEOS-Chem
r = -0.21
Kuala Lumpur: SCIAMACHY vs. GEOS-Chem
r = 0.22
Kuala Lumpur: OMI vs. GEOS-Chem
r = 0.34
Singapore: SCIAMACHY vs. GEOS-Chem
r = 0.81
Singapore: OMI vs. GEOS-Chem
r = 0.36
GEOS-Chem NO2 (10^15molec.cm-2)
SCIAMACHY NO2 (10^15molec.cm-2)
OMI NO2 (10^15molec.cm-2)
Jan-05
Feb-05
Mar-05
Apr-05
May-05
Jun-05
Jul-05
Aug-05
Sep-05
Oct-05
Nov-05
Dec-05

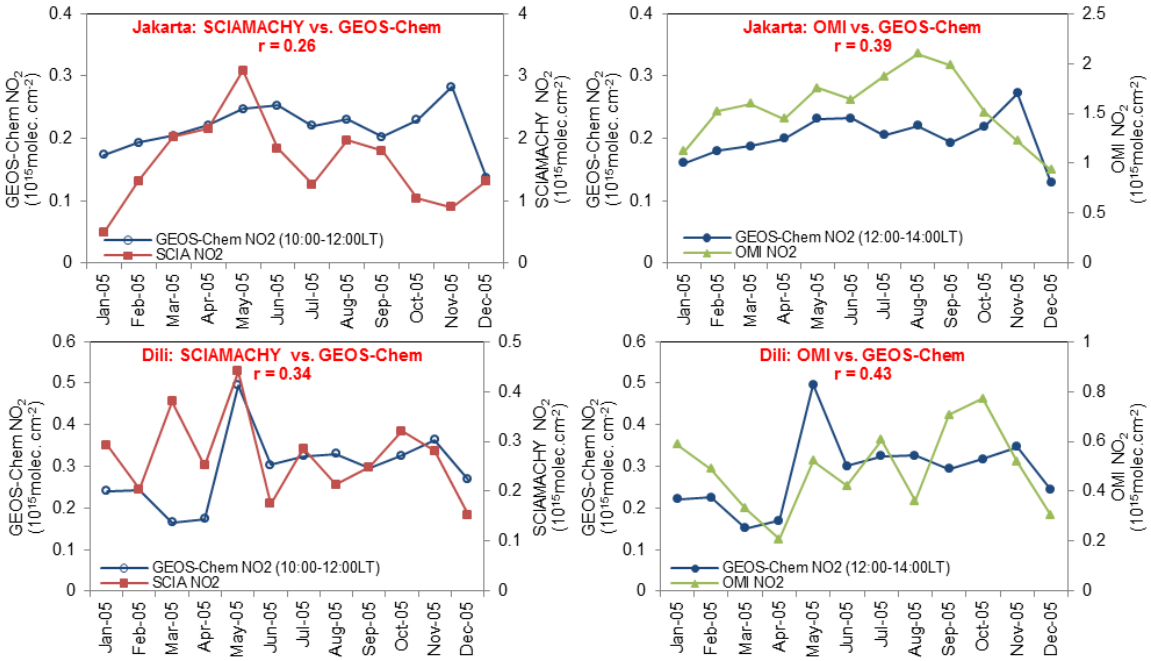
Jakarta: SCIAMACHY vs. GEOS-Chem
r = 0.26
GEOS-Chem NO2 (10:00-12:00LT)
SCIA NO2
GEOS-Chem NO2 (10^15molec. cm-2)
SCIAMACHY NO2 (10^15molec.cm-2)
Jakarta: OMI vs. GEOS-Chem
r = 0.39
GEOS-Chem NO2 (12:00-14:00LT)
OMI NO2
OMI NO2 (10^15molec.cm-2)
Dili: SCIAMACHY vs. GEOS-Chem
r = 0.34
Dili: OMI vs. GEOS-Chem
r = 0.43
Jan-05
Feb-05
Mar-05
Apr-05
May-05
Jun-05
Jul-05
Aug-05
Sep-05
Oct-05
Nov-05
Dec-05